PURIFICATION OF NITROGEN TRIFLUORIDE (NF₃) VIA PHYSICAL SEPARATION

Rasoul Hassanalizadeh
BSc. Eng. Petroleum University of Technology (Iran)
MSc. Eng. University of Science and Technology of Mazandaran (Iran)

Submitted in fulfilment of the Academic Requirements for the Award of

the Doctor of Philosophy Degree in Engineering in the School of

Engineering,

University of KwaZulu-Natal.

March 2020

Supervisor: Prof Deresh Ramjugernath

Co-supervisors: Prof Paramespri Naidoo and Dr Wayne M Nelson

As the candidate's supervisor I agree to the submission of this thesis:

_____   _____

Prof Deresh Ramjugernath   Date

Declaration 1

I, <u>Rasoul Hassanalizadeh</u>, student number <u>216072589</u> declare that:

(i) The research reported in this dissertation, except where otherwise indicated or acknowledged, is my original work.

(ii) This dissertation has not been submitted in full or in part for any degree or examination to any other university.

(iii) This dissertation does not contain other persons' data, pictures, graphs or other information unless specifically acknowledged as being sourced from other persons.

(iv) This dissertation does not contain other persons' writing unless specifically acknowledged as being sourced from other researchers. Where other written sources have been quoted, then:

   a) Their words have been rewritten but the general information attributed to them has been referenced.

   b) Where their exact words have been used, their writing has been placed inside quotation marks, and referenced.

(v) This dissertation is primarily a collection of material, prepared by myself, published as journal articles or presented as a poster and oral presentations at conferences. In some cases, additional material has been included.

_____   _____

Signed   Date

Declaration 2

DETAILS OF CONTRIBUTION TO PUBLICATIONS that form part and/or include research presented in this thesis (include publications in preparation, submitted, *in press* and published and give details of the contributions of each author to the experimental work and writing of each publication)

Publication 1

Hassanalizadeh, R., Nelson, W.M., Naidoo, P., Mohammadi, A.H., Negadi, L. and Ramjugernath, D., 2019. VLE measurements and modelling for the binary systems of (CF_4+ C_6F_{14}) and (CF_4+ C_8F_{18}). *Fluid Phase Equilibria*, *485*, pp.146-152.

Publication 2

Nelson, W.M., Hassanalizadeh, R. and Ramjugernath, D., 2017. Phase equilibrium and critical point data for ethylene and chlorodifluoromethane binary mixtures using a new "static-analytic" apparatus. *Fluid Phase Equilibria*, *451*, pp.106-113.

Signed:

Acknowledgements

I would like to acknowledge the following people for their support in this research study:

Abstract

Nitrogen trifluoride (NF_3) is an important gas used in electrical circuits etching, the manufacture of flat screen displays, hydrogen fluoride lasers and electrical deposits chamber cleaning, all of which require the gas at high purity (99.999 – 99.9999 %). The contaminant in this product is tetrafluoromethane (CF_4) which enters with the fluorine during production. The two gases, CF_4 and NF_3 have very similar physical characteristics making the separation via traditional technologies difficult. Cryogenic distillation at conditions of -100 to -192 ℃ is utilized conventionally for the separation of CF_4 and NF_3 while membrane technology and adsorption using zeolites and molecular sieves have been studied. These processes have a high energy demand and maintenance cost. Further difficulties relate to their batch-wise operation and low production flowrate.

The aim of this research was to study an alternate separation route for purifying NF_3. A detailed literature review of the advantages and disadvantages of existing technologies led to the selection of physical separation technology as a potential method to overcome the current industrial challenges. More than 300 solvents from different chemical families were considered in the solvent screening process. Several solvent screening methods were used, including the Robbins chart, the use of thermodynamic predictive methods, physical property method and phase equilibrium measurements to determine whether the solvents exhibited an affinity to dissolve the gases. The predictive methods included the predictive Soave-Redlich-Kwong (PSRK), Universal quasi chemical Functional-group Activity Coefficients (UNIFAC), and the Conductor-like Screening Model - Segment Activity Coefficient (COSMO-SAC) models. A final list of 6 perfluorinated solvents was chosen for further investigation via experimental work. These solvents were selected based on the physical properties and trends observed in the literature. Other factors such as toxicity, price and availability of the solvents were also considered.

High-pressure vapour liquid equilibrium (HPVLE) measurements were performed as the final screening process to identify the best solvent from the list of selected solvents. This was done using two different high-pressure apparatuses to fast track the measurements and validate the measured data. A considerable amount of time was spent on experimental work to validate the HPVLE measurement technique. A test system of CO_2 + n-hexane was selected at 313.15 K, followed by binary HPVLE measurements for systems of CF_4 + solvents at three temperatures between (283.15 to 303.15) K and pressures up to 20.00 MPa. To generate data for binary systems of NF_3 with a solvent, a significant amount of time was invested in establishing the experimental method, and preparation of the equipment, since NF_3 is a highly toxic gas with major health risks. The exposure limits set are 10 ppm for 8 hrs of working per 5 days of the week. The *immediately dangerous for health and life* (IDLH) threshold is 1000 ppm with no experimental HPVLE data

available for systems of NF_3 + the listed solvents. A comprehensive fault tree analysis was performed prior to the experimental work using NF_3. Major modifications were performed on the experimental apparatus to ensure safe operation. The apparatus was housed in a fume hood and the mixture was prepared in another fume hood. An electricity generator was purchased and installed as a backup power supply to ensure continuous extraction in the event of a power outage. A new experimental procedure was developed by improving the safety procedures of the previous method. New high-quality experimental data were generated for the NF_3 systems within an acceptable range of uncertainties in the measured results.

Overall, more than 10 novel HPVLE binary systems were measured and validated in this study. The experimental data were correlated using a combination of thermodynamic models, with the Peng-Robinson equation of state and Wong-Sandler mixing rule with non-random two-liquid activity coefficient model, yielding the best representation of the data. The least-square objective function was minimized (P and x) using the algorithm of Britt-Luecke to regress the binary interaction parameters. The absolute average relative deviation (AARD(P) %) analysis results showed a good representation of the measured data with the overall average errors of below 1 % and 3.9 % for composition and pressure of CF_4 in the vapour phase, respectively. The results from the screening of new solvents showed promising trends for selected compounds to selectively absorb NF_3. They indicated that tetrafluoroethyl tetrafluoropropropyl ether and perfluorodecalin were the better performing solvents from the list of selected solvents tested in this study.

Preliminary physical absorption simulations were performed using the information from the HPVLE regressions to achieve ultra-high product purity of NF_3. Results showed that the physical absorption process is not capable of producing high purity NF_3. Therefore, the theoretical design with extractive distillation was attempted. The proposed extractive distillation process consists of an extractive distillation column, a stripping column and other auxiliary units such as mixers, pump and heat exchanger. The effects of several parameters such as solvent stage location (2 – 5), gas feed stage location, feed composition (50 to 99 % of NF_3), column pressure (0.10 to 2.50 MPa), reflux ratio (58 - 100) as well as theoretical stage numbers of the extractive distillation column (20 to 100) and stripping column (3 – 6) were investigated during the sensitivity analysis to obtain the most suitable operating conditions that can produce high purity NF_3. The results showed that extractive distillation can enrich NF_3 to the significantly low impurity content of 0.002 ppm (2 ppb). While over the duration of this study the price of the best-selected solvent has increased significantly, undermining the feasibility of the process, the solvent loss of the process is negligible and the costs are attributed to the initial solvent charge to the process. Further recommendations for simulation studies of a cheaper solvent along with intensive energy analysis will enhance the use of extractive distillation for the purification of NF_3.

Nomenclature

English letters

Symbol	Description	Unit
C	Solvent capacity	--
COSMO-SAC	COnductor-like Screening method of MOdel-Segment Activity Coefficient model	--
Eff	Efficiency	--
EoS	Equation of State	--
F	Fugacity	MPa
G	Gibbs free energy	kJ
k_{ij}	Binary interaction parameter	--
L	Liquid	--
N	Number of moles	mol
NRTL	Non-Random Two-Liquid model	--
No.	Number	--
P	Pressure	MPa
PFC	Perfluorocarbon	-
PR	Peng Robinson model	--
PRSK	Predictive-Soave-Redlich-Kwong model	--
R	Universal gas constant	$m^3.Pa.mol^{-1}.K^{-1}$
ROLSI™	Rapid On-Line Sampler-Injector	--
S	Solvent selectivity	--
T	Temperature	K
UNIQUAC	UNIversal QUAsi Chemical model	--
UNIFAC	UNIQUAC Functional-Group Activity Coefficients model	--
V	Volume	m^3
v	Vapour	--
VdW	Van der Waals mixing rule	--
WS	Wong-Sandler mixing rule	--
x	Liquid phase composition	--
y	Vapour phase composition	--

Subscripts

Symbol	Description
C	Critical
calc	Calculated
calib	Calibration
cell	Equilibrium cell
equilib	Equilibrium
exp	Experimental
i and j	Specie i and j
º	Degree

Greek Letters

Symbol	Description	Unit
α	NRTL non-randomness parameter, relative volatility	--
γ	Activity coefficient	--
μ	Chemical potential, viscosity	J/mol, mPa-s
τ	NRTL binary interaction parameters	--
η	Efficiency	--

Abbreviations

Symbol	Description
AAD	Average Absolute Deviation
AARD	Average Absolute Relative Deviation
AC	Absorption Column
ACGIH	American Conference of Governmental Industrial Hygienists
AF	Amorphous Fluoro-plastics
COLA	Council of Labour Affairs
DAU	Data Acquisition Unit
EDC	Extractive Distillation Column
FEI	Fluorochemical Expansion Initiative
FTA	Fault Tree Analysis
GWP	Global Warming Potential
HPVLE	High Pressure Vapour Liquid Equilibrium
IC	Integrated Circuits
IDLH	Immediate Dangerous to Life or Heath
MAC	Maximum Allowable Concentration
JSOH	Japan Society for Occupational Health
NA	Not announced
NECSA	Nuclear Energy Corporation of South African
NIOSH	National Institute for Occupational Safety and Health
NIST TDE	National Institute of Standards and Technology ThermoData Engine
OEL	Occupational Exposure Limit
OSHA	Occupational Safety and Health Administration
PCCC	Post-Combustion Carbon Capture
PCS	Permissible Concentration Standard
PDHIP	Pulsed Discharge Helium Ionization Detector
ppb	Parts per billion
ppm	Parts per million
PEL	Permissible Exposure Limit
REL	Recommended Exposure Limit
SC	Stripping Column
SS	Stainless Steel
TCD	Thermal Conductivity Detector
TLV	Threshold Limit Value
TRU	Thermodynamics Research Unit
ZIF	Zeolite Imidazole Framework

Table of Contents

List of Figures

List of Tables

Chapter 1: Introduction

The global market of fluorochemicals was valued at approximately $2 billion in 2017. This is expected to have an increase of approximately 3.6 % per year, reaching $32 billion by 2026. South Africa supplies 10 % of the global raw fluorochemicals, and due to the crude exports of the fluorspar, it only earns below 0.5 % of its overall value (zionmarketresearch, 2018). The fluorochemical Expansion Initiative (FEI), funded by the South African government and established in 2009 aimed to develop scientific activities regarding the use of fluorine sources to expand their applications to gain financial benefits. FEI activities being integral to the development of the fluorochemicals industry in South Africa is directly linked to Pelchem, which is a subsidiary of the South African Nuclear Energy Corporation (NECSA) (Iannucci, 2009). The activities under the FEI programme are aimed at developing the technology and human capacity to drive the development and expansion of a fluorochemical cluster. Recently, two new fluorspar mines of Nokeng and Wallmannsthal were opened in South Africa, aiming to enter the fluorspar business aggressively. More mines are to be opened by 2026, enabling South Africa to be the world's leading fluorspar provider (Solomons, 2018).

According to the FEI 2020 strategic plan, this study of NF_3 purification, one of the speciality fluoride projects, was identified under commercial research activities. This was classified under the subclass of the development of purification processes for fluorochemicals and electronic gases. The four groups of fluorinated electronic gases, namely, hydrofluorocarbons (CHF_3, CH_3F and CH_2F_2) (French et al., 2003), sulphur hexafluoride (SF_6) (Cheng et al., 2013), perfluorocarbons (e.g., CF_4, C_2F_6 and C_3F_8) (Tsai et al., 2002), and nitrogen trifluoride (NF_3) (Tsai, 2008) are contaminated during production. Limited Electronics South Africa SOC Ltd (LESA) is the subsidiary of Pelchem which is responsible for the manufacture and distribution of NF_3. Pelchem started a strategic relationship with the Linde group in 2008 to distribute NF_3 produced at the Pelindaba Linde plant. The plant was purchased by Pelchem in 2012. LESA SOC Ltd saw a significant rise in net income from R7 731 000 loss in 2010 to R7 195 000 profit in 2017 (NECSA, 2018, NECSA, 2012).

1.1 Background

NF_3 is a colourless and odourless gas that is widely used in the electronics industry (Tsai, 2008). It is used in the production of phosphorus sulfide, the production of carbonaceous thin films, high energy lasers, plasma etching, plasma deposition chamber cleaners and in the production of plasma wafers (Tasaka, 2007). Previously, light perfluorocarbons were used to clean chemical deposition chambers, but due to the excellent performance of the free radicals generated, no

carbonaceous depositions, as well as its better rate of decomposition, the materials were replaced by NF_3 (Wijmans et al., 2004, Singh et al., 2008, Miller et al., 2002). The concentration level of CF_4 in the NF_3 bulk gas has created one of the most important industrial concerns about the purity of this gas. Typically, for industrial applications, such as the semiconductor industry and mass production of integrated circuits (IC), electronic gases such as nitrogen trifluoride are required at ultra-high purities of 99.999 or greater (Flamm, 1993, Howe-Grant, 1993, Branken et al., 2014). There are several classification methods for electronic gases. In the process-based classification, NF_3 gas falls within the categories of etching and sputtering (Woytek and Lileck, 1978). A concentration of more than 20 ppm CF_4 impurity causes serious defects in electronic devices. The increase in impurity produces very low-quality plasma etching products together with undesired residues (Flamm et al., 1983). Commercially produced NF_3 is contaminated by CF_4 from the following sources (Aramaki et al., 1985, Woytek and Lileck, 1978, Tasaka, 2007):

- Raw nitrogen carrier gas for NF_3 synthesis contains carbon which interacts with the fluorine and produces CF_4.
- The fluorine is produced in electrolyte tanks equipped with carbon anodes where the interaction of fluorine with the carbon anodes produces CF_4. Some CF_4 traces are introduced with the fluorine.
- Direct fluorination of the carbon present in the body of the vessel or apparatus.

Separation of CF_4 from the NF_3 bulk gas presents difficulties due to the gases' high similarities in physical and chemical properties. There are currently many commercial methods which are used to purify NF_3, including the use of zeolites (Suenaga et al., 1991), molecular sieves such as carbosphere and 5A (Singh et al., 2008), and the use of conventional distillation methods that operate at cryogenic conditions (Miller et al., 2002). In general, the current methods demand very low operating temperatures down to -192 ^{o} C incurring exorbitant cooling and utility costs. In addition, adsorption methods function with very low production flow rates and require very high maintenance and replacement costs. This adds to the plant downtimes and necessitates batch-wise processing schemes. Therefore, operation at ambient temperatures with greater production flow rates is desirable. Figure 1-1 shows the economic evaluation of several techniques for the CO_2 capture which includes three types of absorption columns, membrane and cryogenic distillation (Tuinier et al., 2011). The total costs of cryogenic technology are almost 2.5 times more than those for absorption technology. Absorption is by far the cheapest technology in terms of capital investment, operating cost and maintenance (Cormos, 2015, Tuinier et al., 2011).
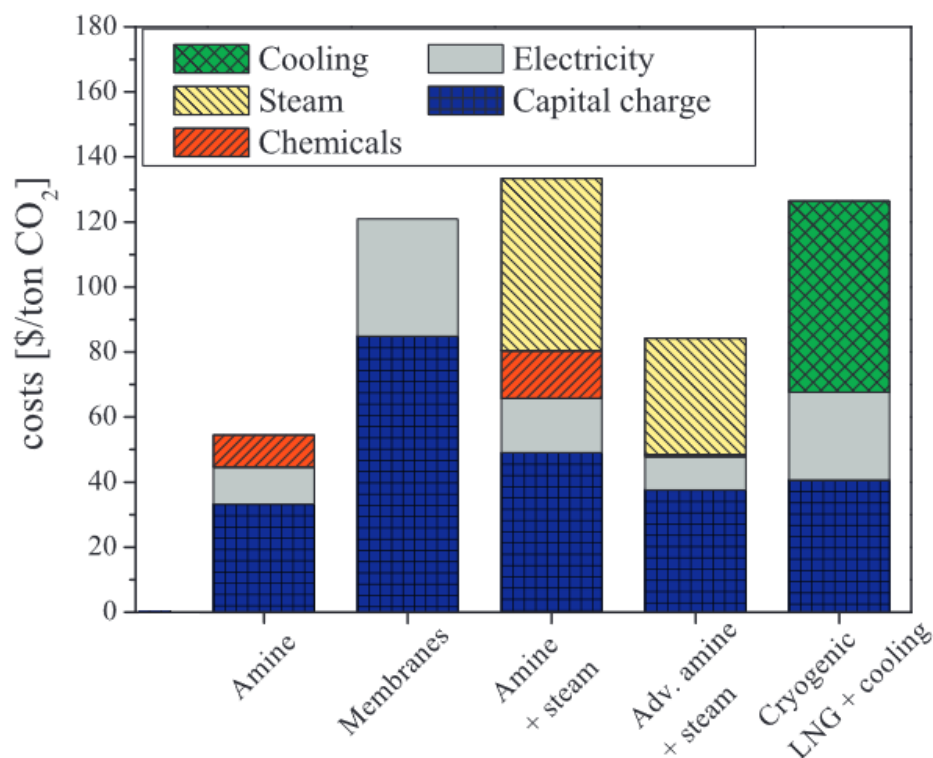
Figure 1-1. Overall costs of different technologies for the CO_2 capture (extracted from (Tuinier et al., 2011)).

1.2 Aim and objectives

The aim of this study was to investigate a suitable technology for the purification of NF_3. The objectives were to:

  i.   Perform an exhaustive literature review to identify a suitable technology.

 ii.   Perform a rigorous solvent screening process using the Robbins chart, predictive methods such as UNIFAC, PSRK and COSMO-SAC and the physical properties-based methods. Several criteria such as toxicity, price, reactivity, boiling point, dielectric constant and availability were considered.

iii.   From a list of solvents selected, to measure high-pressure vapour-liquid equilibrium data for the selected solvents with NF_3 and CF_4. To validate the experimental method, test systems had to be measured first followed by novel measurements.

 iv.   Perform a fault tree analysis on the handling of NF_3 for experimental measurements. This was necessary to eliminate the exposure due to the highly toxic nature of NF_3.

  v.   Perform thermodynamic modelling and correlation of the measured HPVLE such that this could be incorporated in the simulation design work.

 vi.   Upon selection of the best performing solvent from the list of components studied, to perform a preliminary separation by means of simulation work to achieve a 99.999 % purity of NF_3.

Overview of the thesis.

This thesis is presented in 7 chapters. Chapter 1 provides a brief overview of the context of this study. Chapter 2 includes the literature review and expands on the discussion of the available industrial methods for NF_3 purification. One of the essential factors in the physical separation process is the solvent selection which is presented in detail in Chapter 2. Additional insight is given into the process design methodology and thermodynamic modelling.

Chapter 3 explains the thermodynamic phase equilibrium data treatment and modelling approach used to assess the quality of the data and its use in simulation designs. Several models have been tested in this work, and among them, the most appropriate combination of the models has been selected for data regression. Thereafter, the best performing solvent from the systems studied was selected for the preliminary absorption column design.

Chapter 4 presents the experimental equipment used in this work. Two different apparatuses were utilised to measure vapour-liquid equilibrium data. These included the static analytic and static synthetic apparatuses. The necessary information about the apparatuses, calibration methods for the sensors, as well as the experimental procedures are explained in this chapter.

Chapter 5 reports on the novel experimental data and modelling results. The results of the preliminary simulations for the process design is presented in this chapter. Chapter 6 summarises the conclusions from this investigation. Chapter 7 presents recommendations for future work.

Chapter 2: Literature review

The type of separation method for purifying mixtures depends on various factors such as the material and mixture properties, quantity, concentration and the phase of the substance. In general, separation based on the driving force in the separation (such as pressure, electric field and concentration gradient) is divided into five general categories which are, (i) creating a new phase (distillation) (Kister et al., 1992); (ii) adding a new phase (absorption) (Zarzycki and Chacuk, 2013); (iii) creation of a barrier (using membrane) (Lawson and Lloyd, 1997); (iv) using solid particles (adsorption) (Ruthven, 1984); (v) and separation by a magnetic or electric field (Bronkala, 2000). Hybrid technologies include a combination of some of the above.

In this literature review chapter, the five technologies to purify NF_3 are reviewed. These include conventional distillation at cryogenic conditions, extractive distillation, adsorption with the two adsorbents of zeolites and carbosphere, absorption technology and, membrane technology. The latter is still in the research phase. Thereafter, the solvent selection method used in identifying potential candidates for the physical separation processes (i.e. absorption and extractive distillation) is explained. Furthermore, the experimental techniques and type of equipment used to measure high-pressure thermodynamic data are presented in detail. The last part of this chapter discusses the modelling approaches for data treatment and process simulation design.

2.1 Chemical Properties

NF_3 is a colourless and stable gas which exhibits oxidising properties at an elevated temperature. This is due to the low bond energy of 238.9 kJ/mol (Tsai, 2008). The trigonal pyramidal molecular structure and bond dipole moments of the NF_3 molecule is presented in figure 2-1. The dense electron cloud of fluorine atoms and a free electron pair results in a dipole moment of 0.24 (Tro et al., 2011). It is hydrolysed in a basic water solution at 100 °C but does not react with water at ambient temperature (Tsai, 2008). The reaction of NF_3 with metals at temperatures above 300 °C (stainless steel, Bi, and Cu) produces metal fluorides and N_2F_4 (Greenwood and Earnshaw, 2012). Due to its oxidising ability, it generates methaemoglobin which, when inhaled, can result in anoxic death (Pohanish, 2017). Experiments on rats show a slight histolysis of kidneys and livers, together with darkening and enlargement of the spleen. The possibility of mutation is also suspected (Nakajima et al., 2000). The Threshold Limit Value (TLV) is 10 ppm (30 mg/m^3), issued by ACGIH (Meshri, 2000). It has a global warming potential (GWP) of 17200 compared to CO_2, which is equal to one (Forster et al., 2007).
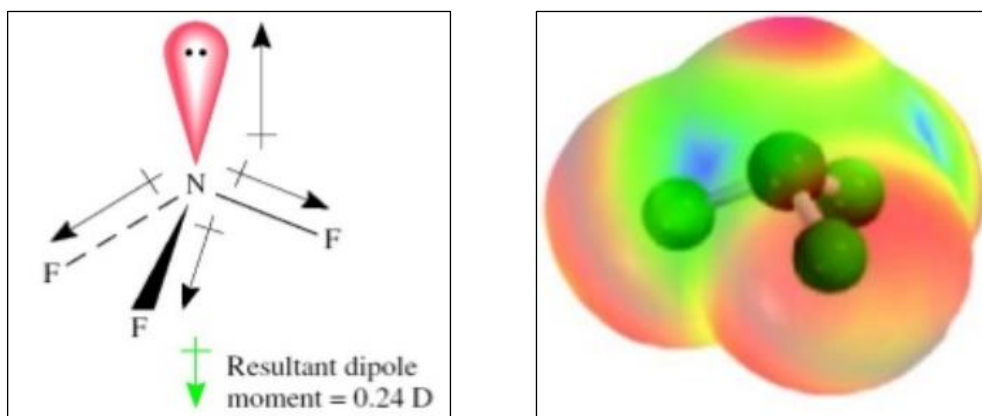
Figure 2-1. Molecular structure and bond moment of NF_3 (Tro et al., 2011).

Tetrafluoromethane, CF_4, is known as the simplest fluorocarbon with a very high bond strength (O'Hagan, 2008). Regarding the four carbon-fluorine bonds and the high electronegativity of fluorine, carbon has a significant positive charge in tetrafluoromethane, which enhances and shortens the carbon-fluorine bond by providing an additional ionic character. Figure 2-2 shows the tetrahedral structure of CF_4 and the evenly distributed electron cloud around it (Molekuul.be). C-F is the most durable single bond among the organic materials which gains its strength from the electrostatic attraction resulting from polarised $C^{\delta+}$ and $F^{\delta-}$ (O'Hagan, 2008). The strong C-F bond established PFCs (perfluorocarbons) as inert chemicals (Riess and Le Blanc, 1982). These class of chemicals remain intact in strong boiling acids and exhibit remarkable thermal stability (Lowe, 1987). Depending on the molecular volume, PFCs dissolve gases such as oxygen, nitrogen and carbon dioxide. This has significant importance in medical science and its applications (Krafft and Riess, 2007). The solubility of gases in PFCs is inversely related to temperature (Riess and Le Blanc, 1982). CF_4 is classified as a greenhouse gas with a GWP of 6500 (Hurley et al., 2005). The chemical properties of CF_4 and NF_3 are listed in table 2-1.
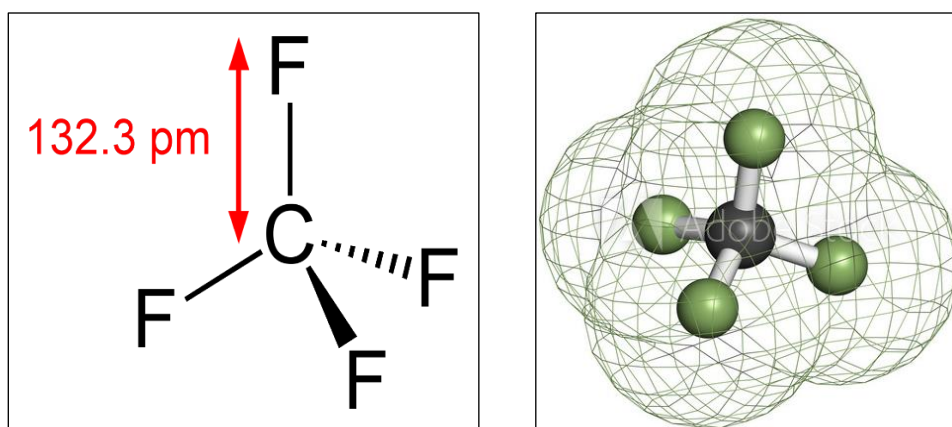
Figure 2-2. Molecular structure and electron cloud of CF_4 (Molekuul.be, 2010).

Table 2-1. List of physical properties for NF_3 and CF_4 (Branken et al., 2013).

Property	NF$_3$	CF$_4$
Boiling point (°C) [a]	-129.0	-128.0
Heat of vaporization (kJ/mol)	11.59	-
Standard heat of formation (kJ/mol) [b]	-131.5	-
Heat capacity (J/mol.K)	53.39	61.27
Critical Temperature (°C)	-39.25	-45.60
Critical Pressure (kPa)	4530	3739
Critical Volume (cm^3/mol)	123.8	139.9
Molecular size (Å)	4.500	4.800
Dipole moment	0.24	0

[a] At 101.325 kPa
[b] At 25 °C, 101.325 kPa

2.2 Technologies to purify NF$_3$ from CF$_4$

Nitrogen trifluoride is among the top four selling inorganic fluorides due to its demand in industrial applications (e.g. electric circuit production and plasma etching). For such applications, it is required in an extremely pure condition at 99.999 % (Nakajima et al., 2000). The presence of high CF_4 content of above 20 ppm in the mixture significantly compromises the product quality (Flamm et al., 1983). This impurity is present in the NF_3 bulk due to the following reasons (Aramaki et al., 1985):

- Due to the interaction of the carbon content of raw nitrogen gas (used for NF_3 production via direct fluorination) with fluorine

- Fluorine is produced in electrolyte tanks equipped with carbon anodes. The fluorine supply would then include CF_4 as a result of its interaction with the carbon anode.

- CF_4 is also produced through the interaction of fluorine with the process equipment and vessels.

When NF_3 is produced, in addition to CF_4, traces of impurities such as N_2F_2, N_2O, CO_2 and H_2O can be detected in the NF_3 bulk flow. N_2F_2 is removed through pyrolysis on the hot surface of metals (Harada et al., 1990) while N_2O, CO_2 and H_2O are removed utilising zeolites (Nakajima et al., 2000). Due to very similar physical properties of NF_3 and CF_4, as well as their small tendency to react, their separation cost is considered exorbitant and the separation process is complicated (Pankratov, 1973). A summary of the technologies available for NF_3 purification is presented in table 2-2.

Table 2-2. Summary of technologies available for NF$_3$ purification.

Technology	T /°C	P /MPa	Capacity (CF$_4$ content) /ppm	References
Cryogenic distillation	-192	0.3	10 to 50	(Jin and Fisher, 1996, Fisher and Jin, 1997, Fisher, 1998, Nagamura and Yamamoto, 1994, Hyakutake et al., 1990, Fidkowski et al., 2001)
Adsorption (zeolites, molecular sieves and carbosphere)	-196 to 600	-	1 to 40	(Suenaga et al., 1991, Harada et al., 1993, Igumnov and Kharitonov, 2006, Singh et al., 2008, Hart et al., 2006, Henderson and Underwood, 2016)
Membrane (research phase)	35 – 160	0.02	3	(Branken et al., 2013)
Extractive distillation	-120	0.6 to 1.1	20 to 200	(Miller, 1966, Shiflett and Yokozeki, 2014)

2.2.1 Cryogenic distillation

The most common method for separating NF$_3$ from CF$_4$ is via cryogenic distillation (refrigeration). In this process, the NF$_3$ + CF$_4$ mixture is liquefied at -129 °C, and it is purified to 99.99 %. While this process can produce high-purity gas, it is a highly energy-intensive process due to the extremely low operating temperatures (Hyakutake et al., 1990). Cryogenic distillation for the purification of NF$_3$ has been further developed by the addition of a washing liquid such as HCl (Jin and Fisher, 1996, Fisher and Jin, 1997, Fisher, 1998). This is used to wash the impurities other than CF$_4$ (mostly fluorinated) from the gas mixture. The washing liquid is recovered for reuse via cryogenic distillation.

A hybrid of a high-pressure and cryogenic distillation columns was proposed to eliminate principle moisture and CO$_2$ from the feed gas mixture (Nagamura and Yamamoto, 1994). In this process, the feed gas mixture is pressurised to 0.9 MPa, cooled down to -166 °C, and passed through an absorber which is maintained at a low temperature to eliminate N$_2$F$_2$, N$_2$F$_4$, N$_2$O, and CF$_4$. The remaining mixture is liquefied in the re-boiler of a second distillation column. The principle of gas separation is the volatility differences of the components. The product mixture then flows through a distillation column operating at low pressure to provide ultra-high purity NF$_3$ as a final product at the medium pressure level supplied by a re-boiler (Nagamura and

Yamamoto, 1994). The advantage of this process is the ultra-high purity NF_3. However, the high energy demand due to the high-pressure requirement to supply NF_3 as a feed stream at an even higher pressure is a major drawback.

Figure 2-3 shows the schematic of a patented process for purifying NF_3 from a gas mixture with different volatilities. This process uses two distillation columns for the raw feed. At first, the liquefied mixture (with NF_3 content of 30 %) is fed into the first column. Thereafter, the cryogenic liquid is introduced to the first stage above the feeding site. The high volatility components are separated from the NF_3 as a lean gas/liquid, and the heavy NF_3 mixture is removed from the bottom. The heavy mixture is then fed to the second distillation column. The second distillation column produces the purified NF_3. This process involves an extra step to remove the less volatile stream in the bottom product of the second distillation column (Fidkowski et al., 2001). This process operates at -192 ^{o} C and 0.3 MPa. The final concentration of the impurities in the product is less than 10 ppm.
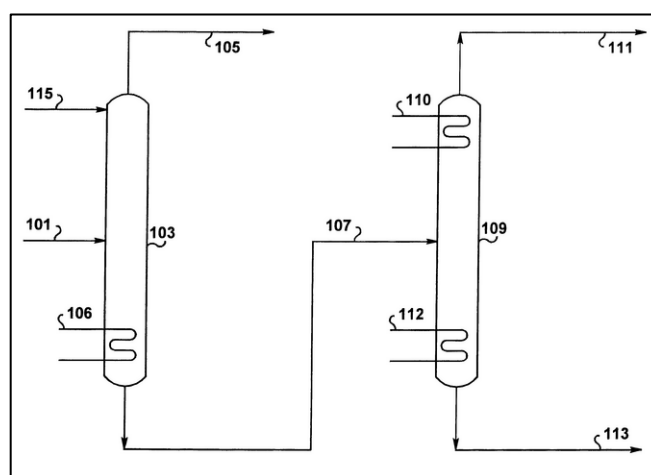
Figure 2-3. Schematic diagram of the cryogenic distillation (Fidkowski et al., 2001).

2.2.2 Adsorption

The main compounds used in physical adsorption of NF_3 purification plants are zeolites, molecular sieves, and carbosphere (Suenaga et al., 1991, Harada et al., 1993, Igumnov and Kharitonov, 2006, Singh et al., 2008). Besides CF_4, there are several other impurities in the NF_3 gaseous stream which needs to be separated. Zeolites were among the first adsorbents used for this purpose. N_2F_2 is one of the oxidizing and decomposing chemicals that are available in NF_3. Using zeolites, this material is adsorbed initially, which decreases the adsorbent capacity significantly to remove other impurities (Harada et al., 1990). NF_3 is also co-adsorbed onto the zeolite, which leads to loss of the gas. Furthermore, due to the accumulation of the N_2F_2, NF_3 decomposition can be initiated on the hot metal plates resulting in heat generation. In an extreme

case, an explosion may occur. Therefore, N_2F_2 needs to be removed before other impurities. Furthermore, nitrogen trifluoride is purified from N_2F_2 utilising a group of candidate adsorbents including metal fluorides of the first three groups of the periodic table, which do not melt at high temperatures. The temperature range of this method is between $150 - 600\,^{\circ}C$ (Harada et al., 1993).

Some of the industrial methods focus on adsorbing NF_3. For example, zeolites with sizes of 4.9 $^{\circ}A$ can purify NF_3 selectively in the temperature range, higher than $10\,^{\circ}C$. An example of a process flowsheet for this separation using a molecular sieve is given in Figure 2-4. In this process, the NF_3 mixture is released into a crystalline and porous synthetic zeolite environment. The adsorbent media produces NF_3 with a final impurity of less than 40 ppm of CF_4 (Suenaga et al., 1991).
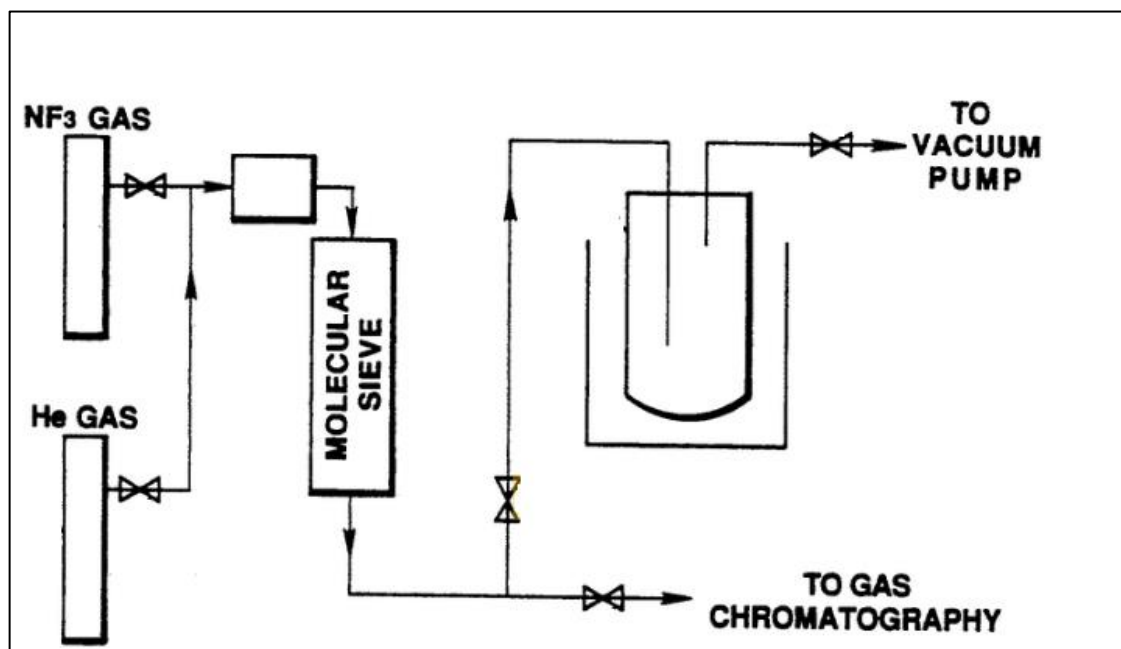
Figure 2-4. Process flowsheet for the NF_3 purification using commercialized 5A zeolites (Suenaga et al., 1991).

Molecular sieves have also been used to adsorb NF_3 selectively at temperatures down to $-196\,^{\circ}C$. The commercially available methods using molecular sieves are capable of cleaning the mixture down to 1 ppm of CF_4 (Igumnov and Kharitonov, 2006, Hart et al., 2006, Singh et al., 2008). The use of pressure swing methods demonstrated complete purification of NF_3 by use of a packed column with Linde Type A® zeolites containing variable pore sizes of 3.6 to $4.6\,^{\circ}A$ (Henderson and Underwood, 2016). A summary of the available adsorption methods is provided in table 2-3.

Table 2-3. A summary of the NF_3 purification methods using adsorption at 1 bar.

Reference	Adsorbent	T/ ºC	CF_4 final impurity (ppm)	Mixture
(Harada et al., 1993)	Metal fluorides	150-600	40	$NF_3 - N_2F_2$
(Suenaga et al., 1991)	4.9 ºA zeolite	>10	40	$NF_3 - CF_4$
(Igumnov and Kharitonov, 2006)	Dehydrated erionite	-50 to 30	10	$NF_3 - CF_4$
(Hart et al., 2006)	Molecular sieves	-179 to -50	10	$NF_3 - CF_4 - HF - F_2$
(Singh et al., 2008)	Polyacrylonitrile molecular sieve	0 to 100	1	$NF_3 - CF_4$

2.2.3 Membrane technology

Membrane technology is highly efficient in the separation of the mixtures with low impurity contents (Reijerkerk et al., 2010). The ZIF-8 mixed matrix membrane has shown promising results in the separation of N_2/NF_3 (Park et al., 2015). NF_3, the target gas, selectively permeates through the membrane due to the smaller size of the molecule in comparison with the contaminant (N_2).

For a mixture of $NF_3 - CF_4$, the Hyflon AD60 and amorphous glassy perfluoropolymer Teflon AF membranes showed good ability to reduce the impurity to 3 ppm. The driving force required for these processes is the particle size difference, which is similar to the filters. These membranes are designed for a small feed stream, which consequently purifies the target gas at very high concentrations (Branken et al., 2014). Figure 2-5 illustrates the separation of NF_3 from CF_4 through the membrane. The membrane is held inside the convection oven to obtain better temperature control. A dual-channel gas chromatography method was used to measure the concentrations of NF_3 and CF_4 using PDHID and TCD detectors in series (Branken et al., 2013). The process described in this study is still in the research phase.
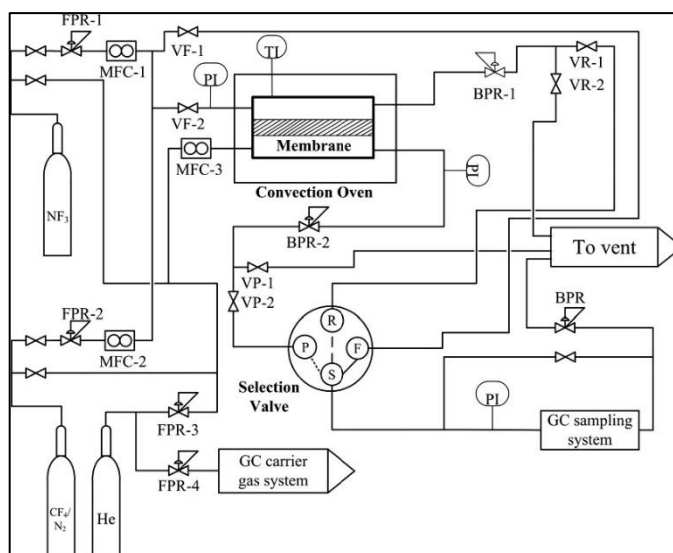
Figure 2-5. The experimental setup used for pure and mixed gas permeation measurements (Branken et al., 2014).

2.2.4 Extractive distillation

Extractive distillation is known as the distillation by the use of a solvent which alters the relative volatility of the component and consequently provides the possibility to separate components. This technique is generally used to separate the chemicals which form azeotrope or close boiling point mixtures. The separator agent or entraining agent changes the fugacity of the chemicals in the mixture which produces repelling force. The component which has the higher repulsive force leaves the liquid phase easily (Noll et al., 2013). A typical extractive process consists of two columns one for separation of the first component from the first mixture and the second column to recover the solvent from the bottom product (Fink, 2016). A simple extractive distillation process for the separation of the two components (A+B) consists of an extractive distillation column and a stripping column in which the gaseous products are obtained from the top of the columns and the solvent (S) is collected from the bottom of the second column (Lei et al., 2003).
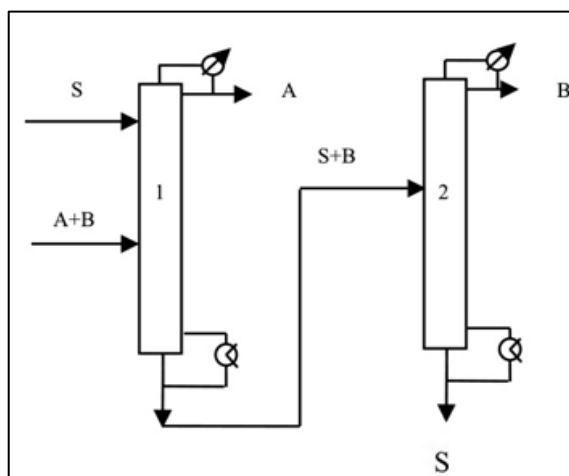
Figure 2-6. Schematic diagram of the two-column extractive distillation process for separation of the binary mixture (A+B) using an entraining solvent (S) (Lei et al., 2003).

The solvent selection for the extractive distillation column design is divided into two major stages of identification of functional groups as well as the comparison of individual candidates (Perry et al., 1997). The first extent includes the use of homologous series, Robbins chart, hydrogen bonding characteristics and polarity characteristics which basically includes the analysis of the molecular interaction. The second extent is based on the comparisons between the identified solvents considering the boiling point differences, infinite dilution selectivities and experimental measurements (Perry et al., 1997).

With extractive distillation, the NF_3 is purified from CF_4 by introducing HCl as the extractive agent which forms an azeotrope. However, a list of 16 different entraining agents from different chemical families of PFCs, CFCs, HDs and refrigerants have been tested, the best results presented are for the case of using HCl as the entraining agent. The use of an extractive agent requires ultra-low temperatures (almost cryogenic conditions) for obtaining a desirable separation (Miller, 1966). Hydrogen chloride is an acid which poses significant problems from the point of view of its disposal. Hence, new energy-efficient and environmentally friendly methods are still required. The proposed method is not commercially justifiable due to the high number of equilibrium stages (120 – 244 stages) as well as massive reflux ratios of up to 1000000 required (Miller et al., 2002).

Furthermore, the use of a long list of ionic liquids has been tested as the extractive agent (Shiflett and Yokozeki, 2014). In this method, depending on the extractive agent selected, either NF_3 or CF_4 can be selectively absorbed. This method is capable of decreasing the impurity level to just above 200 ppm at its best. Due to the oxidising property of nitrogen trifluoride and the probable interaction with ionic liquids (depending on the thermo-physical condition), there is a chance of initiation of explosion regimes. Besides, the ionic liquids listed are not produced on an industrial scale within a feasible price range.

2.2.5 Absorption

Absorption includes simultaneous mass and heat transfer between liquid and gas with the diffusional mass transfer being the most important role (Zarzycki and Chacuk, 2013). It is regularly followed by desorption performed in the stripping column which has equal importance as the absorption process. This process is performed with the major aim of removing one or more components from a gaseous mixture, such as CO_2 removal in ammonia production, and to obtain a specific gas in the liquid component with the aim to produce a new mixture or compound for the case of a chemical reaction (Zarzycki and Chacuk, 2013).

Absorption technology, where applicable, is by far the most widely used application for gas separation processes such as CO_2 capture. This is due to its high efficiency, low capital investment, low operating and maintenance costs, and advanced development of the technology (Edenhofer, 2015). The absorption process is improved at elevated pressure and reduced temperature, as opposed to the stripping process which requires a heating and cooling medium as well as a compressor to pressurise the gas (Mofarahi et al., 2008). Absorption columns are classified according to their internal configurations which are packed, wetted wall, tray and spray columns. A summary of their advantages and disadvantages is presented in table 2-4 (McCabe et al., 1993).

Table 2-4. A summary of the advantages and disadvantages of varying types of absorption columns (McCabe et al., 1993).

Column type	Advantages	Disadvantages
Packed	• High mass transfer obtained from better interphase contact • Low capital, operating and maintenance costs	• Channelling • Only for moderate flow rates
Wetted wall	• Neutralisation of corrosive gas • Multi-stage configurations	• Complex design • High maintenance cost
Tray	• Cost-effective at different flow rates • Adjustable in terms of P and T	• High-pressure drop • Slow reaction rate • Possibility of fouling and plugging
Spray	• Low pressure-drop • Suitable with high solubility	• High pumping cost • Weak mass transfer

Absorption technology has found applications in various industries such as pollution control and wastewater treatment (Ho, 1995), hydrogenation of oil (Bavetta and Deuel JR, 1942), coke plants (Eberly Jr et al., 1966) and in the petrochemical industry (Mehra, 1996). Several factors need to be considered and optimised for the absorption column design. While high operating pressure is recommended for the absorption process, it requires more power which is normally justified by cost-benefit analysis (Chakma, 1995). As the solvent flow rate increases, a reduced number of trays is needed in a tray column, but it poses higher solvent costs and a larger absorber diameter. The optimum flow rate is highly influenced by the balance between the number of trays and solvent cost. Low chemical absorption rate results in weak mass transfer, consequently requiring larger column sizes (Chakma, 1995).

Phase equilibrium data is an essential requirement for the design of an absorption and stripping column. To the best of the author's knowledge, there is no HPVLE data available for NF_3 to date,

and the only available data comprises volumetric dissolution of the NF_3 in a wide range of highly halogenated and perfluorinated solvents within the low-pressure range (Mukhortov et al., 2010). The authors presented in their article design of an absorption column at pressures up to 1.3 MPa.

Furthermore, the name of the solvent(s) selected for the absorption experiment cited was not disclosed. The initial 2000 ppm concentration of CF_4 in the feed was decreased to 8 ppm in the final product. The proposed design included eight equilibrium stages with a gas flow rate of 7775 mole.hr $^{-1}$ and the unknown absorbent flow rate of 1588 mole.hr $^{-1}$ (Blinov et al., 2011). While the use of absorption in cleaning NF_3 looks promising, the purification process falls within a narrow concentration range (from 99.967 to 99.999 %), and the authors suggested more investigations (Blinov et al., 2011).

2.2.6 Summary of the review on technologies

Cryogenic distillation, in addition to its complicated process which requires twice the capital investment of that of an absorption column in relative terms, operates at a very low-temperature condition (*i.e.* down to -192 ^{o} C). Membrane technology has drawbacks such as concentration polarization, clogging of membranes, short membrane life, selectivity, low flow of gas, and the high cost of construction. The maintenance cost is also considerable. The use of extractive distillation using ionic liquids (ILs) suffers from the possibility of ignition and explosion due to the oxidising property of NF_3 and its interaction with ILs, in addition to their high prices and limited availability on a commercial scale. Furthermore, the use of HCl is not recommended as it could pose disposal problems to the environment due to its acidic nature. Adsorption units were mostly designed to operate at low flow rates and in the batch configuration which required plant downtime for cleaning. Among the different types of separation methods proposed for this particular system ($NF_3 – CF_4$), the main objective was to obtain a product with the purity grade of 99.999 % using the most efficient method. Looking at the literature at the available separation techniques, physical separation (i.e. absorption and extractive distillation) comes out as the best separation process for the following reasons:

- Possibility of running the absorption column with the use of commercialised solvents.
- There is no need to shut down the plant for the recovery of absorbent, as required in adsorption and membrane technology.
- Other than membranes, absorbents do not deteriorate and only solvent recovery is required together with compensation for the solvent loss.
- Absorption technology has the potential to produces NF_3 at a high flow rate.

More specifically, the absorption technology operates at a temperature close to ambient conditions, which overcomes the problem of low temperatures required in conventional

distillation and adsorption methods. This decreases the very high energy requirements for NF_3 production with industrial grades. Apart from the benefits of absorption technology, the possibility of corrosion due to the presence of a corrosive solvent, low biodegradation of the solvents as well as the high energy requirements for the solvent regeneration are among the disadvantages of this process (Ben-Mansour et al., 2016).

2.3 Phase equilibrium data in the literature

The number of available phase equilibria data for systems including NF_3 is limited. However, there is a substantial amount of experimental data for CF_4 with different families of chemicals. The data published in the literature are generally (except for a few sets) in the temperature range of 273.15 to 313.15 K. From the literature data, tetrafluoromethane has the highest solubility in the two fluorinated solvents of hexaflurobenzene (C_6F_6) (Evans and Battino, 1971) and perfluorotributylamine ($C_{12}F_{27}N$) (Powell, 1972), with the solubility of 0.005 and 0.015, respectively. It should be noted that the gas exhibits the highest solubility in the latter solvent. Given that the data is reported at ambient pressure, it will certainly show significant improvement with increased pressure. The summary of the experimental data available in the literature is presented in Appendix A.

There are three highly fluorinated compounds among the literature data which are trifluoroethanol ($C_2H_3F_3O$), hexafluorobenzene (C_6F_6), and perfluorotributylamine ($N(C_4F_9)_3$) (Mainar et al., 1996, Evans and Battino, 1971, Powell, 1972). Figure 2-7 shows the structures of these chemicals which are extracted from (SigmaAldrich). The chemical properties of trifluoroethanol ($C_2H_3F_3O$), hexafluorobenzene (C_6F_6), and perfluorotributylamine ($N(C_4F_9)_3$) are listed in table 2-5.
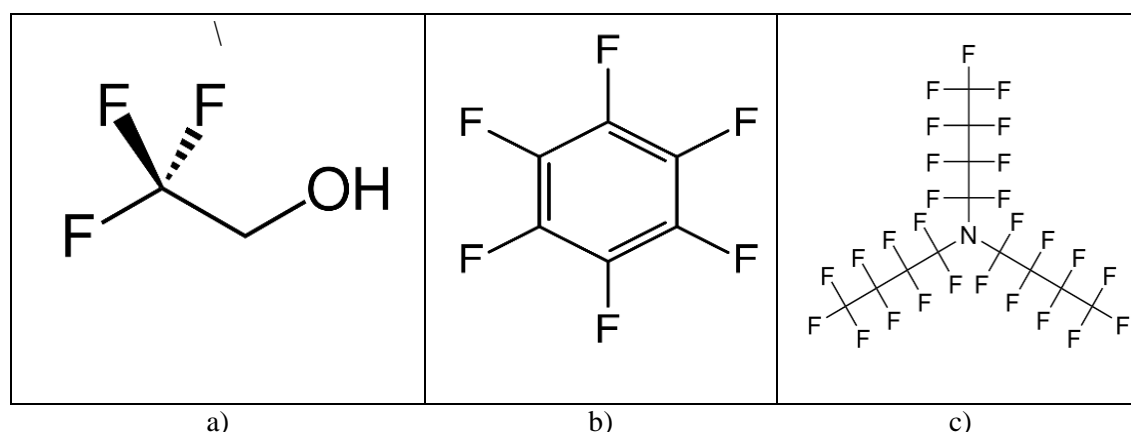
Figure 2-7. The structures of a) trifluoroethanol ($C_2H_3F_3O$), b) hexafluorobenzene (C_6F_6), c) perfluorotributylamine ($N(C_4F_9)_3$) (SigmaAldrich).

Table 2-5. List of physical properties for $C_2H_3F_3O$, C_6F_6 and $N(C_4F_9)_3$. Literature data for the properties are taken from NIST TDE (Frenkel et al., 2005).

Property	$C_2H_3F_3O$	C_6F_6	$N(C_4F_9)_3$
Boiling point (°C) [a]	78	80.2	208.4
Heat of vaporization (kJ/mol)	-	35.72	-
Standard heat of formation (kJ/mol) [b]	-	- 937.22	-
Heat capacity (J/mol.K) [b]	17.68	221.676	-
Critical Temperature (°C)	225.42	243.27	287.94
Critical Pressure (MPa)	48.08	3.28	1.10
Vapour pressure (kPa) [b]	9.44	11.28	0.065

[a] At 101.325 kPa

[b] At 25 °C, 101.325 kPa

The solubility of tetrafluoromethane in trifluoroethanol (0.0013) has an equivalent value to that of straight chain alkanes with C_{10+} (≈0.0017) (Hesse et al., 1996). Hexafluorobezene is a perfluorinated chemical with a symmetric shape and nonpolar structure (Pummer and Wall, 1958). This is also a toxic chemical. The like-like interaction between molecules is prominent, and the solubility of CF_4 is more substantial by far. Perfluorotributylamine consists of three chains of perfluorobutyl which are bonded to the same nitrogen molecule in the centre (Costello et al., 2000). Except for the nitrogen, the structure of perfluorobutane is from the family of perfluoroalkanes, which shows a high potential for the absorption of the CF_4. The available experimental data from the literature has indicated that the solubility of CF_4 is high in perfluorinated chemicals. A detailed analysis of the available experimental data is provided in Appendix A. From the literature studies, the fluorinated solvents are deemed to be the most suitable chemicals to dissolve either NF_3 or CF_4.

2.4 Solvent selection

There are several solvent selection procedures which exist. The Robbins chart (Robbins, 1980), predictive tools such as group contribution methods, the use of the COSMO-SAC prediction tool which allows the prediction of the solvent affinity (Mullins et al., 2006), the use of the primary screening method via phase equilibrium measurements, as well as the physical property method including hydrogen bonding, intermolecular forces, solvent selectivity and capacity via the infinite dilution activity coefficient are among the available techniques. The latter can be estimated by three methods of experimental measurements, correlation to the bubble point data and predicted using predictive models (Perry et al., 1997). Each method requires basic information and assumptions which are discussed in the sections which follow.

2.4.1 Robbins chart on solvent selection

The Robbins chart classifies chemicals into 12 general classes (Robbins, 1980). The main evaluation criteria are to consider the hydrogen bonding among the selected compounds. The Robbins chart studies the electron donor or acceptor property of the chemical, to give an

indication of the interactions of the chemicals in terms of their designated class. The method is capable of identifying the chemicals from the families with several active groups, such as highly active halogenated compounds, non-halogenated paraffin, etc. which is recommended for the liquid phase. For this study, CF_4 falls into class 11 as multi-halo paraffin without active H. However, according to the guidelines of the Robbins chart, there is no group indicated for NF_3, (Perry et al., 1997). Class 11 involves aromatic, olefin, halogen aromatic, multi-halo paraffin without active H and mono-halo paraffin. The reader is referred to (Perry et al., 1997) for more information.

2.4.2 Group contribution methods

The UNIFAC method uses the group contribution approach with functional group parameters, which are calculated from available experimental data. Due to the high number of experimental data used to fit the interaction parameters, in most of the cases, the results are of high quality (Fredenslund et al., 1975). Group surface area, group volume and the energy parameters are the inputs required for the UNIFAC model. There are no experimental high-pressure phase equilibrium data reported in the literature for the NF_3 system which could provide the possibility to fit the parameters. Hence, the prediction of the phase behaviour for systems of NF_3 is not possible. The same condition applies for the PSRK model, another predictive method with a predictive parameter dependent on experimental data.

2.4.3 COSMO-SAC predictions

The use of predictive methods, and in particular the quantum mechanics method, has been used to estimate the phase behaviour of solutions in the last two decades. Due to the lack of experimental data and availability of statistical analysis for the behaviour of molecules, these methods can produce thermodynamic equilibrium data only via modelling. However, these methods have high uncertainty, and in many cases, the accuracy of the results is controversial (Wang et al., 2009). The Conductor-like Screening Models - Segment Activity Coefficient Model (COSMO-SAC) is among the predictive methods which has shown an excellent ability to predict the activity coefficient without the need for experimental data (Borghi et al., 2015). In a set of COSMO-based methods, the first step is calculating the distribution coefficient to obtain the apparent charge density on the surface of the molecule, which is named the Sigma profile (Islam and Chen, 2015).

In ASPEN PLUS software V10, the Sigma profiles have been embedded for more than 1400 compounds (Mullins et al., 2006), including the CF_4 gas. Given that it was possible to measure the phase equilibrium data, the CF_4 system data was measured with hexane solvent at 283.15 K in this study and measured data regressed using the Peng-Robinson equation of state (PR EoS)

(Peng and Robinson, 1976). It was then compared to the predictions of the COSMO-SAC model. Figure 2-8 shows the *P-x-y* plot for the binary system of n-hexane + CF$_4$. The figure compares the experimental data (o) to the results of PR (VdW) model (—) and COSMO-SAC (---) model. It is clear that the COSMO-SAC prediction results provide large discrepancies. The experimental data shows that the composition of CF$_4$ at a pressure of 4.00 MPa is approximately 0.12, compared to a 0.3 as predicted by the COSMO-SAC model. The limitations of COSMO-SAC cannot be generalised for the rest of non-polar systems, but it is clear that for the system including CF$_4$ gas, the prediction is not reliable and it can be either correct or incorrect. It is evident from the results that for the systems studied, the use of COSMO-SAC for the solvent screening is not reliable.
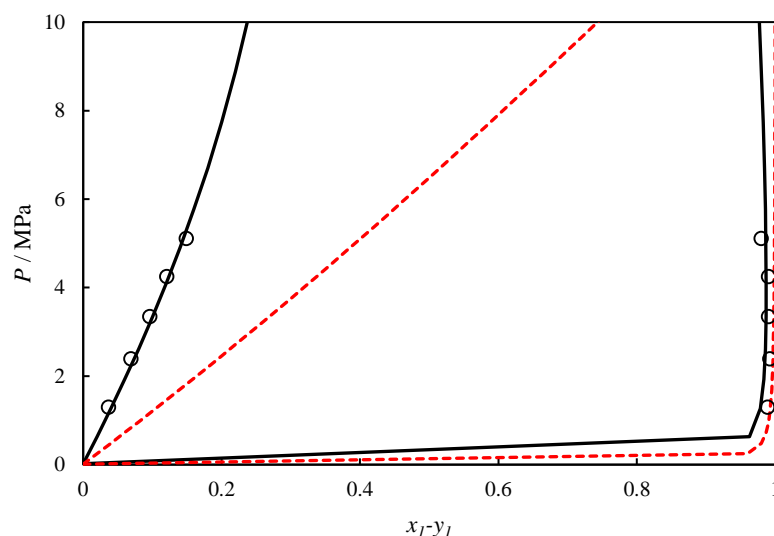
Figure 2-8. *P-x-y* data of the binary system of n-hexane + tetrafluoromethane at 283.15 K. o, experimental VLE data of CF$_4$+C$_6$H$_{14}$; --- COSMO-SAC prediction. — PR (VdW) model.

2.4.4 Physical properties

The physical properties of the solvents were also considered in the solvent screening procedure. From the results of the solubilities studied, 300 solvents from different chemical families were considered which were aromatic, aliphatic, alcohols, ethers, esters, ketones, glycol ether esters, aldehydes and halogenated hydrocarbon. In general, a few substances from different fluorinated families were also included because of their physical property of high absorption capacity. Thereafter, dielectric constant, hydrogen bonding, dipole moment, intermolecular forces, boiling points characteristics, relative volatility, the toxicity level of materials, reactivity, solvent prices, and availability were assessed. The large numerical values of dielectric constant denote highly polar solvents and improved dissolutions are expected for the components with the similar dielectric constants (Lide, 2005). Due to its zero dipole moment, CF$_4$ represents improved dissolution in non-polar components. Table 2-6 shows the list of perfluorinated chemicals screened for the measurements. The chemicals are ranked in the order of non-polar to polar listing them from the most to the least appropriate solvents for CF$_4$ absorption. The chemicals with the properties of lower toxicity as well as price are of interest.

Table 2-6. List of perfluorinated solvents screened for measurements.

Solvent	Properties [a]				Availability	Price/ml (ZAR) [b]
	D [c]	Polar	Toxicity [d]	Boiling point (K)		
Perfluorodibutylester	1.74	-	-	-	-	-
Perfluorooctane	1.79	-	x	376.15	x	164.4
Perfluoroheptane	1.82	-	-	353.15	x	106.8
Perfluorodecalin	1.86	-	-	415.15	x	62
Perfluorohexane	1.98	-	x	329.15	x	37.5
Heptafluoro,1-butanol	14.4	X	x	368.15	x	272
Tetrafluoroethyl-tetrafluoropropyl ether	26.8	X	-	366.15	x	400[e]

[a] Literature data for the properties from NIST TDE (Frenkel et al., 2005).
[b] The prices were taken from the Sigma Aldrich website in February 2019.
[c] Dielectric constant.
[d] Dangerous for the respiratory system (spexcertiprep, 2017).
[e] At the time that this project was started it was R15/L.

To determine the list of suitable solvents for further investigations, several approaches were considered. Due to lack of experimental data for NF_3 in the literature, the conventional screening methods such as Robbins's chart and predictive tools were not powerful enough to help with identifying an affinity of the potential solvents in the dissolution of NF_3 and CF_4. The inclusion of the list of solvents with an affinity to absorb CF_4 was selected from a long list of chemicals as reported in the literature (Borghi et al., 2015, Sousa et al., 2010, Evans and Battino, 1971, Field et al., 1974, Byrne et al., 1975, Sousa and Fonseca, 2014, Wilcock et al., 1977, Hesse et al., 1996, Cosgrove and Walkley, 1981, Gallardo et al., 1987, Powell, 1972, Mainar et al., 1996, Gibanel et al., 1988, Smits et al., 1997, Lobo et al., 1985, Liu et al., 2012). The screening process was continued based on the physical property of the chemicals. A final list containing 7 solvents was prepared for experimental investigations.

2.5 Experimental techniques

There are multiple experimental techniques that can be used to generate high-pressure VLE data which are selected depending on the chemical properties and target phenomenon to be measured. For these type of systems, the techniques in the literature are divided into two major categories of analytic and synthetic systems, depending on the type of composition determination. This classification is based on whether the phase composition is obtained utilising an analytical technique or mixtures are synthesised with a known mixture composition (synthetic method) (Dohrn et al., 2010). With the analytical methods, the analysis is performed either via the withdrawn samples from the phases or implication of the physicochemical techniques without the

requirement to withdraw a sample. The synthetic method only requires either a change in the phase (visual or non-visual) or a material balance. A summary of the available experimental techniques is presented in figure 2-9 (Fonseca et al., 2011).
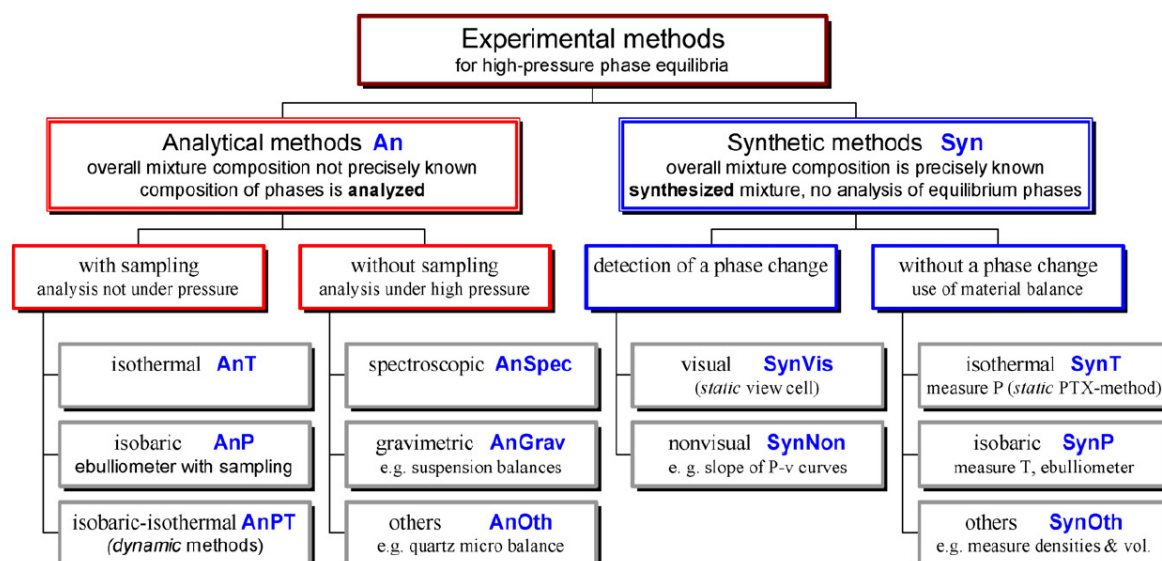
Figure 2-9. Classification of the experimental techniques used in HPVLE (Fonseca et al., 2011).

Sample withdrawal from a high-pressure cell, its handling and analysis is among the substantial source of errors added to maintain the system at the pressure after the sample (of vapour and/or liquid) is taken. The analytical methods without sampling are generally used to study the phase equilibria based on the reactive systems. The accurate analysis of the samples to obtain the phase composition is among other drawbacks of the analytic methods (Dohrn et al., 2010, Fonseca et al., 2011).

The synthetic methods are preferred in the case of failure of the analytic techniques. For example, this may occur for mixtures of similar densities of the coexisting phases such as near-critical conditions (Dohrn et al., 2012). On the contrary, with testing the static analytic apparatus used in this work, we were able to measure data at the critical point (Nelson et al., 2017). The main source of error in synthetic methods arises from imprecise preparation of the mixture, inability to determine the correct thermophysical property for the phase change and limitations in obtaining further properties to evaluate the raw data. In contrast to the analytic method, the use of synthetic techniques to measure the solubility of extremely low volatile compounds in supercritical fluids does not produce reliable results. Due to the abovementioned reasons, over 63 % of the data published in the literature were obtained by the synthetic methods (Dohrn et al., 2010, Dohrn et al., 2012). Readers are referred to the review articles on the HPVLE techniques and experimental

results for more information (Knapp et al., 1981, Fornari et al., 1990, Dohrn and Brunner, 1995, Christov and Dohrn, 2002, Dohrn et al., 2010, Fonseca et al., 2011, Dohrn et al., 2012).

The use of ROLSI™ sampler connected to the GC has shown considerable improvement in the appropriate sampling from the cell, as well as handling and analysis of the samples withdrawn from the high-pressure mixtures (Duran-Valencia et al., 2001, Valtz et al., 2004). Furthermore, the volume of the samples withdrawn from the cell is adjustable to volumes as small as $100 - 500$ μl from a cell with an approximate volume of 50 ml. The small sample volumes do not interfere with the equilibrium conditions of the test chamber. According to the data published using such apparatus, the exact critical point is measurable (Nelson et al., 2017). The new advancements in the sampling devices provided a significant decrease in the uncertainties associated with the high-pressure VLE measurements.

From the literature review around the equipment and experimental procedure, it was found that the isothermal analytic apparatus equipped with the ROLSI™ sampler is the best technique to measure HPVLE data for this type of system. From the research that has been done using this apparatus, good results with high reliability of the experimental data have been obtained (Ramjugernath et al., 2018, Nelson et al., 2017, Uusi-Kyyny et al., 2016). The thermodynamic consistency tests (point and direct tests) that have been done which gave very good confidence in the use of the thermodynamic data (Narasigadu et al., 2013). That is why this technique was selected to measure the HPVLE data in this work. In addition, a previously tested synthetic apparatus (Nelson and Ramjugernath, 2017) with the ability to track the phase change (both visual and non-visual) was utilised to confirm the data measured for all of the systems studied, giving a very high degree of confidence in the quality of the data measured. The experimental apparatuses and techniques used in this work will be explained in detail in chapter 4.

2.6 VLE data and design process

The diagram shown in figure 2-10 illustrates how phase data fits into the design process. After experimental phase equilibrium data is measured, the data is fitted to a model and the physical property is estimated. The model parameters are then used for the simulation of the chemical process which is normally performed via commercial simulation packages such as Aspen Plus®. Thereafter, the pilot plant studies are done. The preliminary design is performed based on the data gathered from the previous stage. Eventually, the process is designed. This illustrates the importance of phase data.
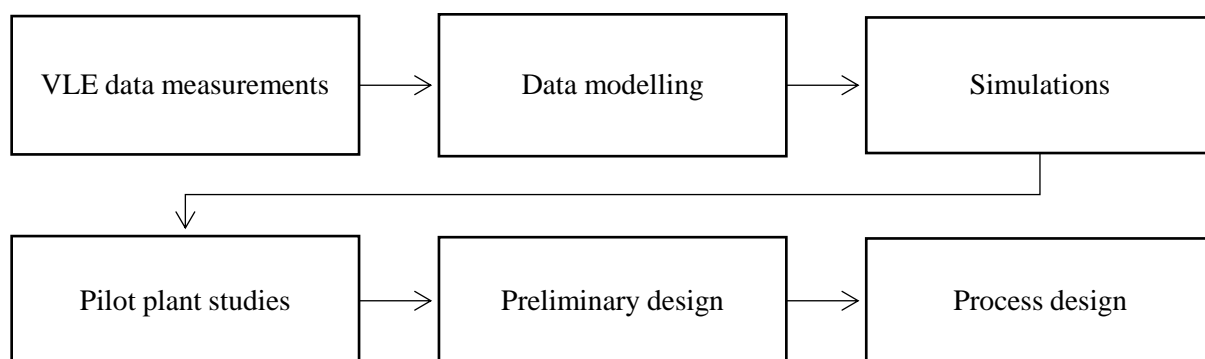
Figure 2-10. How phase data fits into the design of a chemical process.

2.7 Modelling

There are two general methods to interpret the high-pressure phase data, namely combined and direct methods (Mühlbauer and Raal, 1995). The combined method employs the activity coefficient for the liquid phase and the fugacity coefficient (using EoS) for the vapour phase. This method has given excellent data interpretation in low to medium pressure ranges since it has limitations once the pressure of the system tends to the critical pressure of the chemical. On the other hand, direct methods utilise only the fugacity coefficient to describe the phase behaviour of the mixture (Mühlbauer and Raal, 1995, Smith et al., 2005). Due to the empirical nature of the EoS model coefficients, the application of the direct method is not accurate enough for modelling of the highly polar systems and liquid phase (Mühlbauer and Raal, 1995).

Due to the high-pressure range of the experiments, the direct method ($\emptyset - \emptyset$) was utilised to treat the data. This method has been used in the literature and is able to describe these types of systems very well. An extensive description of the modelling approaches used in this work along with their theoretical background will be explained in chapter 3.

2.8 Simulation of the physical separation processes

Process simulation provides the ability to model a plant in great detail without incurring exorbitant costs in the construction of a plant. This is usually implemented on the basis of the experimental data and phase properties during the study phase to obtain ideal operating conditions along with the pros and cons. The design can be in either steady-state or dynamic form depending on the stage of the project phase. Thereby, engineers can run a virtual process to ensure the safety and operation conditions of the factory.

A typical absorption plant consists of an absorber followed by a stripping column to recover the solvent and separate the gas dissolved in it. The solvent then is combined with the make-up flow to compensate for the lost solvent and used again as the absorbent. An example of a physical

absorption process designed for post-combustion carbon capture (PCCC) process is shown in figure 2-11 (Ahmad et al., 2017).
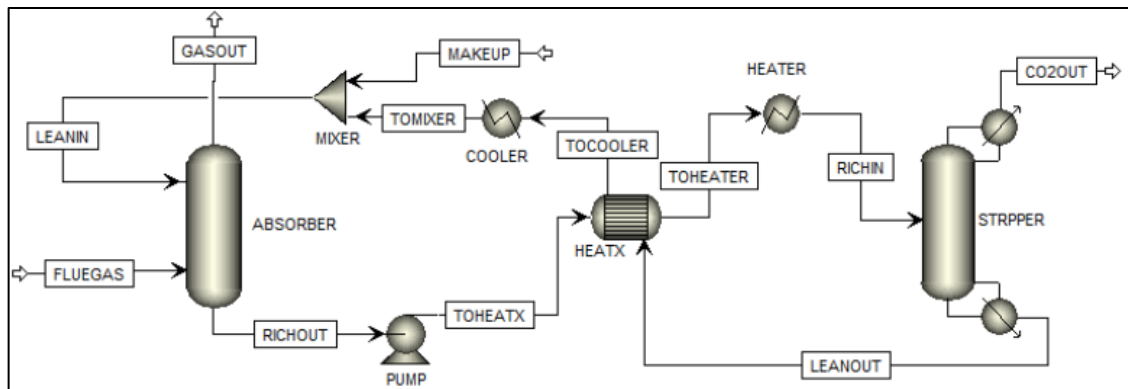
Figure 2-11. A typical process flow diagram for absorption and desorption of PCCC (Ahmad et al., 2017).

A typical extractive distillation plant consists of an extractive distillation column followed by a stripping column. Similar to the absorption process, the solvent then is combined with the make-up flow to compensate for the lost solvent and used again as the separator agent. An example of the extractive distillation process designed for separation of acetone (distillate) and methanol (bottom) using the water as the separation agent is presented in figure 2-12 (Langston et al., 2005).
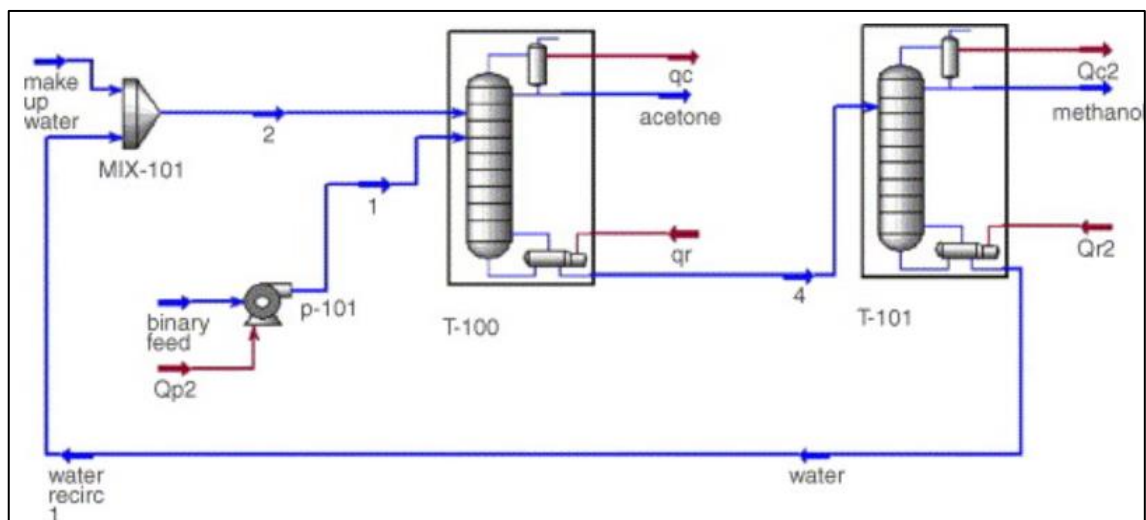
Figure 2-12. A typical process flow diagram for extractive distillation designed for the separation of acetone from methanol using the water as an entraining agent (Langston et al., 2005).

The step by step methodology of Aspen Plus® design for the simulation of this work is explained below:

a. The Aspen Plus® simulation models are developed including the essential units of the physical separation plants which are absorber, stripper and other main parts for absorption

plant. These are an extractive distillation column, a stripping column and other auxiliary units including heat exchanger and pump for the extractive distillation plant.

b. The physical absorption option is selected from the navigation panel for the absorption column design and the best solvent from the experimental measurements was tested.

c. After the model is analysed and validated, several parameters including gas flow rate, operating temperature and pressure, gas and solvent location stage, etc. were investigated through sensitivity studies with an aim to obtain the highest possible purity.

In summary, the literature review was presented on the different available technologies for purifying NF_3, together with their advantages and disadvantages. The solvent screening procedure and available experimental data in the literature were then explained. Thereafter, a background on the experimental apparatuses and techniques was discussed. A brief discussion on the modelling background and simulation methodology was presented in the final part of this chapter.

Chapter 3: Modelling

This chapter illustrates the approaches followed in this work to model the measured HPVLE data. Experimental phase equilibria data is the foundation stone of separation process design in the chemical industry. Precise experimental data is required to achieve process safety and a better understanding of the process optimisation. The thermodynamics of the phase equilibrium data is highly influenced by pressure, temperature and volume by interfering with the density of the mixture, phase change, solubility promotion, and reaction in the gas phase (Peper et al., 2019).

The binary phase equilibrium behaviour can be estimated depending on the measured data, including liquid-liquid and vapour-liquid equilibrium data to gain information on multi-component behaviour (Mühlbauer and Raal, 1995). The experimental data for the binary systems should be treated theoretically for calculation of excess Gibbs energy, considering the uncertainties of the measurements in the laboratory condition. Chemical thermodynamics is the basic requirement to make it possible.

This chapter studies the basics of chemical thermodynamic phase equilibrium data reduction or parameter fitting, as well as the basics of the modelling and calculations of the activity coefficient. The combined method ($\gamma - \emptyset$) and direct method ($\emptyset - \emptyset$) are studied as the recognised methods to treat experimental data. Thereafter, the equations of state (EoS) and the activity coefficient models are included. More information on the fundamentals of the thermodynamic modelling approaches are presented in the related textbooks (Walas, 2013, Raal and Mühlbauer, 1998).

3.1 Theoretical background for modelling

The Van der Waals EoS (Van der Waals, 1873), was the first equation which could represent the coexistence of vapour and liquid phases. Redlich-Kwong EoS (Redlich and Kwong, 1949) was the inflexion point of the modification on the Van der Waals EoS which retained its hard-sphere term and included a new term that was temperature-dependent. Soave replaced the original temperature-dependent term with a new term which is known as Soave-Redlich-Kwong (SRK EoS) (Soave, 1972). The new EoS showed remarkable improvements in the data fit results.

Peng-Robinson EoS (Peng and Robinson, 1976) provided a better prediction of the liquid volume's critical compressibility factor. SRK and PR found widespread applications in the industry due to their capability in relating temperature, pressure and mixture composition with the requirement for only the acentric factor and critical properties of the component (Mühlbauer and Raal, 1995).

The EoS models and their mixing rules have been modified to improve their representation of data for the liquid phase and polar mixtures. The traditional VdW mixing rule is incapable of modelling excess Gibbs energy in a wide range of pressures. The Huron and Vidal local composition mixing rule was the first modification which related the EoS to an activity coefficient model via excess Gibbs energy. This mixing rule has a linear relationship, which does not satisfy requirements for the quadratic EoS in the low-density range (Mühlbauer and Raal, 1995). The Wong-Sander mixing rule replaces the excess Helmholtz energy with excess Gibbs energy which eliminates the requirement of applying the mixing rule to accommodate pressure. Hence, it satisfies the quadratic requirement for the second virial coefficient.

The activity coefficient models are developed based on the excess Gibbs energy. Among the several activity coefficient models which have been developed based on the local composition concept, the Wilson, NRTL (Renon and Prausnitz, 1968) and UNIQUAC (Abrams and Prausnitz, 1975) models provide expressions to estimate activity coefficient applied to the group contribution model of UNIFAC (Fredenslund et al., 1975). Due to the temperature-dependence of the model parameters for the local composition activity coefficient models, the NRTL model is more reliable for prediction purposes. The Wilson model was the first excess Gibbs energy model to use the local composition idea which is applicable to slightly polar mixtures. It has shortcomings when applied to highly polar mixtures and for the prediction of the immiscibility of two liquids (Smith et al., 2005).

CF_4 is a small nonpolar molecule with the tetrahedral structure which exhibits behaviours that can be justified by both Lenard-Jones potential (similar to CH_4) and spherical shell models (similar to CCl_4) in statistical thermodynamics (Rubio et al., 1985). While the phase equilibria data of the $CH_4 - CF_4$ mixture behaves strongly non-ideal due to difference in their intermolecular potential, its compressibility factor is justifiable by the corresponding states law (Holleran and Gerardi, 1969).

Among the binary mixtures studied, the phase data of the binary mixture of $CF_4 + CHF_3$, C_2H_6 and $CClF_3$ were measured in the pressure ranges up to 0.2 MPa and modelled using excess Gibbs energy where the satisfactory results were obtained by up to 4 % error (Croll and Scott, 1964). However the use of PR (VdW) model gave satisfactory results for the latter system (CF_4 - $CClF_3$) without regressing any parameter and errors of below 1 % (Kubic Jr and Stein, 1981). Among the models developed for prediction of phase behaviour as well as data regression, a new functional group, namely CF_4, was introduced for the PSRK model in 2005 (Horstmann et al., 2005). A summary of the literature modelling approaches used for the binary system of CF_4 with different

chemicals is listed in table 3-1. The study indicates that the data fit results of PR (VdW) model represents the least deviations among others used.

Table 3-1. Summary of the modelling approaches used for systems including CF_4.

System	Model combination	T/ K	P/ MPa	Deviations	Reference
CH_4	- Strobridge EoS with either least square or maximum likelihood (Strobridge, 1962) - Perturbation theory	95 – 413	110	0.86 – 6 %	(Rubio et al., 1985)
$CClF_3$ CHF_3 C_2H_6	- Excess Gibbs energy with the least square objective function	108 - 150	0.2	0.5 – 4 %	(Croll and Scott, 1964)
$CClF_3$	- PR (VdW) model	200 - 288	0 - 7	< 1 %	(Kubic Jr and Stein, 1981)
CHF_3	- Martin-Huo equation (Martin and Hou, 1955)	243 - 363	10	1.1 %	(Lange and Stein, 1970)
C_8H_{16}	- Scaled particle theory (Reiss et al., 1959)	289 - 313	0.1	3 %	(Wilcock et al., 1977)
$C_8H_{24}O_4Si_4$	- Scaled particle theory (Reiss et al., 1959)	292 - 313	0.1	3 %	(Wilcock et al., 1978)
HCl	- Perturbation theory	159, 173	0.1	5 – 90 %	(Lobo et al., 1985)
C_3H_8	- PR (VdW) model	142 - 293	0.02 -0.6	< 1 %	(Liu et al., 2012)
C_2H_6	- PR (Huron−Vidal) model	179 - 210	0.01 -0.4	< 1 %	(Zhu et al., 2006)

The HPVLE data treatment of this work was performed using the direct method ($\emptyset - \emptyset$), as it has a better representation of experimental data at elevated pressures. The PR EoS is selected to regress the data. The WS mixing rule was used due to its better ability in the use of local composition models and its independence from pressure. The NRTL model is used to satisfy the Gibbs free energy requirement of the mixing rule.

3.2 Fugacity and Fugacity Coefficients

According to (Smith et al., 2005), an equilibrium condition is obtained when there is no change in the macroscopic properties of a system over time. At equilibrium, the main rule is the stability of chemical potential throughout the system. The calculation of the chemical potential is not possible quantitatively, since the results from integration and an integration constant is unknown. Rather, the difference in the chemical potentials of the two conditions can be evaluated using the fugacity concept. Equation 3-1 shows the relationship between chemical potential and the fugacity coefficient.

$$\overline{G}_1 = \Gamma_i(T) + RTlnf_i \qquad \text{3-1}$$

$\Gamma_i(T)$ denotes the integration constant at the respective temperature. The partial molar property of the Gibbs excess energy is defined as follows:

$$\overline{G}_\iota = \left[\frac{\partial(nG)}{\partial n_i}\right]_{T,P,n_j} \qquad \text{3-2}$$

Hence for the chemical potential in terms of fugacity:

$$\overline{\mu}_\iota = \Gamma_i(T) + RTlnf_i \qquad \text{3-3}$$

Equations 3-1 and 3-3 are simply the same. At equilibrium, the chemical potential in all phases at a constant temperature should be equal, all terms of equation 3-3 are cancelled and the equilibrium is only dependent on equality of the fugacity of all phases (the reader is referred to the textbook for a full derivation (Smith et al., 2005)):

$$\hat{f}_i^\alpha = \hat{f}_i^\beta = \cdots = \hat{f}_i^\pi \qquad \text{3-4}$$

Where β, α and π represent the phase. Hence, for the vapour-liquid equilibrium, equation 3-4 reduces to:

$$\hat{f}_i^l = \hat{f}_i^v \qquad \text{3-5}$$

Where l is a liquid phase, and v is the vapour phase ($i \in$ natural numbers, indicating the component in solution). The fugacity of the liquid and vapour phases in the non-ideal solution is corrected by a factor named activity coefficient. Equations (3-6) and (3-7) are used for a binary VLE:

$$\hat{f}_i^v = y_i\hat{\emptyset}_i P \qquad \text{3-6}$$
$$\hat{f}_i^l = x_i\gamma_i f_i^0 \qquad \text{3-7}$$

Where $\emptyset$ and γ are fugacity and activity coefficients, respectively. While the fugacity is equal to the product of partial pressure and the fugacity coefficient, activity is calculated from the product

of mole fraction and the activity coefficient. The activity is often used to represent the chemical potential in liquid. The ratio of the fugacity coefficient can be obtained using equation 3-8.

$$\Phi_i = \frac{\widehat{\emptyset}_i}{\emptyset_i^{sat}} exp\left[\frac{-V_i^{sat}\left(P - P_i^{sat}\right)}{RT}\right] \qquad \text{3-8}$$

In the ideal solution, the vapour phase and liquid phase represent an ideal gas and liquid, respectively. Any system which has no deviation from Raoult's law is considered the simplest VLE system known as the ideal system (Smith et al., 2005). In equation 3-8, the term in bracket is known as the Poynting factor, which is almost equal to unity (Smith et al., 2005). There is a negligible difference in Poynting factor at low and medium pressures, hence it is neglected. For non-polar components, elimination of this factor does not make a significant difference at low pressures, but for mixtures containing polar compounds, it will show a significant deviation (Prausnitz, 1980).

3.2.1 Fugacity coefficient with an EoS

The cubic equation of state (EoS) is utilised to determine the fugacity coefficients. The simplest EoS is Van der Waals, which is capable to exhibit the deviation from the ideal gas low (Van der Waals, 1873). The proposed EoS considers intermolecular interaction forces amongst available compounds in the mixtures. Van der Waals created a simple, comprehensive semi-experimental, semi-empirical EoS that satisfied the fluid behaviour above and below the critical point. With all the novelty that he proposed, the parameters were independent, which led to a limited version of this model. Several scientists tried to resolve the problems of the Van der Waals EoS and as the first highly successful method, (Redlich and Kwong, 1949) and (Soave, 1972) proposed a revision of this model. The later model of (Peng and Robinson, 1976) known as PR EoS, is one of the most successful models. Due to applicability and extensive use of the (Peng and Robinson, 1976) EoS, it will be explained in more detail.

3.3 The Peng-Robinson (PR) EoS

The PR EoS was proposed to overcome the inability of the other models to predict fluid density as well as modelling of experimental data close to the critical region (Peng and Robinson, 1976). Equation 3-9 shows the PR EoS:

$$P = \frac{RT}{V - b} - \frac{a(T)}{V(V + b) + b(V - b)} \qquad \text{3-9}$$

Where *a* and *b*, are the attractive and co-volume parameters, respectively, which can be calculated as follows:

$$a_i(T_c)_i = 0.45724 \frac{R^2 (T_c)_i^2}{(P_c)_i} \qquad 3\text{-}10$$

$$b_i(T_c)_i = 0.07780 \frac{R(T_c)_i}{(P_c)_i} \qquad 3\text{-}11$$

$$k_i = 0.37464 + 1.54226\omega_i - 0.26992\omega_i^2 \qquad 3\text{-}12$$

The corresponding equation for the equation (3-9) is for the composite compression factor:

$$Z^3 - (1 - B_m)Z^2 + (A_m - 3B_m^2 - 2B_m)Z - (A_m B_m - B_m^2 - B_m^3) = 0 \qquad 3\text{-}13$$

The expression of the fugacity $(\widehat{\emptyset}_i)$ in a mixture is:

$$\widehat{\emptyset}_i = exp \left\{ \begin{array}{c} (Z-1)\dfrac{b_i}{b_m} - Ln(Z - B_m) - \\ \dfrac{A_i}{2\sqrt{2}B_m}\left(\dfrac{2\sum_j Z_k a_{ki}}{a_m} - \dfrac{b_i}{b_m}\right) Ln\left[\dfrac{Z + \left(1 + \sqrt{2}\right)b_m}{Z + \left(1 - \sqrt{2}\right)b_m}\right] \end{array} \right\} \qquad 3\text{-}14$$

Due to fewer calculations time required for the hydrocarbon systems and the need for only critical properties of the components, SRK and PR EoS gained popularity in the industry. However, the SRK and PR EoS exhibit poor ability in the estimation of liquid densities, polar fluid parameters, phase behaviour of the long-chain hydrocarbons (C_{10+}), critical region behaviour, and phase behaviour of the systems with the pressures below 1.3 kPa. The reader is referred to textbooks for comprehensive information on the cubic EoSs (Abbott, 1979, Martin, 1979).

A precise cubic EoS for the phase equilibrium calculations should estimate the vapour pressure of the pure components accurately (Twu et al., 1991). The α function, also known as temperature attraction term, plays an essential role in the estimation of the vapour pressure, while the mixing rule significantly affects the mixture properties.

3.3.1 Mixing rules of EoS

Mixing rules are utilised in the EoS to correctly display the phase behaviour of mixtures to fit the phase data, which is indicative of the molecular interactions in the mixtures. The mixing rules utilised by Soave and PR EoS are known as classical mixing rules (VdW mixing rule). The literature presents multiple mixing rules with various categories that have been developed and

improved over the decades. (Mühlbauer and Raal, 1995) provided a detailed examination of such mixing rules.

According to (Hernández-Garduza et al., 2001), different mixing rules do not necessarily show similar deviations from the experimental data, especially when it comes to the diluted region. The attraction (*a*) and co-volume (b) parameters of PR EoS using the Van der Waals mixing rule are calculated as follows:

$$b = \sum_i x_i b_i$$

$$a = \sum_i \sum_j x_i x_j (a_i a_j)^{0.5} (1 - k_{ij})$$

One of the mixing rules that is accurate for simple mixtures containing hydrocarbons and inorganic gases, and mixtures containing polar, aromatic and associating species over a wide range of pressures is the WS mixing rule, which is popular industrially (Wong and Sandler, 1992). The mixing parameters are calculated as follows:

$$\frac{a_m}{RT} = \frac{QD}{(1-D)} \tag{3-15}$$

$$b_m = \frac{Q}{(1-D)} \tag{3-16}$$

$$Q = \sum_i \sum_j x_i x_j \left(b - \frac{a}{RT}\right)_{ij} \tag{3-17}$$

$$D = \sum_i x_i \frac{a_i}{b_i RT} + \frac{A_\infty^E}{cRT} \tag{3-18}$$

Where A_∞^E is the Helmholtz energy, which is calculated at infinite pressure. Also, the governing equation for the mixing rule is used considering partial molar derivatives with the mole numbers to assess the fugacity coefficients obtained from EoS. The reader is referred to the original paper for more information (Orbey et al., 1993). The Helmholtz free energy was used in WS mixing rule instead of Gibbs energy due to the smaller dependence on pressure. Consequently, the correct behaviour was achieved at both infinite dilution and low pressures (Wong and Sandler, 1992). To explain the Helmholtz energy at the infinite dilution activity coefficient ($ln\gamma_i^\infty$) and low pressure, the NRTL activity coefficient model was used.

3.4 NRTL (Non-Random Two Liquid) activity coefficient model

The NRTL activity coefficient model (Renon and Prausnitz, 1968) was developed using the local composition model (Scott, 1956) and the non-random assumption similar to the one used by

(Wilson, 1964). The NRTL model is significantly advantageous over Wilson's general equation, in which both miscible and immiscible mixture can be regressed. Additionally, the NRTL model can be utilised to the highly unpredictable systems to provide a satisfactory representation of the phase behaviour (Raal and Mühlbauer, 1998). The NRTL equation for a binary system is as follows:

$$\frac{G^E}{RT} = x_1 x_2 \left[\frac{\tau_{21} G_{21}}{x_1 + G_{21} x_2} + \frac{\tau_{12} G_{12}}{x_2 + G_{12} x_1} \right] \qquad \text{3-19}$$

$$G_{12} = exp(-\alpha_{12}\tau_{12}) \qquad \text{3-20}$$

$$G_{21} = exp(-\alpha_{21}\tau_{21}) \qquad \text{3-21}$$

$$\tau_{12} = \frac{g_{12} - g_{22}}{RT} \qquad \text{3-22}$$

$$\tau_{21} = \frac{g_{21} - g_{11}}{RT} \qquad \text{3-23}$$

The binary interaction parameter for the NRTL model in Aspen Plus® is defined as follows:

$$\tau_{ij} = A_{ij} + \frac{B_{ij}}{T} + C_{ij} \ln(T) + D_{ij}(T) \qquad \text{3-24}$$

Where A, B, C and D denote the asymmetric temperature (T)-dependant parameters. In this case, only B was used for this work. The activity coefficient is given by:

$$ln\gamma_1^L = x_2^2 \left[\tau_{21} \left(\frac{G_{21}}{x_1 + x_2 G_{21}} \right)^2 + \frac{G_{12}\tau_{12}}{x_2 + x_1 G_{12}} \right] \qquad \text{3-25}$$

$$ln\gamma_2^L = x_1^2 \left[\tau_{12} \left(\frac{G_{12}}{x_2 + x_1 G_{12}} \right)^2 + \frac{G_{21}\tau_{21}}{x_1 + x_2 G_{21}} \right] \qquad \text{3-26}$$

The NRTL equation contains the following adjustable parameters: τ_{21}, τ_{12}, α_{12} and α_{21}. The parameters τ_{21} and τ_{12} are the interaction between the two constituents. The parameter α represents the random characteristics of a mixture whose zero value indicates that the mixture is entirely random. Over the previous 50 years, numerous researchers have indicated that the instructions given by (Renon and Prausnitz, 1968) are too limited and other α values provide better representation for phase equilibrium. If an estimate is made for α, it should be 0.3 for non-polar mixtures and 0.47 for the polar organic-aqueous mixture (Walas, 2013). In this work, the PR EoS was used with either VdW or WS mixing rules. The NRTL activity coefficient model was used to satisfy the WS mixing rule requirement. The k_{ij}, τ_{21}, and τ_{12} were regressed to the experimental data. The non-randomness parameter of α_{ij} is set to 0.3 for non-polar mixtures and

0.47 for polar mixtures. The ordinary least squares objective function was used, which implemented the Britt-Luecke algorithm (Britt and Luecke, 1973) to minimise the pressure and composition of the vapour phase. For the case that the data were generated for the liquid phase (bubble point data), only the pressure of the liquid phase was minimised. The average absolute deviation (AAD) and average absolute relative deviation (AARD) were estimated to assess the quality of the data-fit statistically.

$$AAD(\bar{\theta}) = \frac{1}{N_p} \sum_{1}^{N_p} \left| \bar{\theta}_{exp} - \bar{\theta}_{calc} \right| \qquad \text{3-27}$$

$$AARD(\bar{\theta}) = \frac{1}{N_p} \sum_{1}^{N_p} \frac{\left| \bar{\theta}_{exp} - \bar{\theta}_{calc} \right|}{\bar{\theta}_{exp}} \qquad \text{3-28}$$

where $\bar{\theta}_{exp}$ and $\bar{\theta}_{calc}$ are the experimental and calculated quantities. N_p is the total number of data points. The statistical assessments of each binary system will be presented in the results chapter.

Chapter 4: Experimental methods

This chapter presents the two high-pressure apparatuses used for experimental measurements in this research study. These apparatuses were based on the "static-analytic (SA)" and "static-synthetic (SS)" methods. The static analytic method involved measurement of *P-x-y* data for the CF_4 + (perfluorohexane/perfluoroheptane/perfluorooctane/tetrafluoroethyl tetrafluoropropyl ether (TFE-TFP ether)) systems at isothermal conditions, with analyses of the withdrawn samples of both the liquid and vapour phases. The static synthetic method was selected mainly for systems of NF_3 + solvents due to the safety hazards of NF_3. These will be discussed further in this chapter.

The pre-test safety consideration to start VLE data generation for NF_3 system took just more than 6 months. Prior to NF_3 measurements, major modifications were implemented to the experimental technique and apparatus to avoid health risks associated with the release of NF_3 to the environment.

4.1 The Static Analytic (SA) apparatus

The equilibrium cell consists of a hollow tube made of cylindrical sapphire tubes (manufactured by Rayotek Scientific), sealed using two O-rings between the two flanges made of SS 316L (thickness 15 mm) (Nelson et al., 2017). The picture of the experimental apparatus is shown in figure 4-1. The excellent corrosion and thermal resistance of sapphire, while fully transparent, makes it perfectly suitable for the equilibrium cell. The sapphire tube is 70 mm high, with the outside diameter of 55 mm, and the inner diameter of 32 mm. The total volume of the cell is approximately 50 cm^3.

Figure 4-1. Photograph of the equilibrium cell (Williams-Wynn, 2018).

The design of 12 mm thickness SS 316L flanges, sapphire tube, Parker valves, pressure transmitter, and high-pressure Valco fittings allow the cell to withstand pressures up to 25.0 MPa. Sealing between the SS flanges and the sapphire cell was accomplished using Viton® (including FKM®), Vespel®, polyurethane or Teflon® O-rings depending on the material compatibility with the solvents studied. The chemical compatibility with the solvents used in this work is presented in Appendix B.

Two holes in the top flange and a hole in the bottom flange were drilled and connected to Valco fittings with the sizes of 1/8". The inlet holes of the bottom and top flanges were connected to two needle valves (Parker: 10V series; 1/8"; 103.4 MPa) each. The top valve stem was extended by 40 cm to provide the ability to discharge or fill the cell while it was inside the thermo-regulated bath.

An impeller was situated in the cell to agitate the cell contents via a magnetic field introduced by the outside magnetic configuration. The outside configuration consisted of an overhead stirrer (Maxon: model A-max) to drive a Neodymium magnet (OD 28 mm; grade N40H; nickel-plated). The internal magnet (grade N40H; gold-plated) was placed in a ball bearing configuration via a closed cover to prevent friction. The magnet was covered with a stainless-steel cap attached to four blades to initiate turbulence while spinning. Figure 4-2 displays the photo of the stirring mechanism.
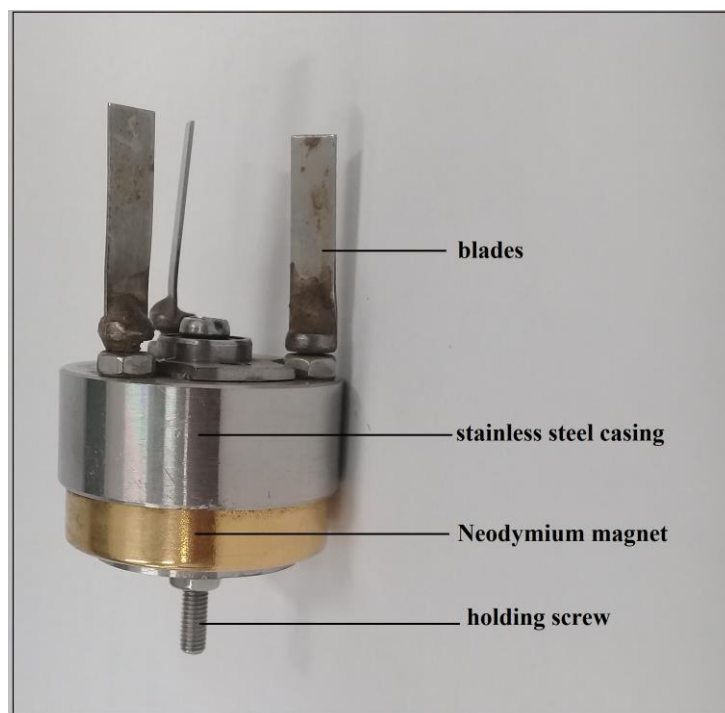
Figure 4-2. Photograph of the stirring mechanism.

A ROLSI™ online sampler was fitted onto the top flange of the equilibrium cell. The autosampler was utilised to withdraw between 50 to 500 μl of the vapour and liquid samples. The tip of the 3 mm diameter capillary was movable to allow sampling of both phases. The withdrawn samples were then moved to the GC via a 1/16" SS 316L line.

The equilibrium cell was placed in a SS 316L frame in a thermo-stated liquid bath with an approximate volume of 30 dm^3. The bath inner dimensions were $30 \times 33 \times 41$ cm. The bath was equipped with two viewing windows of 100 mm OD and thickness of 8 mm. The space between the internal and external walls of the bath was filled with compressed polyester foam and glass wool to provide insulation. The temperature of the bath was regulated using a programmable Grant immersion circulator (TX 150). A circular disc of compressed foam of diameter 10 mm was utilised to insulate the surface of the bath liquid. A cold finger chiller (Thermo Scientific EK20 Immersion Cooler) was employed to reach temperatures below ambient condition.

A Valco fitting outlet was connected to a pressure transducer via a 1/8" SS line. The transducer was placed in a temperature-regulated block with two heating cartridges inserted in the block. A temperature sensor was placed in the block which was connected to a temperature controller to maintain the heater block at a set temperature of 313 K. The two Pt100 Ω platinum resistance probes were placed in the holes drilled in the top and bottom flanges. These were used to measure the temperature of the cell accurately while measuring the equilibrium phase composition. The feature of having two temperature probes allows recording the temperature at the bottom and top

of the cell to monitor the temperature fluctuations. In this case, the fluctuations were not significant, and the average temperature of the bottom and top probes was used. This was well within 0.01 K.

A DAU (Agilent; HP34970A) was connected to the PC to log the pressure and temperature simultaneously every 2 seconds. A two-stage vacuum pump (Edwards; RV3) was utilised to evacuate the loading lines and equilibrium cell. Figure 4-3 shows the schematic diagram of the SA apparatus.
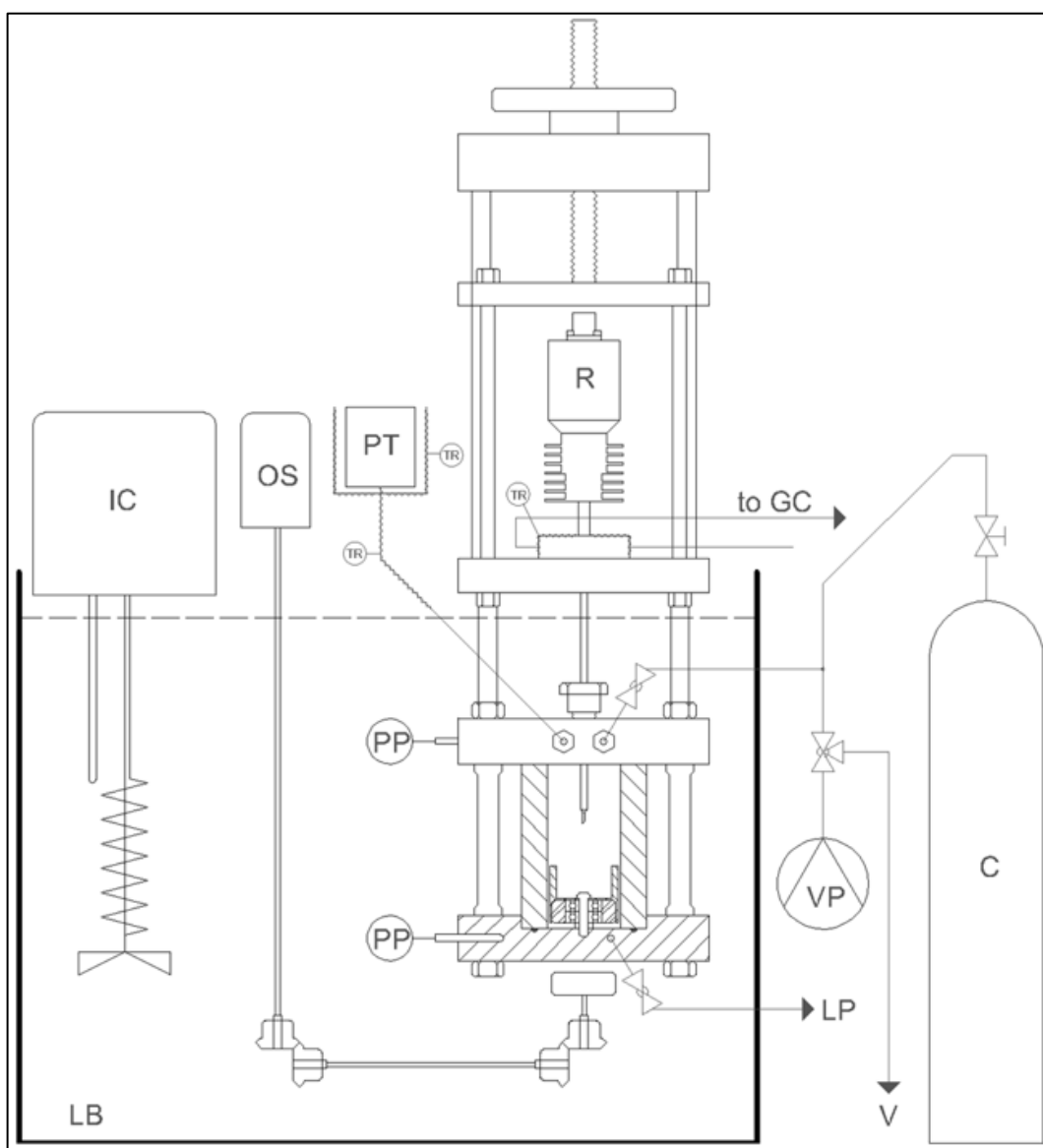
Figure 4-3. Schematic diagram of the SA apparatus. VP: vacuum pump, OS: overhead stirrer, TR: temperature regulation, R: ROLSI™, PT: pressure transmitter, PP: platinum resistance temperature probe, GC: Gas chromatograph, LP: liquid venting port, LB: liquid bath, IC: immersion circulator, C: Gas cylinder (Nelson et al., 2017).

4.2 The Static Synthetic (SS) apparatus

The main part of the equilibrium cell is a sapphire tube with an approximate volume of 10 cm^3. Two SS 316L thick flanges enclose the transparent sapphire tube. The internal volume can be varied using a hydraulically movable SS 316L made piston which is sealed via either Viton or polyurethane (depending on the used solvent). Two Teflon O-rings located at the top and bottom of the piston were used to stabilise the piston. The piston was driven by pressurising the hydraulic fluid (typically water) using a high-pressure ISCO pump (model 100DM). The two sides of the piston were equipped to two needle valves (Parker; 10V series; 1/8") enabling the cell to operate up to 35 MPa.

The two 1/8" Valco fittings were connected to the bottom flange to use in feeding/drainage and to connect to a pressure transducer, respectively. The stirring mechanism consisted of an internal mixer made of Teflon to agitate the contents of the cell. It was driven externally via a Maxon motor (Maxon; A-max).

The cell was submerged into a thermo-stated bath. The temperature of the bath was maintained by an immersion circulator (Grant; TX 150). The top and bottom temperature of the cell is recorded via two Pt100 Ω platinum resistance thermometer (Pt100) probes (WIKA; 1/10 DIN). A 25 MPa pressure transducer (WIKA; P-10) was utilised to measure the pressure. The signals were recorded to a PC via a DAU (Agilent; HP34970A). The schematic diagram of the experimental apparatus is shown in figure 4-4 (Nelson and Ramjugernath, 2017).
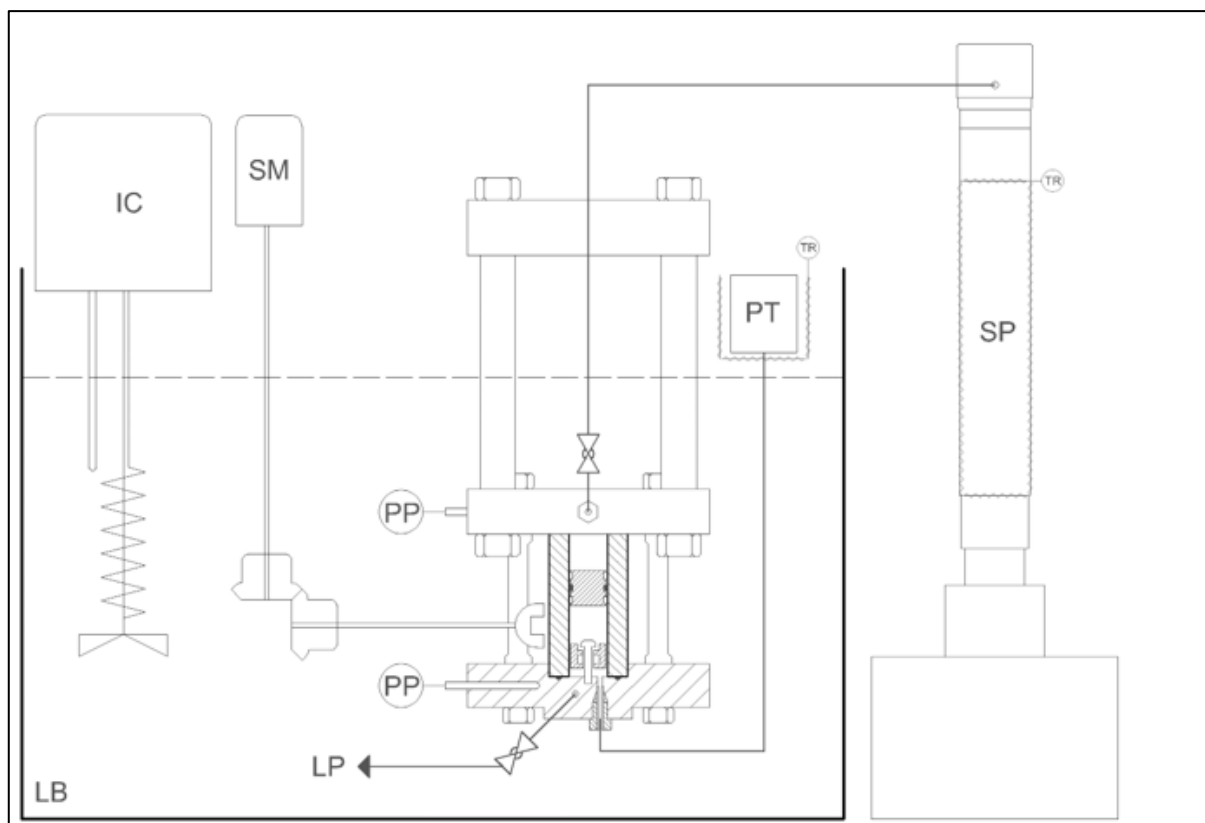
Figure 4-4. Schematic of the SS apparatus incorporating a variable-volume sapphire cell. IC: immersion circulator, LB: liquid bath, LP: loading port, PP: platinum resistance temperature probe, PT: a pressure transducer, SM: stirrer motor, SP: syringe pump, TR: temperature regulation (Nelson and Ramjugernath, 2017).

4.2.1 Modifications to the SS apparatus

The modification to the equipment included adding a stainless-steel chamber to the equilibrium cell to release the gas in two stages once the experiment was finished. The chamber inlet was connected to a 1/8" SS 316L valve, and the outlet port was connected to a tube and extended to the top side of the fume cabinet for better suction of the toxic gas. The weight of the cell was also decreased by machining some parts of the top and bottom flanges for ease of its moving and weighing. This also could decrease the hit impact in the case that the cell falls from the hand. Furthermore, another fume hood is utilised to be used for the mixture preparation which was done outside the fume cabinet originally. This eliminates the chance of exposure to NF_3 in case of major gas leakage during the mixture preparation.

Due to gravimetric preparation of the mixture, the balance is moved to a spot nearby the second fume hood and calibrated. As there was no access to the NF_3 detector in the proximity of the experimental apparatus, extra precautions were taken, such as the use of an M3 6500 mask with a special filter and cartridge. An electricity generator was purchased and placed inside the mixture preparation fume hood for the case of a power outage. It can provide up to 30 to 45 minutes power

for the fume cabinet. A power source was added to the second fume hood to drive the overhead stirrer motor to replace the manual stirring required for the mixture preparation.

4.3 Experimental procedure

The experimental methods for the SA and SS apparatuses are explained in the sections which follow. The calibration of temperature and pressure sensors, calibration of gas chromatograph for the SA apparatus, evacuating and loading the equilibrium cell, measurement of vapour pressure in the SA unit followed by phase equilibrium measurements is discussed. Furthermore, degassing of the solvent is explained for the SA method. The safety procedures developed for the measurements with NF_3 is also presented.

4.3.1 Temperature Calibration

The two Pt-100 probes were calibrated against a WIKA CTH 6500 thermometer probe for each method (4 probes). The WIKA CTH 6500 thermometer had been calibrated directly by the WIKA standard with the internal uncertainty of 0.02 K. The temperature probes were submerged into the temperature regulated bath to the same depth. The controller temperature of the thermo-stated bath was adjusted incrementally and then decreased. At any constant temperature, each temperature probe was measured for 3-4 minutes. The temperature of the Pt-100 probes was recorded through a data acquisition unit, while the measured values of the reference probe were read from the unit's display and recorded manually.

The collected data was fitted to first and second-order polynomials with least squares regression. The Pt100 probe response should behave linearly, so the values calculated using a polynomial (first or second order) should be the same. If there is a big difference between the calculated values of each polynomial, the Pt100 probes are damaged. Temperature probes may need to be re-calibrated if the probe's internal resistance changes, such as a change in the length of the wire or probe bending. Calibration should be reviewed periodically to make sure the internal resistance of the probe is reliable. The standard probe, in this case, the WIKA CTH 6500 underwent annual calibration as per schedule.

4.3.2 Pressure calibration

Three pressure transducers were calibrated against a pressure transmitter WIKA CPT 6000 0-250 mm (0.025% accuracy declared). The WIKA CPT 6000 pressure transducer was calibrated directly by WIKA Instruments (in ambient conditions) with the maximum internal uncertainty of 0.022 kPa (0.00002 MPa).

The reference pressure transducer was connected to the liquid outlet of the equilibrium cell, and the equilibrium cell was pressurized under high-pressure nitrogen. Isothermal conditions were maintained during calibration by controlling both isothermal fluid baths and the temperature of the P10. Then the cell pressure was increased and steadily decreased throughout the range of work for each pressure transducer by 10 bar steps. At each pressure setting, an average pressure measurement was recorded over 2-3 minutes. The data were recorded from the pressure transducers through the data acquisition unit, while the values of the reference pressure transmitter were recorded manually. The collected data were fitted to first and second-order polynomials. The calibrations were to be confirmed periodically to record drifts.

4.4 Calibration of gas chromatograph detector

The GC detector calibration can be performed via either standard solution, direct injection or monomeric methods dependent on the available phases in the system at the ambient condition. In the standard solution method, multiple binary mixtures are prepared gravimetrically with varied compositions. Thereafter, the constant volume of each mixture is injected into the GC column. The mole numbers are calculated via multiplying the response factor to the peak area. The response ratio was calculated over a wide range of peaks using several synthesised mixtures. In this work, the standard solution method was used for the diluted mixtures of the gases to extend the calibration range. The uncertainties arising from the mixture preparation were considered in uncertainty calculations.

The monomeric method is used for preparing the mixtures by the partial pressure of the gaseous compounds. The binary mixtures could be made of gas/gas systems or vaporised liquid/gas systems. The latter is applicable in theory. The ratio of the number of moles is then calculated at a constant temperature using ideal gas law (Nelson, 2012). Despite the accurate calibration results obtained from this method, it is limited to completely gaseous mixture preparation inside the equilibrium cell. This was not utilised in this work due to the presence of liquid components.

In the direct injection technique, a specific volume of pure liquid or pure gas is injected into the chromatograph. Then, using the direct calculation, the relationship between the number of injected moles and the area under the curve is found, which is called the response ratio. For this calculation, ambient temperature and pressure are required. Since the selected volume is adjusted by hand, there is always a human error in volume selection, and there will be an inevitable difference between the volume of the injected and computed value. This difference should be considered in the uncertainty calculations. The uncertainty of liquid volume chosen can be due to the fixed point selection for each injection and sealing of the syringe.

Due to the low dependence of the volume of liquids on ambient temperature and pressure, the volume does not significantly affect these results. However, in the case of injected gas volumes, attention should be paid to the compressibility factor of gases, which is strongly influenced by pressure and temperature. As 5 subsequent repeated injections are required for the calibration of each selected volume, there is a probability for the syringe needle to get warmer from the previous injection, which will have a heat transfer effect. However, the effect of pressure changes will not be high. The GC detector calibration is highly sensitive, and one must pay careful attention to the technique to perfect the method since the human error will change the entire result.

The effect of human accuracy or error can be due to the lack of consistency in the injection method, as well as the manual choice of the setpoint for volume on the syringe. Another factor that affects the precision and accuracy of the selected volume is that the accuracy is related to the characteristics of the injection gas. The larger the volume of the selected setpoint, the smaller the relative error on the set point. It indicates the difficulty of reproducibility and reliability of the data measured in the dilute ranges and at low volumes injected (i.e. below 100 μl for gases and below 0.1 μl for liquids).

4.5 Equilibrium Measurements
4.5.1 Preparation of the cell
The equilibrium cell was initially opened and washed with acetone to remove any source of organic impurities as well as moisture. After the O-rings were changed, the cell was tested for any leaks.

4.5.2 Leak testing
The cell was pressurised with nitrogen gas to 16.0 MPa. Then, the leak detection fluid (Snoop®) was used to locate the possible leakage from fittings. As another approach, the cell was submerged to a water bath and waited for possible bubbles to emerge, which indicates the leakage. Thereafter, the cell pressure was recorded in the isothermal environment over a period of 24 hours to record the leak rate. In the case of no leakage, the test was finished and the cell was ready for experiments. The same leak test approaches were followed before every system measurement. If there were leaks present it was resolved and measurement was started.

4.5.3 HPVLE measurements using the SA apparatus
After the leak test, experiments were started by measuring the vapour pressure of solvents. The purpose of measuring the vapour pressure was to first confirm the calibration of temperature and pressure, and the purity of the materials used. At the same time, before the start of an experiment, the complete characterisation of the material was carried out by measuring the refractive index

(Bellingham & Stanley; Abbe 60LR; expanded uncertainty of 0.001) and density (Anton Paar; DMA 5000; expanded uncertainty of 0.001 g/ml). The cell was then flushed a few times to prepare for testing. The evacuation of the cell was carried out for 20 minutes. The pump was turned off, and the solvent was then introduced into the cell using a syringe.

The minimum volume of the solvent used for measurements was 13 to 16 ml. Due to the height of the magnet and the mixer body, it is not possible for the capillary tip to reach the liquid to remove samples using smaller volumes. After transferring the solvent to the cell, the degassing was performed using a valve and a vacuum pump to remove dissolved gases from the solvent. Then the gas was introduced to the equilibrium cell, and the cell was submerged into the bath. The bath controller was set to the desired temperature to regulate the temperature of the cell.

Once the temperature of the cell body and the contents had stabilised, the mixer was turned on to achieve the chemical equilibrium at the set temperature. The duration that the mixer was active depended on the solubility of the gas in the liquid. The greater the solubility of the gas, the less time is required. The mixer was then switched off to allow the liquid and vapour phases to settle and prepare the system for sampling. Sampling started at the vapour phase because, before starting the sampling, purging was carried out several times through the ROLSI™, so that the remaining fluids were evacuated from the capillary. During the experiment, the concentrations of liquid and gas phases were always measured at the same pressure. If the liquid phase was sampled before the gas phase, there is a probability of a difference in the pressures measured for the two phases.

In each phase, at least 6 or more repeatable samples must be withdrawn until the GC composition analysis indicates comparable results. Samples were always adjusted to be within the calibration range so that the response ratio could be properly used to estimate the mole numbers and the composition of the solution. Therefore, after confirming the concentration of the vapour phase, the capillary tip was moved to the liquid phase to obtain its concentration in the same manner.

The average pressure and temperature were recorded for each phase. After obtaining the corresponding temperature, pressure and concentration of liquid and vapour phases, the next point should be measured. The next composition could be prepared either by topping up the pressure or by discharging the pressure of the compartment, with the latter being due to higher pressures. At the same time, it was important to take care that the liquid level was not decreased too low to prevent sampling. The method described for measuring the concentration was similarly repeated for each pressure.

4.5.4 *P-x* measurements using the SS apparatus

Before commencing with experiments, an extensive fault tree analysis was performed. The drafted safety document was based on the existing safety codes and was approved by all supervisors and the safety authorities within the department.

During the course of NF_3 measurements, a person had to be stationed outside the lab to monitor the procedure of the experiment from outside in case of emergency incidents. Two lab technicians were put in the access section during the test. The total lab area was clear of other students and staff members during the experiments. Due to the limitations of the possible working hours, only one mixture was prepared each day. There are no available experimental data for the phase equilibria of NF_3 and each data point was generated carefully to maintain the safety and experimentation standards. Overall, the generation of the binary data for NF_3 + solvents took almost a year from pre-test safety actions and equipment modifications to the final data modelling stage.

The experimental procedure for the mixture preparation was modified in such a way that the cell was mostly kept inside the fume hood. The cell was only removed from the cabinet for weighing. One of the most important stages of the mixture preparation was to transfer the high-pressure NF_3 gas to the cell. The general procedure is to invert the cell and turn the mixer manually to obtain the better dissolution of the gas. While the measurements with NF_3 is difficult, time-consuming and complex, a substantial amount of high-quality data was generated for the NF_3 + solvents.

To prepare the mixture inside the cell, the equilibrium cell must be separated from the water bath and the pressure pump. Due to the fact that the mixture preparation was based on the mass of the introduced material into the cell, it was necessary to ensure the absence of moisture on its body. At first, the cell was placed under vacuum and weighed to obtain the empty chamber weight. This manner was always followed because the water level of the other side of the piston was variable, and the weight could not be considered constant for the evacuated cell. Then, a small amount of gas was injected into the system (slightly above the barometric pressure), which, if the degassing process was prolonged, it was not likely to introduce the air to the cell under vacuum condition.

The solvent was then degassed inside a Büchner flask attached to the vacuum pump to eliminate any dissolved gas and air of the solvent. It should be noted that in the case of the presence of air in the solvent, the measured bubble point will not be reliable. After carrying out the degassing process, the solvent was transferred to the compartment and then weighed. Due to the fact that the solvent was fed into a cell using a conventional syringe, there was a probability of the presence

of some solvent in the outer portion of the feed valve. This was dried by the vacuum pump and the use of a hairdryer.

The cell was then inverted, and the mixer motor was switched on to agitate the content and help the full dissolution. After loading the cell with the gas, it was weighed again. At this stage, the concentration of the mixture introduced into the test chamber was calculated. Then the cell was again attached to the pump and immersed into the water bath. After ensuring the temperature equilibrium inside the compartment, the pressure of the compartment was increased with the flow of water to the upper part of the piston.

It was important to increase the pressure of the test chamber by considering the water injection rate. If the pressure was increased with considerable speed and gradient, the bubble point measured did not have enough accuracy. The pressure gradient varied according to the type of mixture and solubility of the material. In the test series for this project, the injection speed was varied between (0.5 to 20 μl/s). In the region near the bubble point, small bubbles of the solution were visible. This step required a great deal of precision because, when the pressure was recorded, there was an adequate time to take readings and observe the formation of the bubbles.

Given that the systems' pressure was recorded every two seconds using the data acquisition unit, the process of variation of pressure was recorded as pressure versus time graph. When the system reached the bubble point, a discontinuity occurred in the P vs time plot and a jump in the slope of the pressure was observed on the recorded trend, indicating the bubble point. After reaching the bubble point, the pressure of the system was reduced using the pump, and this process was repeated twice to obtain the required precision for the bubble point pressure.

4.6 Shutdown procedure

Once the experimental phase equilibrium measurements were completed, the running auxiliary units of the equipment were turned off. These parts include the stirring mechanism, chilling unit, temperature controllers, and data acquisition unit. The discharge method of both apparatuses was the same except before draining the SS cell, the flow rate of the syringe pump was returned to decrease the level of the compression fluid (i.e. water) in the equilibrium cell. Thereafter, the cell contents were drained into a chamber. On all occasions, it was necessary to connect the chamber to the drain/feed valve of the equilibrium cell and discharge the cell directly to the chamber to avoid major toxic gas leakage. The gaseous components were then vented and directed to the top side of the fume cabinet using a tube to direct the flow of gas. The vacuum pump was used to discharge the contents of the cell. Eventually, the compartments were washed and cleaned to

prepare for the next run. For the discharge of the toxic gas (NF$_3$), a carefully developed method was followed and is explained in Appendix C.

Chapter 5: Results and discussions

This chapter presents the solvent selection procedure with the finalised list of the selected solvents identified for further investigations. The experimental VLE measurements for the test system along with new data measurements are presented along with the thermodynamic modelling. The experimental data measured following the static-analytic (SA) apparatus were validated following the static-synthetic (SS) apparatus.

A significant amount of experimental time was spent on experimental apparatus and procedure validation which took just above 6 months. The test system measurements were carried out until confidence was obtained in the regeneration of the data for a system that was previously measured in the literature.

The aim of this project was to find appropriate solvents for the purification of NF_3 gas removing the CF_4 impurity. Accordingly, binary data for the gas with the solvent were studied to determine the solvent capacity. The data is presented in two parts: results generated for binary systems of CF_4 and 6 solvents, followed by binary data generated for NF_3 and 4 solvents. Ultimately, the behaviour of the solvents is discussed and compared against these gases.

An extensive review of the literature indicated that no vapour liquid equilibrium data have been published for NF_3 to date. The experimental measurements for the systems including nitrogen trifluoride were only performed using the SS method due to the hazardous risks associated with the toxic nature of the chemical. From the experimental results, the best performing solvent was selected for the preliminary design of the physical separation processes (i.e. the absorption process and extractive distillation process). The results from the Aspen Plus® V10 simulation are presented and discussed.

5.1 Solvent screening

There are various methods proposed for solvent selection which were explained in chapter 3. Based on the results from the Robbins chart, tetrafluoromethane fits into group 11 while there is no designated group for nitrogen trifluoride. Based on the results from the group contribution methods, due to the lack of experimental data for NF_3, the functional groups do not exist. As discussed in chapter 3, the prediction of the phase data for the $CF_4 + C_6H_{14}$ has demonstrated that the use of COSMO-SAC is not reliable for solvent selection. The experimental data from the literature identifies that CF_4 has a higher tendency to dissolve in fluorinated compounds. Before finalising the list of chemicals, some experimental test systems were measured to aid in the

screening process. The list of identified solvents is provided in table 5-1. These chemicals are fluorinated components some of which were also identified by (Mukhortov et al., 2010).

Table 5-1. List of the selected solvents for this study.

Solvent	Properties [a]			Availability	Price/ml (ZAR)[b]	VLE data[c]
	polar	Toxicity [d]	boiling point (K)			
Perfluorodibutylester	x	-	-	-	-	-
Perfluorohexane	-	x	329.15	x	37.5	● & ◆
Perfluoroheptane	-	-	353.15	x	106.8	◆
Perfluorooctane	-	x	376.15	x	164.4	◆
Perfluorodecalin	-	-	415.15	x	62	● & ◆
Heptafluoro,1-butanol	x	x	368.15	x	272	● & ◆
Tetrafluoroethyl-tetrafluoropropyl ether	x	-	366.15	x	400	● & ◆

[a] Literature data for the properties from NIST TDE (Frenkel et al., 2005).
[b] The prices are adapted from Sigma Aldrich website in February 2019.
[c] Systems measured in this work; ◆: CF_4 ●: NF_3.
[d] Dangerous for the respiratory system (spexcertiprep, 2017).

Table 5-1 includes the properties of the solvents (polarity status, toxicity and boiling point), availability, price and the systems as published in the available literature (Frenkel et al., 2005, Williamson, 2013, González et al., 2010). As mentioned in chapter 3, the literature data has proven the higher capability of fluorinated compounds in CF_4 intake and the selected compounds from several fluorinated families. The fluorinated chemicals are expensive (e.g. TFE-TFP ether and heptafluoro,1-butanol are R400 and R272 per ml according to Sigma Aldrich at February 2019) which is affected by annual inflation rate added to the fluctuations in currency. Furthermore, some fluorinated chemicals such as perfluorodibutylester, identified by (Mukhortov et al., 2010), are not available. In addition, some of the available and cheaper PFCs are toxic if inhaled, including perfluorohexane with a lethal dose (LD50) Oral-Rat- > 5,000 mg/kg, and perfluorooctane with LD50 of 5628 mg/kg (spexcertiprep, 2017). The compounds selected have a wide range of polarity, enabling the study of chemical behaviour in both polar and non-polar mixtures.

The supplier and critical properties of the chemicals used for experimental screening measurements, test systems and new systems are provided in table 5-2. The chemical purity analysis is presented in table 5-3. This purity analysis includes the purity provided by the supplier, the purity obtained by direct injection of the material into the gas chromatograph to obtain the GC peak area percentage, the refractive index and density measurements, and comparison to the literature data. In case of the inability to access literature data, results were compared to the manufacturer purity. The GC peak area percentage for the chemicals is reported in table 5-3. A

thermal conductivity detector (TCD) with either Porapak Q or Rtx-5ms columns, was used to test for the GC peak area.

Two different grades of perfluorohexane were used from two different suppliers. The TCD detector with either the packed or capillary column at different GC conditions was unable to separate the impurity from the chemical. Due to the purity stated by Acros Organics with >97 %, further characterisations were performed. The TCD was used first for the GC peak area with various packed or capillary columns which were unable to separate the impurities at different speeds of carrier gas as well as column temperatures. Thereafter, a GC-MS was utilised with an Rtx-5ms column to detect the impurities and peak area percentage. The suggested impurities after analysis with the GC-MS were from heavier PFCs. C_6F_{14} from SynQuest Laboratories had a GC peak area of 99.9 % while the C_6F_{14} from Acros Organics had a GC peak area of 96.7 %.

All experimental data of density and refractive index compared well with the literature data. Only one literature data was used to compare the densities measured for C_6F_{14} from both suppliers. The refractive index data measured in this work compared well to the values stated by the suppliers.

Table 5-2. Critical properties of the materials used in this study.

Component	Formula	T_c/K [a]	P_c/MPa [a]	ω [a]
Carbon dioxide	CO_2 [b]	304.2	7.38	0.224
Tetrafluoromethane	CF_4	227.5	3.75	0.179
Nitrogentrifluoride	NF_3	234.0	4.46	0.120
n-Hexane	C_6H_{14} [b]	507.6	3.03	0.301
Perfluorohexane [c]	C_6F_{14}	449.6	1.80	0.543
Perfluorohexane [d]	C_6F_{14}	449.6	1.80	0.543
Perfluoroheptane	C_7F_{16}	475.7	1.61	0.508
Perfluorooctane	C_8F_{18}	502.2	1.48	0.443
Heptafluorobutanol	$C_4H_3F_7O$	506.0	2.75	0.656
Tetrafluoroethyl-tetrafluoropropyl ether	$C_5H_4F_8O$	510.7	2.58	0.537
Perfluorodecalin	$C_{10}F_{18}$	565.1	1.78	0.499

[a] Literature data for the properties from NIST TDE (Frenkel et al., 2005).

[b] The test system material.

[c] Perfluorohexane purchased from SynQuest Laboratories

[d] Perfluorohexane purchased from Acros Organics

Table 5-3. Supplier and purity analysis of the chemicals used in this work.

Chemical	CAS number	Supplier	Supplier purity (wt. %)	GC peak area [a]	liquid density [b] Experimental	Literature	refractive index [c] Experimental	Literature
CO_2	124-38-9	Afrox	99.99	>99.9	-NA-	-NA-	-NA-	-NA-
CF_4	75-73-0	Air liquid	99.99	>99.9	-NA-	-NA-	-NA-	-NA-
NF_3	7783-54-2	Air liquid	99.99	none	-NA-	-NA-	-NA-	-NA-
C_6H_{14}	110-54-3	Sigma Aldrich	99.8	>99.9	0.659	0.659	1.375	1.375
C_6F_{14}	355-42-0	SynQuest Labs	99.99	>99.9	1.670	1.670	1.251	1.251
C_6F_{14}	355-42-0	Acros Organics	>97	>96.7 [d]	1.701	1.670	1.252	1.253
C_7F_{16}	335-57-9	SynQuest Labs	99.98	>99.9	1.724	1.720	1.265	1.265
C_8F_{18}	307-34-6	SynQuest Labs	99.98	>99.9	1.768	1.777	1.268	1.268
$C_4H_3F_7O$	375-01-9	DLD Scientific	98	>98	1.599	1.600	1.294	1.294
$C_5H_4F_8O$	16627-68-2	DLD Scientific	99.95	>99.9	1.528	1.532	1.276	1.276
$C_{10}F_{18}$	306-94-5	SynQuest Labs	99.5	>99.9	1.939	1.941	1.314	1.314

[a] A thermal conductivity detector was used to identify the area percentage of the chemicals by gas chromatography. The Rtx-5ms column was used for liquid analysis and Porapak Q column for gases.

[b] The liquid density (ρ/g.cm^{-3}) ($P = 101$ kPa) data at $T = 298.15$ K; $U(T) = 0.05$ K; $U(\rho) = 0.001$ g.cm^{-3}; $U(P) = 1$ kPa.

[c] The refractive index data ($P = 101$ kPa) at $T = 293.15$ K; $U(T) = 0.05$ K; $U(n_D) = 0.001$; $U(P) = 1$ kPa.

[d] GS-MS with Rtx-5ms capillary column for perfluorohexane

5.2 Modelling approaches

Thermodynamic modelling enables design and property estimation when performing rigorous column sizing of extractive distillation and absorption columns. A detailed study of the modelling approach was provided in chapter 3.

Regarding the fairly ideal nature of most of the binary systems of CF_4 + n-perfluoroalkanes, the data measured were predicted using the PR EoS. The Wong-Sandler (WS) mixing rule was utilised together with the NRTL activity coefficient model to provide a better representation of the vapour phase composition. All models were utilised using ASPEN PLUS® V10 software. In several studies (Mühlbauer, 1997, Narasigadu, 2011), it has been pointed out that the direct method of vapour and liquid phase data modelling by utilising a single EoS model and mixing rule can describe the phase equilibrium data with high accuracy. In this study, the interaction parameter of WS mixing rule (k_{ij}) and two adjustable parameters of the NRTL model ($\tau_{2,1}$ and $\tau_{1,2}$) were regressed. The recommended value for the non-randomness parameter ($\alpha_{1,2}$) is between 0.2 and 0.47. It was set equal to 0.3 for the nonpolar systems and 0.47 for systems with hydrogen bonding (Marina and Tassios, 1973). The modelling results of each system will be explained in the relevant section. For statistical analysis, the average absolute deviation (AAD) and average absolute relative deviation (AARD %) were used to determine the model fit.

$$AAD(\bar{\theta}) = \frac{1}{N_p} \sum_{1}^{N_p} |\bar{\theta}_{exp} - \bar{\theta}_{calc}|$$ 5.1

$$AARD(\bar{\theta}) \% = \frac{1}{N_p} \sum_{1}^{N_p} \frac{|\bar{\theta}_{exp} - \bar{\theta}_{calc}|}{\bar{\theta}_{exp}} \times 100$$ 5.2

Calc, exp, $\bar{\theta}$ and N_p are the calculated value, the experimental value, the corresponding property (i.e. vapour phase pressure or composition) and numbers of experimental data for each isotherm, respectively.

5.3 Pressure and temperature calibrations

A summary of the calibration results is provided in this section and detailed information on the method was explained in chapter 4. Table 5-4 presents the list of uncertainties associated with the pressure transmitters used in this study.

Table 5-4. Standard uncertainty influences and estimates for the pressures reported in this study.

Uncertainty source	Estimate [a]	Distribution
P reference/MPa; 25 MPa (gauge) [b]	0.01%	normal
P reference/MPa; 300 kPa [c]	0.01%	normal
Correlation for *P*/kPa (500 kPa)	0.1	rectangular
Correlation for *P*/MPa (10 MPa(gauge))	0.001	rectangular
Correlation for *P*/MPa (25 MPa(gauge))	0.002	rectangular

[a] Estimate treated as a type B distribution
[b] Mensor CPC 8000
[c] Mensor CPC 6000

The overall uncertainty for the vapour pressure measurement was 1 kPa. For the phase data measured using the SS apparatus, the pressure uncertainty was 0.005 MPa. The pressure uncertainty for the SA apparatus was 0.007 MPa. Table 5-5 shows a summary of correlations and calculated uncertainties for the pressure transmitters. Refer to chapter 4 for detailed information on the pressure calibration.

Table 5-5. Pressure calibration data for the pressure transducers.

Range	Calibration range	$U(P)$	Correlation / bar
0-25 (MPa)	0-230	0.01 (MPa)	$P_{calc} = 0.999 \times P + 0.071$
0-10 (MPa)	0-90	0.007 (MPa)	$P_{calc} = 1.001 \times P + 0.005$
0-500 (kPa)	0.2-1	1 (kPa)	$P_{calc} = 0.999 \times P$

In total, four temperature probes were calibrated. Table 5-6 shows a summary of the correlations and calculated uncertainties for the temperature probes. The calibrations were checked every six months.

Table 5-6. Temperature calibration data for the four different probes.

Calibration range/K	$U(T)$ / K	Correlation / K
273.15 - 348.15	0.07	$T_{CALC} = 1.001 \times T - 1.547 + 273.15$
273.15 - 348.15	0.06	$T_{CALC} = 0.997 \times T - 1.527 + 273.15$
273.15 - 353.15	0.04	$T_{CALC} = 0.997 = \times T - 1.773 + 273.15$
273.15 - 353.15	0.03	$T_{CALC} = 0.998 \times T - 1.480 + 273.15$

5.4 GC detector calibration

Detailed information on the calibration method was presented in chapter 4. A summary of the GC detector calibrations is presented below. The gas chromatograph detector was calibrated for two gases and four solvents. The calibration polynomials and errors are listed in table 5-7. The error reported in the table is the difference between the experimental and calculated values of the moles injected to the

GC column. The calibration errors were within 3 % and only the calibration of diluted CF_4 had 4 % error which is within acceptable range compared to the pure component.

Table 5-7. Calibration polynomial and associated error for GC detector calibrations.

Chemical	Correlation [a]	Error %
CO_2	$n_{calc} = 9.933 \times 10^{-13} A - 5.320 \times 10^{-8}$	1.5
CF_4	$n_{calc} = 8.004 \times 10^{-13} A + 8.332 \times 10^{-8}$	2.5
$CF_{4\ (diluted)}$	$n_{calc} = 7.842 \times 10^{-13} A + 6.142 \times 10^{-12}$	4.0
C_6H_{14}	$n_{calc} = 4.610 \times 10^{-13} A - 1.133 \times 10^{-8}$	3.0
C_6F_{14}	$n_{calc} = 3.278 \times 10^{-13} A - 2.037 \times 10^{-11}$	2.0
C_7H_{16}	$n_{calc} = 3.278 \times 10^{-13} A - 2.037 \times 10^{-11}$	2.0
$C_5H_4F_8O$	$n_{calc} = 3.653 \times 10^{-13} A - 2.466 \times 10^{-7}$	2.0

[a] n = number of moles, A = GC peak area.

5.5 Experimental test system

The VLE data measurement for a previously presented system in the literature provides the ability to evaluate the technique and the device to generate novel data. Hence a mixture of n-hexane + carbon dioxide at 313.15 K was selected as the test system, since:

- Both n-hexane and the target solvents present the same range of boiling point which is an important factor in the thermal conductivity detector (TCD).

- The abundance of previously published thermodynamic data for this system which is an indicator of ability to perform a comparative study on the measured data and the predictive model.

- The temperature of the system studied should be close to the temperature range considered for the main systems.

The data measured using the SA method for the n-hexane + carbon dioxide system at 313.15 K is shown in figure 5.1. The uncertainties associated with the data measured are shown by error bars in the figure. The uncertainty is reported per data point and for each phase. These are presented in tables 5-8 and 5-9. The uncertainty estimated at lower compositions for data measured using the SA apparatus is usually smaller and it expands as the composition of the liquid phase increases to the equimolar. Thereafter it decreases as the composition departs from the equimolar region. It is due to the similar contribution of each component to the uncertainty in the equimolar region and lower contribution of one of the components in either high or low compositions. By contrast, as the composition increases (using the SS apparatus), the uncertainty constantly decreases, which is due to the rise in the mass of the gas filled. Hence, the relative uncertainty proportion for the mass loaded decreases.
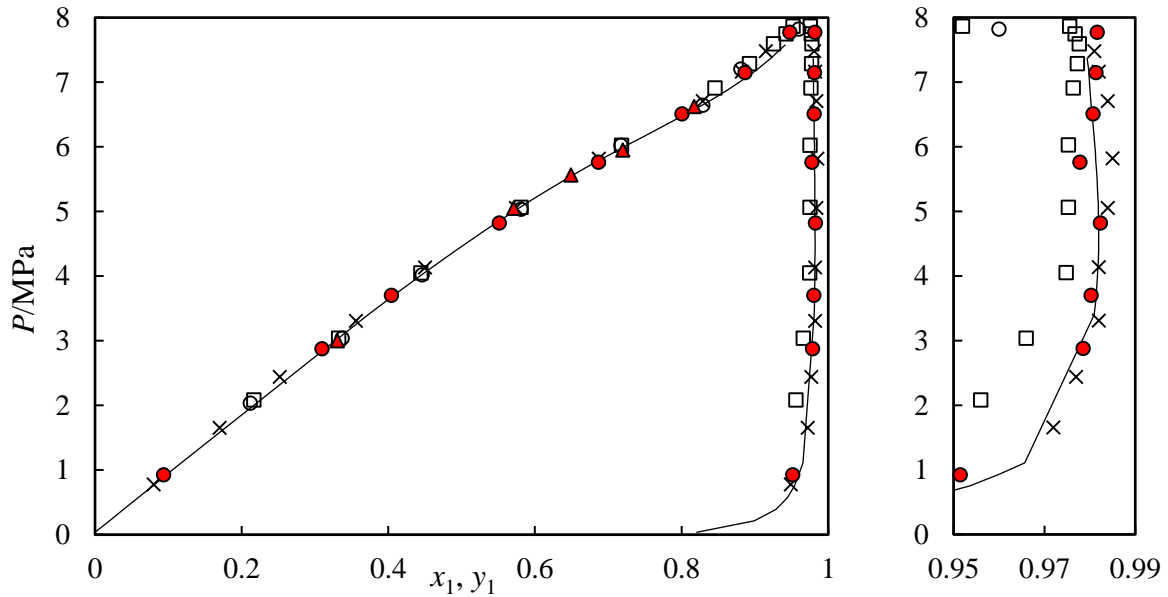
Figure 5-1. HPVLE data for the carbon dioxide (1) + n-hexane (2) binary system at a temperature of 313.15 K, •; Experimental (This work - measured using a SA apparatus), ▲; Experimental (This work - measured using a SS apparatus) ×; (Li et al., 1981), □; (Wagner and Wichterle, 1987) and o; (Chen and Chen, 1992). Solid lines, —, PSRK model.

The measured data compares well with the predictive PSRK model, as well as against the data of (Li et al., 1981). A notable point is the good correlation between the generated data and model prediction. The comparison between the data is better than some data provided in the literature. There is some discrepancy in the data reported in literature especially that of (Chen and Chen, 1992). Another point to mention is the ability of the equipment to generate data at high pressures, close to the critical region. Based on the measured data, it can be concluded that the measurement technique was accurate. The experimental data with the associated uncertainties are listed in tables 5-8 (SA method) and 5-9 (SS method).

Table 5-8. Experimental HPVLE data for the carbon dioxide (1) + n-hexane (2) binary system at 313.15 K including the vapour phase composition (y_1), the liquid phase composition (x_1), measured pressure (P) and the expanded uncertainty[a].

P/MPa	x_1	y_1	$U(x_1)$	$U(y_1)$
0.925	0.094	0.9515	0.007	0.0008
2.878	0.310	0.9786	0.009	0.0007
3.704	0.405	0.9803	0.009	0.0004
4.823	0.551	0.9817	0.011	0.0021
5.762	0.687	0.9778	0.009	0.0013
6.511	0.801	0.9807	0.009	0.0011
7.150	0.887	0.9813	0.008	0.0004
7.772	0.948	0.9823	0.007	0.0009

[a] $U(P) = 0.007$ MPa; $U(T) = 0.05$ K.

Table 5-9. Experimental data for the carbon dioxide (1) + n-hexane (2) binary system at 313.17 K using the SS apparatus, including liquid phase composition (x_1) and the pressure (P), listing the expanded uncertainty[a].

P/MPa	x_1	$U(x_1)$
3.00	0.330	0.008
5.05	0.571	0.003
5.57	0.649	0.003
5.95	0.720	0.003
6.63	0.817	0.003

[a] $U(P) = 0.01$ MPa; $U(T) = 0.07$ K.

5.6 Experimental data

The data is presented in two parts; results generated for CF_4 with six solvents with the corresponding thermodynamic modelling, followed by data generated for NF_3 with four solvents. An overview of the measured data is presented in table 5-10.

Table 5-10. Overview of the test and novel binary VLE systems measured in this work, 'l' and 'g' denotes whether the component is either a liquid or gas at ambient conditions.

Gas	Liquid solvent	T/ K	P/ MPa	Method	No. points
CO_2 (g)	C_6H_{14} (l)	313.15 (test)	1-7.7	SA - SS	20
CF_4 (g)	C_6H_{14} (l)	283.15	1.2-6.4	SA	5
CF_4 (g)	C_6H_{12} (l)	283.15	1.3-5.8	SA	5
CF_4 (g)	C_6F_{14} (l)	283.15- 303.15	1.5-9.0	SA - SS	42
CF_4 (g)	C_7F_{16} (l)	283.15- 303.15	1.5-9.6	SA - SS	35
CF_4 (g)	C_8F_{18} (l)	283.15- 303.15	1.6-10.8	SA - SS	39
CF_4 (g)	$C_{10}F_{18}$ (l)	283.15- 303.15	3.0-8.0	SA	23
CF_4 (g)	$C_5H_4F_8O$ (l)	283.15- 303.15	1.6-20.0	SA-SS	36
CF_4 (g)	$C_4H_3F_7O$ (l)	283.15- 303.15	2-11.5	SS	18
NF_3 (g)	C_6F_{14} (l)	283.15- 303.15	2.4-9.3	SS	18
NF_3 (g)	$C_5H_4F_8O$ (l)	283.15- 303.15	3-24	SS	18
NF_3 (g)	$C_{10}F_{18}$ (l)	283.15- 303.15	2-7.1	SS	18
NF_3 (g)	$C_4H_3F_7O$ (l)	283.15- 303.15	3.5-8.7	SS	12

5.6.1 CF_4 + C_6F_{14} (perfluorohexane)

New HPVLE data were measured for the tetrafluoromethane + perfluorohexane binary system at three isotherms in the range of (283.15 to 303.15) K. The experimental data are listed in table 5-11 (SA apparatus) and table 5-12 (SS apparatus) and are shown in figure 5-2. The results obtained from the two experimental apparatuses represent a good thermodynamic consistency. The phase equilibrium data measured with two different grades of perfluorohexane show very good overlap in the measured data. The model provides a satisfactory correlation of the experimental data.

On comparison of the CF₄ solubility in perfluorohexane at constant pressure (e.g. 6.0 MPa), as the temperature of the mixture decreases from 303.15 K to 283.15, the solubility of the gas increases from 0.575 to 0.666 indicating better solubility at the lower temperature.

Figure 5-2. HPVLE data for the tetrafluoromethane (1) + perfluorohexane (2) binary system. Experimental data generated by the SS apparatus (C_6F_{14} purchased from SynQuest Laboratories); ●, at 283.16 K; ▲, at 293.17 K; ■, at 303.17 K; (C_6F_{14} purchased from Acros Organics); ●, at 283.17 K; ▲, at 293.15 K; ■, at 303.15 K. Experimental data generated by the SA apparatus; ○, at 283.15 K; △, at 293.15 K; □, at 303.15 K. — PRWS (NRTL) model.

Table 5-11. HPVLE data for the tetrafluoromethane (1) + perfluorohexane [a] (2) binary system using the SA apparatus, listing the measured pressure (P), temperature (T), liquid (x_1) and vapour (y_1) phase compositions, and the expanded uncertainty [b].

T/K	P/MPa	x_1	y_1	$U(x_1)$	$U(y_1)$
283.14	1.535	0.218	0.977	0.009	0.001
283.15	2.147	0.293	0.987	0.011	0.001
283.13	2.792	0.367	0.988	0.013	0.001
283.15	3.343	0.425	0.980	0.013	0.001
283.15	4.062	0.500	0.980	0.014	0.001
283.15	4.709	0.557	0.976	0.013	0.002
283.15	5.544	0.630	0.971	0.013	0.002
283.15	7.060	0.760	0.970	0.010	0.002
283.14	7.804	0.859	0.933	0.007	0.004
293.16	2.026	0.255	0.979	0.010	0.001
293.15	3.666	0.415	0.983	0.013	0.001
293.14	5.207	0.556	0.980	0.013	0.001
293.15	5.994	0.618	0.976	0.013	0.002
293.16	6.978	0.701	0.968	0.011	0.002
293.15	7.774	0.762	0.955	0.010	0.003
293.15	8.449	0.850	0.915	0.007	0.005
303.15	2.535	0.283	0.973	0.011	0.002
303.15	3.632	0.388	0.976	0.013	0.002
303.15	4.635	0.470	0.974	0.014	0.002
303.15	5.753	0.560	0.970	0.013	0.002
303.15	6.726	0.632	0.965	0.013	0.002
303.15	7.840	0.716	0.950	0.011	0.003
303.15	8.605	0.796	0.918	0.009	0.005
303.16	8.776	0.823	0.901	0.008	0.006

[a] Perfluorohexane purchased from Acros Organics.
[b] $U(P) = 0.007$ MPa; $U(T) = 0.05$ K.

Table 5-12. P-x data for the tetrafluoromethane (1) + perfluorohexane (2) binary system using the SS apparatus including the liquid phase composition (x_1), pressure (P), temperature (T), and the expanded uncertainty[a].

T/K	P/MPa	x_1	$U(x_1)$
	Perfluorohexane [b]		
283.17	3.91	0.472	0.004
283.17	5.48	0.617	0.003
283.18	7.12	0.757	0.002
293.15	4.35	0.472	0.004
293.15	6.05	0.617	0.003
293.16	7.78	0.757	0.002
303.15	4.75	0.472	0.004
303.15	6.55	0.617	0.003
303.16	8.85	0.835	0.002
	Perfluorohexane [c]		
283.15	2.68	0.344	0.004
283.17	5.58	0.624	0.002

Table 5-12 continued

T/K	P/MPa	x_1	$U(x_1)$
283.17	6.38	0.689	0.002
293.16	2.97	0.344	0.004
293.20	6.19	0.624	0.002
293.14	7.02	0.689	0.002
303.15	3.26	0.344	0.004
303.17	6.67	0.624	0.002
303.18	7.59	0.689	0.002

[a] $U(P) = 0.01$ MPa; $U(T) = 0.07$ K.
[b] Perfluorohexane supplier: Acros Organics.
[c] Perfluorohexane supplier: SynQuest Laboratories.

The model parameters, as well as statistical analysis of the model results against experimental data, are listed in tables 5-13 (PRWS (NRTL) model) and 5-14 (PR (VdW) model). The binary interaction parameter of the PR (VdW) model shows the system deviates positively (weak deviation) from Raoult's law with an average k_{ij} of 0.001. The magnitude of the interaction parameters shows that the system can be predicted with $k_{ij} = 0$ and the deviations are in the uncertainties estimated for composition and pressure. In addition, the PR (VdW) and PR (WS) models show the same average AAD(P) of 0.01 MPa. While the average uncertainty of the CF_4 composition in the vapour phase is 0.002, the deviation of the CF_4 composition in the vapour phase is ±0.004 (PRWS model).

Table 5-13. Regressed binary interaction parameters (k_{ij} and B_{ij}) and statistical analysis for the PRWS (NRTL) model for the binary system of tetrafluoromethane (1) + perfluorohexane (2).

	$T = 283.15$ K	$T = 293.15$ K	$T = 303.15$ K
k_{12} [a]	0.526	0.535	0.540
B_{12}/ K [b]	52.8	35.2	4.8
B_{21}/ K [b]	5.1	-3.3	8.0
AAD(P/MPa)	0.008	0.010	0.010
AARD(P/MPa)/%	1.16	0.77	0.77
AAD(y_1)	0.003	0.004	0.005
AARD(y_1)/%	0.47	0.44	0.51

[a] k_{12} is the interaction parameter of the WS mixing rule.
[b] B_{12} and B_{21} are the temperature-dependent adjustable parameters of the NRTL model and a non-randomness factor of α_{12} set to 0.3.

Table 5-14. Regressed binary interaction parameters (k_{ij}) and statistical analysis for the PR (VdW) model for the binary system of tetrafluoromethane (1) + perfluorohexane (2).

	$T = 283.15$ K	$T = 293.15$ K	$T = 303.15$ K
k_{12} [a]	0.002	0.000	0.001
AAD(P/MPa)	0.010	0.012	0.010
AARD(P/MPa)/%	0.98	1.26	1.16
AAD(y_1)	0.005	0.002	0.002
AARD(y_1)/%	1.35	0.33	0.47

[a] k_{12} is the binary interaction parameter for the classical mixing rule in the PR (VdW) model.

5.6.2 CF$_4$ + C$_7$F$_{16}$ (perfluoroheptane)

VLE data for the system of CF_4 + C_7F_{16} were measured at three temperatures between (283.15 to 303.15) K. The experimental results are reported in tables 5-15 (SA method) and 5-16 (SS method). The graphical view is presented as a *P-x-y* plot in figure 5-3. The consistency between the measured experimental data from both methods is notable. The model gives a good representation of the experimental data. Two different models were utilised to regress the experimental data including the PR and PRWS (NRTL) model. The binary interaction parameter of k_{ij} for the temperatures of 283.15, 293.15 and 303.15 K is 0.006. The magnitude of the interaction parameters shows that the system can be predicted with $k_{ij} = 0$. The pressure range was 1.5 to 10 MPa throughout the three isotherms. The system shows a slight deviation from ideality which is due to weak interactions between similar compounds.

Figure 5-3. HPVLE data for the tetrafluoromethane (1) + perfluoroheptane (2) binary system. Experimental data generated by the SS apparatus; ●, at 283.17 K; ▲, at 293.15 K; ■, at 303.15 K. Experimental data generated by the SA apparatus; ○, at 283.15 K; △, at 293.15 K; □, at 303.15 K. — PRWS (NRTL) model.

To confirm the experimental data for the SA method, six different mixtures were measured at temperatures between (283.15 to 303.15) K. The pressure range was 1.6 to 9.5 MPa throughout the three isotherms. As the pressure of the mixture was close to the critical region, the system was more unstable with a very small withdrawal of the sample. The cell pressure is controlled with the syringe pump by the flow rate of the compression fluid into it. At high flow rate, the bubble point is obtained at higher pressure compared to the real bubble point. Hence, the speed of the syringe pump was decreased to below 0.1 µl/min to reach the equilibrium slowly.

Every filling was independent of the previous measurement to make sure that any chance of introducing an impurity into the cell was avoided and minimised. The results confirm the measured data for each isotherm as the minor differences between the measured data following both methods are within the uncertainties associated with both methods (±0.003).

Table 5-15. HPVLE data measured for the tetrafluoromethane (1) + perfluoroheptane (2) binary system using the SA apparatus, listing the measured pressure (P), temperature (T), liquid (x_1) and vapour (y_1) phase compositions, and the expanded uncertainty[a].

T/K	P/MPa	x_1	y_1	$U(x_1)$	$U(y_1)$
283.17	1.647	0.227	0.994	0.007	0.001
283.16	2.706	0.363	0.995	0.009	0.002
283.16	3.418	0.421	0.994	0.009	0.001
283.18	4.594	0.524	0.993	0.011	0.001
283.14	5.559	0.606	0.991	0.011	0.001
283.16	6.678	0.694	0.987	0.010	0.001
283.15	7.594	0.767	0.978	0.009	0.001
283.13	8.495	0.845	0.955	0.008	0.001
293.18	1.457	0.186	0.989	0.008	0.001
293.17	2.356	0.285	0.990	0.009	0.001
293.15	3.495	0.393	0.990	0.010	0.001
293.15	4.494	0.483	0.990	0.012	0.001
293.16	6.513	0.637	0.986	0.012	0.003
293.14	7.582	0.708	0.979	0.010	0.001
293.16	8.570	0.782	0.964	0.010	0.001
293.15	9.194	0.841	0.937	0.007	0.003
303.14	1.497	0.181	0.985	0.008	0.002
303.13	2.535	0.279	0.988	0.009	0.001
303.14	3.495	0.368	0.987	0.009	0.001
303.16	4.594	0.453	0.987	0.011	0.001
303.16	5.694	0.533	0.985	0.012	0.002
303.17	6.544	0.591	0.982	0.011	0.004
303.15	7.494	0.656	0.976	0.010	0.003
303.15	8.594	0.730	0.964	0.008	0.004
303.15	9.595	0.823	0.928	0.006	0.001

[a] $U(P) = 0.007$ MPa; $U(T) = 0.05$ K.

Table 5-16. Experimental P-x data of tetrafluoromethane (1) + perfluoroheptane (2) binary system at temperatures between (283.15-303.15) K measured using the SS apparatus, and the expanded uncertainty[a].

T/K	P/ MPa	x_1	$U(x_1)$
283.17	2.51	0.324	0.005
283.17	4.78	0.542	0.002
283.18	7.24	0.736	0.001
293.15	2.84	0.324	0.005
293.17	5.31	0.542	0.002
293.16	7.97	0.736	0.001
303.14	3.14	0.324	0.005
303.16	5.87	0.542	0.002
303.15	8.61	0.736	0.001

[a] $U(P) = 0.01$ MPa; $U(T) = 0.07$ K.

The regressed model parameters and results of the statistical analysis are provided in tables 5-17 (PRWS (NRTL) model) and (PR (VdW) model) 5-18. Due to the ideal nature of the binary system, the PR (VdW) model gives good correlation results. Although, the PR (VdW) model gives a satisfactory result the statistical comparison between the associated errors for the vapour phase pressure and composition indicates that the PRWS (NRTL) model has a smaller error of below 0.1 %, due to the addition of fitting parameters.

By the increases in temperature, there is a decrease in concentration. For example, at 6 MPa and 283.15 K, the concentration of the CF_4 is 0.66, which decreases to 0.60 and 0.55 for temperatures of 293.15 and 303.15 K, respectively.

Table 5-17. Regressed binary interaction parameters (k_{ij} and B_{ij}) and statistical analysis for the PRWS (NRTL) model for the binary system of tetrafluoromethane (1) + perfluoroheptane (2).

	$T = 283.15$ K	$T = 293.15$ K	$T = 303.15$ K
k_{12} [a]	0.598	0.590	0.601
B_{12}/ K [b]	491.9	5634.6	586.3
B_{21}/ K [b]	-318.3	-25.9	-371.1
AAD (P/MPa)	0.003	0.002	0.007
AARD (P/MPa)/%	1.41	0.52	0.76
AAD (y_1)	0.000	0.000	0.002
AARD (y_1)/%	0.13	0.25	0.23

[a] k_{12} is the interaction parameter of the WS mixing rule.
[b] B_{12} and B_{21} are the temperature-dependent adjustable parameters of the NRTL model, and a non-randomness factor of α_{12} set to 0.3.

Table 5-18. Regressed binary interaction parameter (k_{ij}) and statistical analysis of the PR (VdW) model, for the binary system of tetrafluoromethane (1) + perfluoroheptane (2)

	$T = 283.15$ K	$T = 293.15$ K	$T = 303.15$ K
k_{12} [a]	0.006	0.006	0.006
AAD (P/MPa)	0.015	0.013	0.043
AARD (P/MPa)/%	1.85	1.14	2.24
AAD (y_1)	0.001	0.002	0.001
AARD (y_1)/%	0.13	0.27	0.22

[a] k_{12} is the binary interaction parameter for the classical mixing rule in the PR (VdW) model.

5.6.3 CF$_4$ + C$_8$F$_{18}$ (perfluorooctane)

VLE data for the system of CF_4 + C_8F_{18} were measured at three temperatures between (283.15 to 303.15) K and are reported in tables 5-19 (SA method) and 5-20 (SS method). The graphical view is presented as a *P-x-y* plot in figure 5-4. The consistency between the measured data from both methods confirms the quality of the data measured. Two different models were utilised to regress the experimental data which were the PR and PRWS (NRTL) model. The binary interaction parameter of k_{ij} for the temperatures of 283.15, 293.15 and 303.15 K is 0.016, 0.026 and 0.025, respectively. The regressed k_{ij} shows a higher deviation from ideality for perfluorooctane throughout the measured isotherms compared to C6 and C7 systems. This deviation is because of induced-dipole-induced-dipole interactions associated with long-chain PFCs. A molecule with a temporary dipole is capable of inducing the nearby molecule which consequently creates the polarity in the mixture. As the chain length increases, the polarity also becomes stronger (Bruice, 2003). The pressure ranged from 1.6 to 11 MPa throughout the three isotherms. The system shows a slight departure from ideality and small interaction between components.
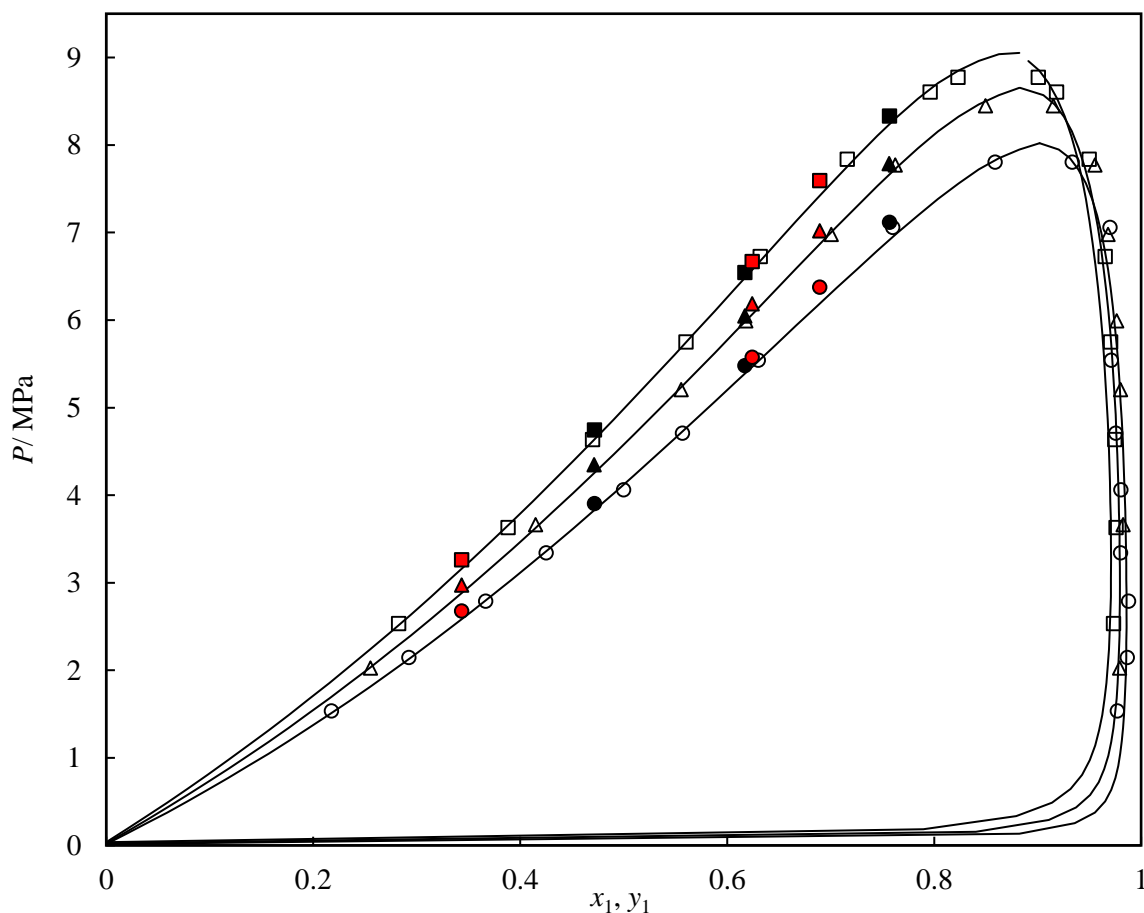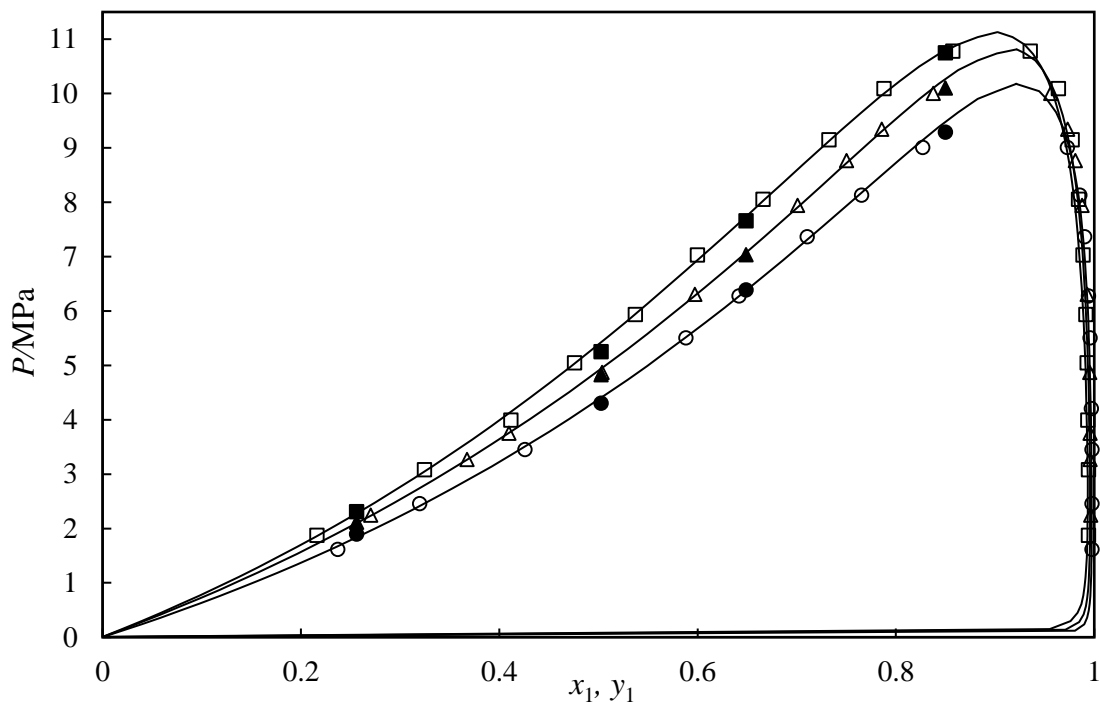
Figure 5-4. HPVLE data for the tetrafluoromethane (1) + perfluorooctane (2) binary system. Experimental data generated by the SS apparatus; ●, at 283.17 K; ▲, at 293.15 K; ■, at 303.15 K. Experimental data generated by the SA apparatus; ○, at 283.15 K; △, at 293.15 K; □, at 303.15 K. — PRWS (NRTL) model.

Table 5-19. HPVLE data measured for the tetrafluoromethane (1) + perfluorooctane (2) binary system using the SA apparatus, listing the measured pressure (P), temperature (T), liquid (x_1) and vapour (y_1) phase compositions, and the expanded uncertainty[a].

T/K	P/MPa	x_1	y_1	$U(x_1)$	$U(y_1)$
283.15	1.617	0.237	0.9977	0.010	0.0002
283.15	2.456	0.320	0.9976	0.012	0.0002
283.15	3.453	0.426	0.9977	0.013	0.0002
283.15	5.508	0.588	0.9959	0.013	0.0003
283.12	6.279	0.642	0.9940	0.012	0.0004
283.15	7.364	0.710	0.9901	0.011	0.0006
283.12	8.129	0.765	0.9853	0.010	0.0009
283.15	9.006	0.827	0.9727	0.008	0.0017
293.15	2.244	0.270	0.9964	0.011	0.0003
293.16	3.271	0.367	0.9958	0.013	0.0003
293.15	3.753	0.410	0.9956	0.013	0.0003
293.15	4.867	0.504	0.9953	0.014	0.0003
293.16	6.303	0.597	0.9928	0.013	0.0005
293.15	7.941	0.701	0.9875	0.011	0.0008
293.15	8.767	0.750	0.9810	0.010	0.0012
293.16	9.345	0.786	0.9730	0.009	0.0017
293.15	9.999	0.838	0.9561	0.007	0.0027
303.15	1.874	0.216	0.9941	0.009	0.0004
303.14	3.079	0.325	0.9941	0.012	0.0004

Table 5-19 continued

T/K	P/MPa	x_1	y_1	$U(x_1)$	$U(y_1)$
303.15	3.990	0.412	0.9935	0.013	0.0004
303.16	5.044	0.476	0.9926	0.014	0.0005
303.15	5.936	0.537	0.9914	0.014	0.0006
303.16	7.032	0.600	0.9885	0.013	0.0007
303.16	8.056	0.666	0.9843	0.012	0.0010
303.16	9.151	0.733	0.9775	0.011	0.0014
303.16	10.088	0.788	0.9636	0.009	0.0023
303.16	10.780	0.857	0.9352	0.007	0.0039

[a] $U(P)$ = 0.007 MPa; $U(T)$ = 0.05 K.

Table 5-20. Experimental P-x data of tetrafluoromethane (1) + perfluorooctane (2) binary system at temperatures between (283.15-303.15) K measured using the SS apparatus, and the expanded uncertainty[a].

T/K	P/MPa	x_1	$U(x_1)$
283.18	1.89	0.256	0.007
283.16	4.30	0.503	0.004
283.14	6.39	0.649	0.003
283.17	9.28	0.850	0.001
293.16	2.11	0.256	0.007
293.14	4.82	0.503	0.004
293.16	7.03	0.649	0.003
293.19	10.10	0.850	0.001
303.16	2.31	0.256	0.007
303.15	5.26	0.503	0.004
303.12	7.66	0.649	0.003
303.14	10.75	0.850	0.001

[a] $U(P)$ = 0.01 MPa; $U(T)$ = 0.07 K.

The regressed model parameters and results of the statistical analysis of the model fit are provided in tables 5-21 (PRWS (NRTL) model) and 5-22 (PR (VdW) model). A comparison of the statistical analysis from data regression using either the PRWS (NRTL) or PR (VdW) model, shows smaller errors with the former. With the PR (VdW) model, the AAD(P) and AARD(P) % magnitudes of the errors are higher for pressure and composition indicating the better data fit of PRWS (NRTL) model. The average AAD(P) and AARD(P) % of PRWS model are 0.007 MPa and 1.42. The highest discrepancy is obtained for the system at 283.15 K isotherm with AAD(P) and AARD(P) % of 0.005 MPa and 2.31. The average AAD(y_1) and AARD(y_1)/% with PRWS model are 0.0007 and 0.13, respectively, and are 0.001 and 0.15 for their PR (VdW) model counterparts. It indicates that the PRWS model obtained a better fit to the experimental data.

Table 5-21. Regressed binary interaction parameters (k_{ij} and B_{ij}) and statistical analysis for the PRWS (NRTL) model for the binary system of tetrafluoromethane (1) + perfluorooctane (2)

	T = 283.15 K	*T* = 293.15 K	*T* = 303.15 K
k_{12} [a]	0.667	0.663	0.660
B_{12}/ K [b]	-112.8	422.2	544.7
B_{21}/ K [b]	106.6	-288.8	-351.0
AAD(*P*/MPa)	0.005	0.008	0.010
AARD(*P*/MPa)/%	2.31	0.72	1.23
AAD(y_1)	0.0004	0.0002	0.0015
AARD(y_1)/%	0.08	0.15	0.18

[a] k_{12} is the interaction parameter of the WS mixing rule.
[b] B_{12} and B_{21} are the temperature-dependent adjustable parameters of the NRTL model, and a non-randomness factor of α_{12} set to 0.3.

Table 5-22. Regressed binary interaction parameters (k_{ij}) and statistical analysis for the PR (VdW) model for the binary system of tetrafluoromethane (1) + perfluorooctane (2).

	T = 283.15 K	*T* = 293.15 K	*T* = 303.15 K
k_{12} [a]	0.016	0.021	0.020
AAD(*P*/MPa)	0.126	0.079	0.081
AARD(*P*/MPa)/%	3.90	2.13	2.65
AAD(y_1)	0.001	0.001	0.002
AARD(y_1)/%	0.10	0.17	0.19

[a] k_{12} is the binary interaction parameter for the classical mixing rule in the PR (VdW) model.

Summary of the data measured

The three systems presented in sections 5.6.1 to 5.6.3 compare the solubility of tetrafluoromethane with straight-chain perfluoroalkanes (C6, C7 and C8) which is shown in figure 5-5 for the temperature of 283.15 K. Considering a constant composition of x_{CF_4}= 0.5 and temperature of 283.15 K, the isotherm with the lowest pressure is 4 MPa with the perfluorohexane solvent. The highest pressure is 4.6 MPa with perfluorooctane solvent.

As the length of the carbon chain decreases, the solubility improves and the solvent-solute interactions become ideal. As the C-chain increase, the molecular interactions show an increasing departure as evident in the k_{ij} values reported in tables 5-14, 5-18 and 5-22. The solubility of tetrafluoromethane in the three solvents is almost similar up to the equimolar condition though for compositions greater than 0.5, it is improved for the smaller chain perfluoroalkanes (C6).
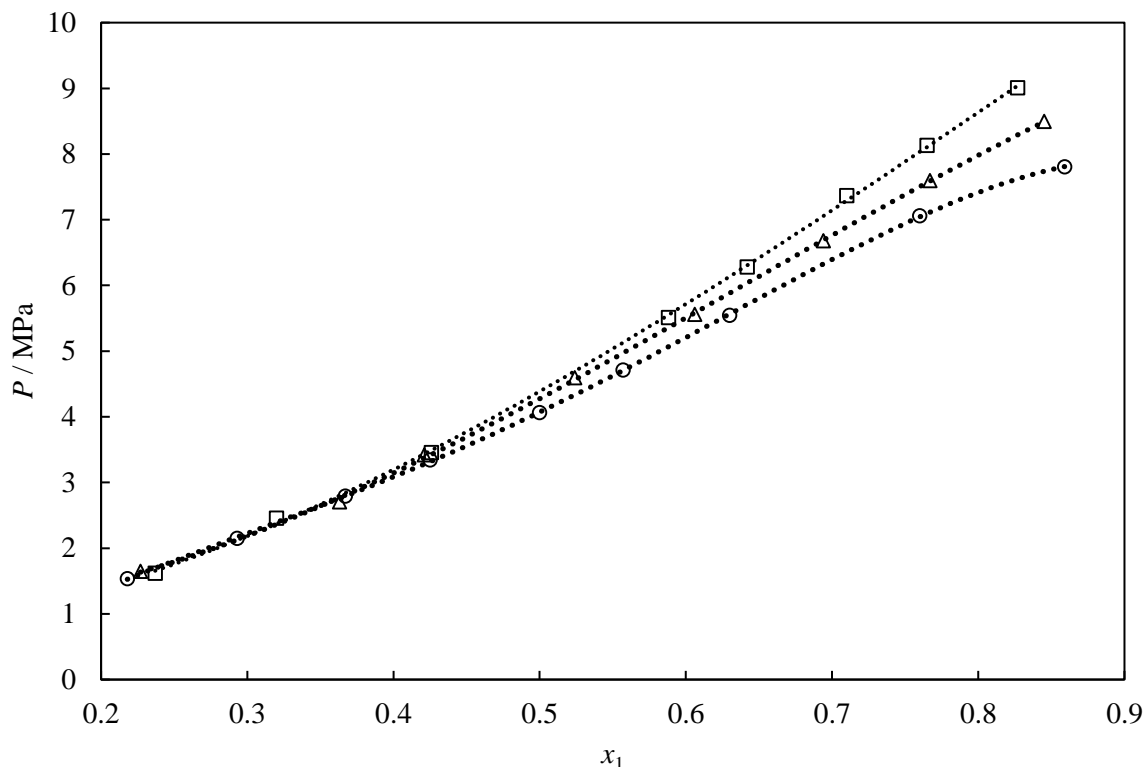
Figure 5-5. *P-x* data for the tetrafluoromethane (1) + either ○, perfluorohexane (2) △, perfluoroheptane (2) or □, perfluorooctane (2) binary systems at the temperature of 283.15 K.

5.6.4 CF$_4$ + C$_{10}$F$_{18}$ (perfluorodecalin)

New *P-x* data were measured for the tetrafluoromethane + perfluorodecalin binary system at three isotherms in the range of (283.15 to 303.15) K. The experimental data are listed in table 5-23 and are shown in figure 5-6. The experimental data were modelled using the PRWS (NRTL) model. The specified error bars on the figure are the uncertainties associated with the data points which were within ±0.012.

The pressure of the data measured is in the range between (2.1 to 7.1) MPa. As the data generated from both apparatuses were consistent and given the high price of perfluorodecalin, the experimental data were measured only via the SS apparatus. The amount of material required for every experiment following the SS method is at most 3.5 ml, and it can be recovered while venting the mixture. A minimum volume of 13 ml was required for measurements using the SA apparatus with several top up of solvent which is another important factor to consider.
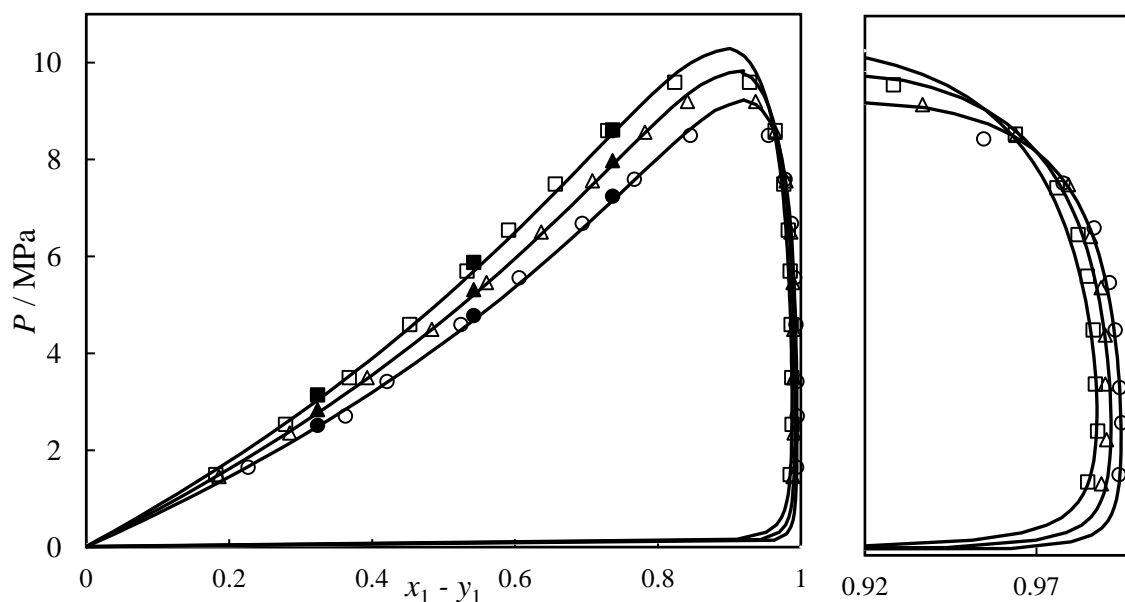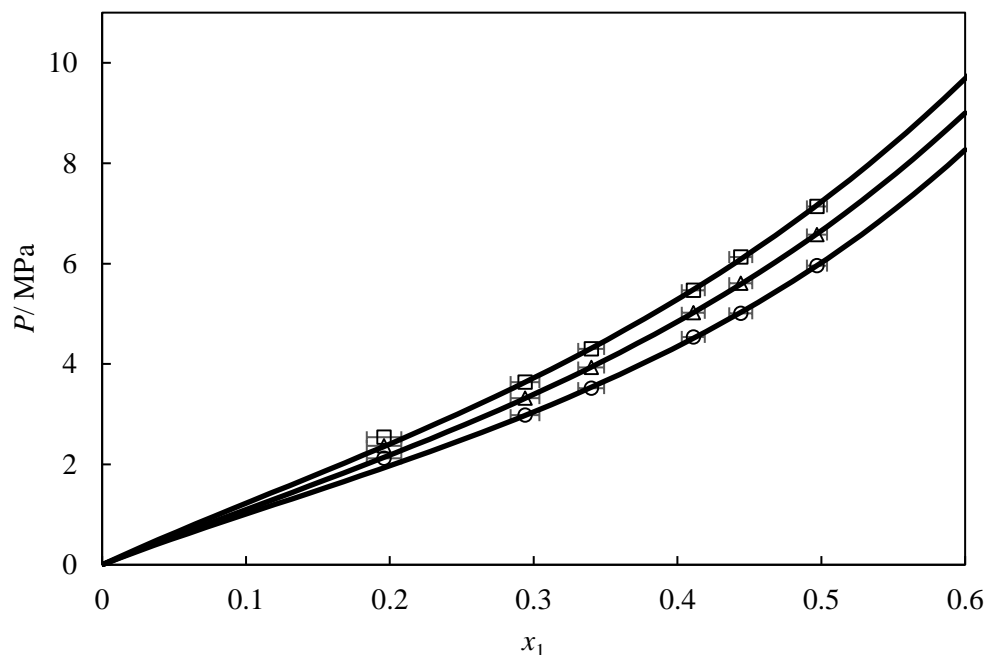
Figure 5-6. *P-x* data for the tetrafluoromethane (1) + perfluorodecalin (2) binary system. Experimental data generated by the SS apparatus; ○, at 283.14 K; △, at 293.15 K; □, at 303.16 K. — PRWS (NRTL) model.

Table 5-23. Experimental *P-x* data of tetrafluoromethane (1) + perfluorodecalin (2) binary system at temperatures between (283.15-303.15) K measured using the SS apparatus, and the expanded uncertainty[a].

T/K	*P*/MPa	x_1	$U(x_1)$
283.15	2.12	0.196	0.012
283.16	2.98	0.294	0.010
283.15	3.52	0.340	0.009
283.15	4.54	0.411	0.008
283.14	5.01	0.444	0.008
283.16	5.96	0.497	0.007
293.17	2.37	0.196	0.012
293.14	3.32	0.294	0.010
293.15	3.93	0.340	0.009
293.12	5.02	0.411	0.008
293.16	5.61	0.444	0.008
293.16	6.58	0.497	0.007
303.14	2.54	0.196	0.012
303.16	3.64	0.294	0.010
303.13	4.30	0.340	0.009
303.18	5.47	0.411	0.008
303.18	6.13	0.444	0.008
303.15	7.14	0.497	0.007

[a] *U(P)* = 0.01 MPa; *U(T)* = 0.07 K.

The model parameters regressed and results of the statistical analysis are provided in tables 5-24 (PRWS (NRTL) model) and (PR (VdW) model) 5-25. Only bubble point data were measured using the SS apparatus disabling the statistical analysis for the vapour phase composition. On comparison of the two model results, the PR (VdW) model shows greater errors (maximum AAD(P) of 0.037 MPa and maximum AARD(P) % of 0.78) compared to that of the PRWS (NRTL) model (maximum AAD(P) of 0.019 MPa and maximum AARD(P) % of 0.32).

Table 5-24. Regressed binary interaction parameters (k_{ij} and B_{ij}) and statistical analysis for the PRWS (NRTL) model for the binary system of tetrafluoromethane (1) + perfluorodecalin (2).

	$T = 283.15$ K	$T = 293.15$ K	$T = 303.15$ K
k_{12} [a]	0.728	0.718	0.714
B_{12}/ K [b]	-1.215	-1.179	-1.220
B_{21}/ K [b]	2.060	1.925	2.034
AAD(P/MPa)	0.013	0.011	0.019
AARD(P/MPa)/%	0.30	0.20	0.32

[a] k_{12} is the interaction parameter of the WS mixing rule.
[b] B_{12} and B_{21} are the temperature-dependent adjustable parameters of the NRTL model, and a non-randomness factor of α_{12} set to 0.3.

Table 5-25. Regressed binary interaction parameters (k_{ij}) and statistical analysis for the PR (VdW) model for the binary system of tetrafluoromethane (1) + perfluorodecalin (2).

	$T = 283.15$ K	$T = 293.15$ K	$T = 303.15$ K
k_{12} [a]	0.026	0.024	0.021
AAD(P/MPa)	0.037	0.033	0.031
AARD(P/MPa)/%	0.78	0.62	0.55

[a] k_{12} is the binary interaction parameter for the classical mixing rule in the PR (VdW) model.

5.6.5 CF$_4$ + C$_5$H$_4$F$_8$O (tetrafluoroethyl, tetrafluoropropyl ether)

New HPVLE data were measured for the tetrafluoromethane + tetrafluoroethyl, tetrafluoropropyl ether binary system at three isotherms in the range of (283.15 to 303.15) K. The experimental data are shown in tables 5-26 (SA apparatus), and 5-27 (SS apparatus) and are displayed in figure 5-7. The experimental data measured from two equipment display a satisfactory thermodynamic consistency. The model gives a good representation of the experimental data. Only at the pressures higher than 20.00 MPa, slight departure is noticeable between experimental data and modelling results. For the measurements of the phase behaviour data following the SA method, it was observed that there was poor temperature dependency of the mixture at 293.15 and 303.15 K. Hence the data were measured at 303.15 K up to pressures of 10 MPa. The temperature of the bath was then decreased to 293.15 K to measure the remaining data points for the full isotherm. For measurements at pressures higher than 20.00 MPa, the PTFE O-rings was not able to withstand the conditions and failed to seal the

equilibrium cell. The test was repeated with a new polyurethane O-ring which failed at pressures higher than 20 MPa once more.
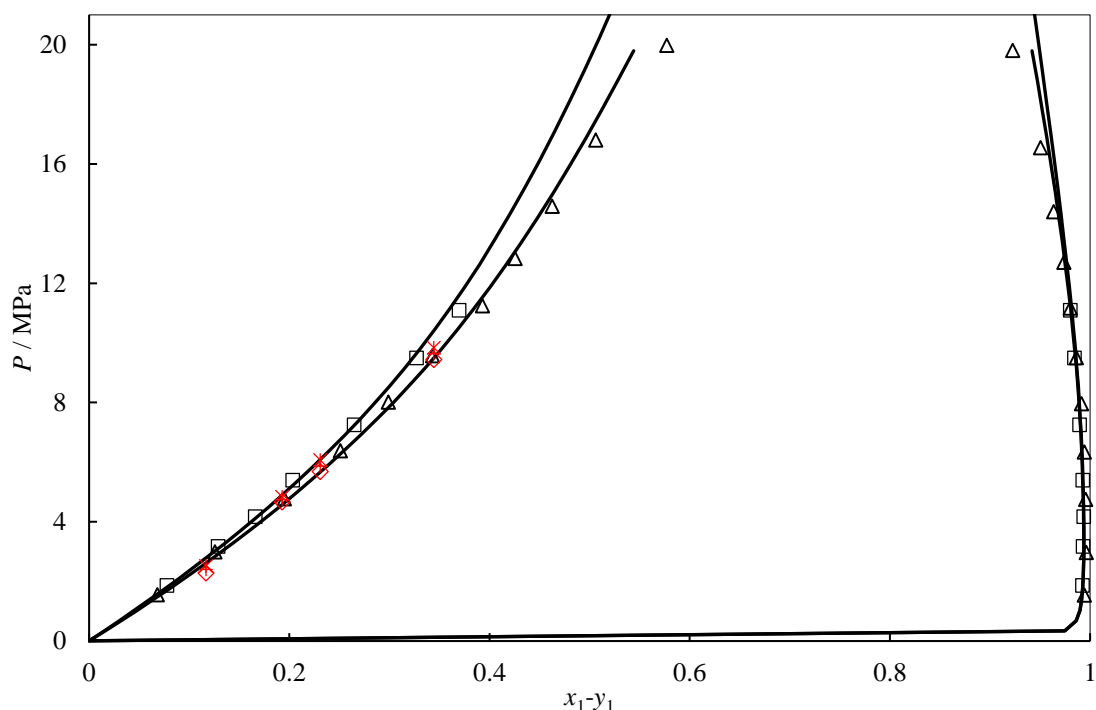
Figure 5-7. HPVLE data for the tetrafluoromethane (1) + 1,1,2,2-1,1,2,2-tetrafluoroethyl 2,2,3,3-tetrafluoropropyl ether (2) binary system. Experimental data generated by the SS apparatus; ◊, at 283.16 K; ×, at 293.19 K; ∗, at 303.14 K. Experimental data generated by the SA apparatus; △, at 293.15 K; □, at 303.16 K. ― PR (VdW) model.

Table 5-26. HPVLE data measured for the tetrafluoromethane (1) + 1,1,2,2-tetrafluoroethyl 2,2,3,3-tetrafluoropropyl ether (2) binary system using the SA apparatus, listing the measured pressure (P), temperature (T), liquid (x_1) and vapour (y_1) phase compositions, and the expanded uncertainty[a].

T/K	P/MPa	x_1	y_1	$U(x_1)$	$U(y_1)$
293.15	1.559	0.068	0.9941	0.006	0.0006
293.15	2.996	0.126	0.9963	0.007	0.0008
293.15	4.778	0.195	0.9959	0.009	0.0007
293.16	6.385	0.251	0.9941	0.011	0.0013
293.16	8.010	0.299	0.9908	0.012	0.0008
293.16	9.574	0.343	0.9857	0.012	0.0009
293.16	11.242	0.393	0.9804	0.013	0.0008
293.15	12.830	0.426	0.9741	0.013	0.0006
293.15	14.582	0.463	0.9640	0.013	0.0017
293.15	16.801	0.506	0.9504	0.015	0.0011
293.14	19.978	0.577	0.9229	0.014	0.0009
303.16	1.863	0.078	0.9923	0.012	0.0006
303.15	3.171	0.129	0.9926	0.012	0.0005
303.16	4.170	0.166	0.9937	0.010	0.0011
303.16	5.394	0.204	0.9925	0.010	0.0006
303.16	7.251	0.265	0.9898	0.018	0.0015

Table 5-26 continued.

T/K	P/MPa	x_1	y_1	$U(x_1)$	$U(y_1)$
303.16	9.498	0.327	0.9835	0.007	0.0011
303.16	11.095	0.370	0.9802	0.007	0.0007

[a] $U(P) = 0.007$ MPa; $U(T) = 0.05$ K.

Table 5-27. Experimental P-x data of tetrafluoromethane (1) + 1,1,2,2-tetrafluoroethyl 2,2,3,3-tetrafluoropropyl ether (2) binary system at temperatures between (283.15-303.15) K measured using the SS apparatus, and the expanded uncertainty[a].

T/K	P/MPa	x_1	$U(x_1)$
283.16	2.28	0.117	0.007
283.15	4.66	0.193	0.005
283.15	5.69	0.231	0.004
283.15	9.45	0.344	0.003
293.14	2.40	0.117	0.007
293.17	4.74	0.193	0.005
293.17	5.87	0.231	0.004
293.16	9.64	0.344	0.003
303.15	2.53	0.117	0.007
303.18	4.84	0.193	0.005
303.18	6.08	0.231	0.004
303.17	9.84	0.344	0.003

[a] $U(P) = 0.01$ MPa; $U(T) = 0.05$ K.

The regressed binary interaction parameters are listed in tables 5-28 (PRWS (NRTL) model) and 5-29 (PR (VdW) model). The experimental results show a large deviation from ideality which can be justified due to the difference in intermolecular forces resulting from the mixing of a completely non-polar gas with a hydrogen-bonding compound. The results of the modelling show that the deviation of the model from experimental data is less with the PRWS (NRTL) model compared to results obtained from PR (VdW) model.

Table 5-28. Regressed binary interaction parameters (k_{ij} and B_{ij}) and statistical analysis for the PRWS (NRTL) model for the binary system of tetrafluoromethane (1) + 1,1,2,2-tetrafluoroethyl 2,2,3,3-tetrafluoropropyl ether (2).

	$T = 283.15$ K	$T = 293.15$ K	$T = 303.15$ K
k_{12} [a]	---	0.401	0.604
B_{12}/ K [b]	---	326.6	620.3
B_{21}/ K [b]	---	269.5	-126.6
AAD(P/MPa)	---	0.080	0.002
AARD(P/MPa)/%	---	9.198	0.531
AAD(y_1)	---	0.017	0.0001
AARD(y_1)/%	---	2.00	0.06

[a] k_{12} is the interaction parameter of the WS mixing rule.
[b] B_{12} and B_{21} are the temperature-dependent adjustable parameters of the NRTL model, and the non-randomness factor of α_{12} set to 0.3.

Table 5-29. Regressed binary interaction parameters (k_{ij}) and statistical analysis for the PR (VdW) model for the binary system of tetrafluoromethane (1) + 1,1,2,2-tetrafluoroethyl 2,2,3,3-tetrafluoropropyl ether (2).

	$T = 283.15$ K	$T = 293.15$ K	$T = 303.15$ K
k_{12} [a]	---	0.112	0.125
AAD(P/MPa)	---	0.15	0.05
AARD(P/MPa)/%	---	6.16	2.21
AAD(y_1)	---	0.002	0.001
AARD(y_1)/%	---	0.27	0.07

[a] k_{12} is the binary interaction parameter for the classical mixing rule in the PR (VdW) model.

5.6.6 CF$_4$ + C$_4$H$_3$F$_7$O (heptafluoro, 1-butanol)

New HPVLE data were measured for the tetrafluoromethane + heptafluoro, 1-butanol binary system at three isotherms in the range of (283.15 to 303.15) K. The experimental data are shown in table 5-30 (SS method) and are displayed in figure 5-8. The HPVLE data were modelled using the PRWS (NRTL) and PR (VdW) models. Regressed binary interaction parameters are listed in tables 5-31 (PRWS (NRTL) model) and 5-32 (PR (VdW) model).

The uncertainties associated with the data points are shown in the figure by the error bars with a maximum uncertainty of ± 0.009. As mentioned previously, due to time constraints and limited chemicals, the measurements were performed following the SS method. The smaller liquid volume resulted in a low mass of gas loaded. As it was mentioned in chapter 4, the mixtures were prepared gravimetrically and the masses played an essential role in the uncertainty of the composition. Due to the low masses loaded into the equilibrium cell, the uncertainties associated with the experimental data are relatively high.
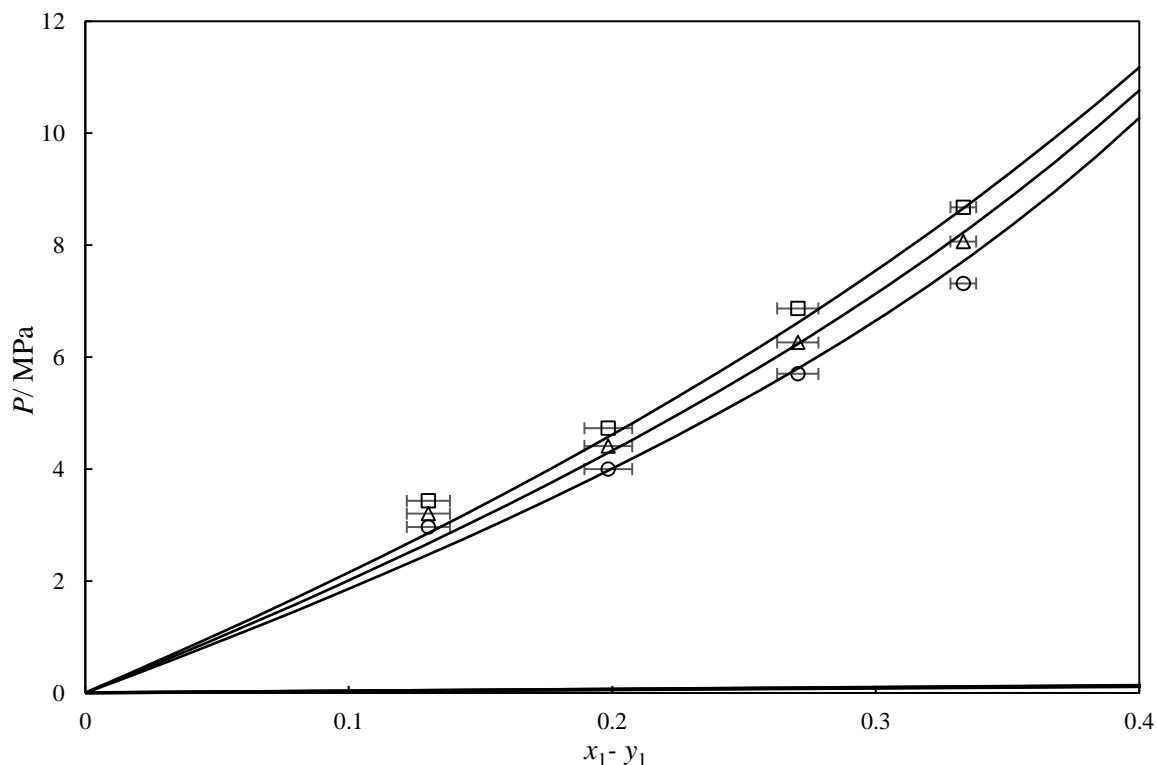
Figure 5-8. *P-x* data for the tetrafluoromethane (1) + heptafluoro, 1-butanol (2) binary system. Experimental data generated by the SS apparatus; ○, at 283.14 K; △, at 293.15 K; □, at 303.16 K. — PRWS (NRTL) model.

Table 5-30. Experimental *P-x* data of tetrafluoromethane (1) + heptafluoro, 1-butanol (2) binary system at temperatures between (283.15-303.15) K measured using the SS apparatus, and the expanded uncertainty[a].

T/K	P/MPa	x_1	$U(x_1)$
283.13	2.96	0.130	0.008
283.13	4.00	0.198	0.009
283.14	5.70	0.270	0.008
283.13	7.32	0.333	0.005
293.15	3.20	0.130	0.008
293.18	4.41	0.198	0.009
293.15	6.26	0.270	0.008
293.15	8.07	0.333	0.005
303.18	3.43	0.130	0.008
303.18	4.73	0.198	0.009
303.19	6.87	0.270	0.008
303.17	8.68	0.333	0.005

[a] $U(P) = 0.01$ MPa; $U(T) = 0.07$ K.

Table 5-31. Regressed binary interaction parameters (k_{ij} and B_{ij}) and statistical analysis for the PRWS (NRTL) model for the binary system of tetrafluoromethane (1) + heptafluoro, 1-butanol (2).

	T = 283.15 K	*T* = 293.15 K	*T* = 303.15 K
k_{12} [a]	0.980	1.001	1.022
B_{12}/ K [b]	-457.9	-485.9	-512.8
B_{21}/ K [b]	1333.6	1421.6	1520.3
AAD(*P*/MPa)	0.031	0.046	0.063
AARD(*P*/MPa)/%	2.988	3.221	3.642

[a] k_{12} is the interaction parameter of the WS mixing rule.
[b] B_{12} and B_{21} are the temperature-dependent adjustable parameters of the NRTL model, and a non-randomness factor of α_{12} set to 0.3.

Table 5-32. Regressed binary interaction parameters (k_{ij}) and statistical analysis for the PR (VdW) model for the binary system of tetrafluoromethane (1) + heptafluoro, 1-butanol (2).

	T = 283.15 K	*T* = 293.15 K	*T* = 303.15 K
k_{12} [a]	0.071	0.074	0.078
AAD(*P*/MPa)	0.044	0.026	0.008
AARD(*P*/MPa)/%	6.00	5.51	4.74

[a] k_{12} is the binary interaction parameter for the classical mixing rule in the PR (VdW) model.

Summary of the solubility of tetrafluoromethane in solvents.

The solubility data of tetrafluoromethane in six different systems were presented. The system (CF_4 + C_6F_{14}) presented in section 5.6.1 shows the highest solubility of tetrafluoromethane, while the system (CF_4 + $C_5H_4F_8O$) presented in section 5.6.6 displays the lowest solubility for tetrafluoromethane. For example, at the pressure of approximately 5.50 MPa and temperature of 283.15 K, the solubility of tetrafluoromethane was just above 0.61. This is well over twice as much of its solubility in heptafluoro, 1-butanol at 0.28 mole fraction. The phase data for CF_4 + C_6F_{14} confirms the like-like interactions, showing improved solubility as per classification of physical properties method.

5.7 Phase equilibrium measurements for systems with NF₃

Due to the highly toxic nature of NF_3, data for the NF_3 systems were measured via the SS method. Hence, only the bubble point data was measured. Before starting the measurements, a meticulous safe operating method was designed and a test system of CO_2 + C_6H_{14} measured following the exact procedures. After the confirmation of the technique, four different binary systems of NF_3 with liquid solvents, perfluorohexane, perfluorodecalin, perfluoroalcohol and perfluoroether were measured.

The systems presented consisted of the same chemicals tested with tetrafluoromethane, however, due to the improved solubility in PFCs, only C6 (perfluorohexane) was tested from the straight-chain PFCs with NF_3. An overview of the systems measured (NF_3 + solvents) is presented in table 5-33.

Table 5-33. Overview of the binary systems (NF_3 + solvents) measured in this work, 'l' and 'g' denotes whether the component is either a liquid or gas at ambient conditions.

Gas	Liquid solvent	Temperature/ K	Pressure/ MPa	No. of points
NF_3 (g)	C_6F_{14} (l)	283.15 – 303.15	2.4 – 9.3	18
NF_3 (g)	$C_5H_4F_8O$ (l)	283.15 – 303.15	3 – 8.4	18
NF_3 (g)	$C_{10}F_{18}$ (l)	283.15 – 303.15	2 – 7.1	18
NF_3 (g)	$C_4H_3F_7O$ (l)	283.15 – 303.15	3.5 – 8.7	12

5.7.1 NF_3 + C_6F_{14} (perfluorohexane)

New HPVLE data were measured for the nitrogen trifluoride + perfluorohexane binary system at three isotherms in the range of (283.15 to 303.15) K and pressures ranging from (1.9 to 8.3) MPa. The experimental data are shown in table 5-34 (SS apparatus) and are displayed in figure 5-9. The experimental data were modelled using the PR (VdW) model. The maximum expanded uncertainty associated with the experimental data was ± 0.011 which is indicated for each data point by the error bars in figure 5-9.

The solubility of NF_3 in C_6F_{14} is similar to that of CF_4 with a minor improved solubility of NF_3. Due to the helical structure of the perfluoroalkanes (C4 <), the solvent has a dipole moment (Fournier et al., 2011). Two free electrons exist in the structure of the NF_3, which are delocalized in the presence of a polar component. The delocalised molecule interacts with the molecule (Bruice, 2003). The system of NF_3 + C_6F_{14} represents a gaseous molecule with a delocalised electron mixed with a slightly polar molecule. The interactions in the mixture increase the solubility of NF_3.

Figure 5-9. *P-x* data for the nitrogen trifluoride (1) + perfluorohexane (2) binary system. Experimental data generated by the SS apparatus; ○, at 283.14 K; △, at 293.15 K; □, at 303.16 K. ― PRWS (NRTL) model; --- tetrafluoromethane (1) + perfluorohexane (2) at 293.15 K.

Table 5-34. Experimental *P-x* data of nitrogen trifluoride (1) + perfluorohexane (2) binary system at temperatures between (283.15-303.15) K measured using the SS apparatus, and the expanded uncertainty[a].

T/K	P/MPa	x_1	$U(x_1)$
283.15	1.96	0.281	0.011
283.16	2.56	0.343	0.009
283.15	3.88	0.473	0.008
283.15	5.01	0.580	0.006
283.14	6.05	0.671	0.002
283.16	6.93	0.747	0.003
293.17	2.24	0.280	0.011
293.14	2.83	0.337	0.009
293.15	4.28	0.466	0.008
293.12	5.59	0.577	0.006
293.16	6.80	0.674	0.002
293.16	2.24	0.282	0.003
303.14	2.47	0.283	0.011
303.16	3.10	0.341	0.009
303.13	4.73	0.465	0.008
303.18	6.03	0.583	0.006
303.18	7.24	0.669	0.002

[a] $U(P) = 0.01$ MPa; $U(T) = 0.07$ K.

The regressed model parameters and results of the statistical analysis are provided in tables 5-35 (PRWS (NRTL) model) and (PR (VdW) model) 5-36. In terms of model errors, the PR (VdW) model gives a better representation of experimental data (maximum AAD(P) of 0.171 MPa and maximum AARD(P) % of 3.93) compared to that of PRWS (NRTL) model (maximum AAD(P) of 0.188 MPa and maximum AARD(P) % of 7.04).

Table 5-35. Regressed binary interaction parameters (k_{ij} and B_{ij}) and statistical analysis for the PRWS (NRTL) model for the binary system of nitrogen trifluoride (1) + perfluorohexane (2).

	$T = 283.15$ K	$T = 293.15$ K	$T = 303.15$ K
k_{12} [a]	0.637	0.666	0.667
B_{12}/ K [b]	175	192	233
B_{21}/ K [b]	-191	-208	-260
AAD(P/MPa)	0.107	0.143	0.188
AARD(P/MPa)/%	5.40	5.03	7.04

[a] k_{12} is the interaction parameter of the WS mixing rule.
[b] B_{12} and B_{21} are the temperature-dependent adjustable parameters of the NRTL model, and a non-randomness factor of α_{12} set to 0.3.

Table 5-36. Regressed binary interaction parameters (k_{ij}) and statistical analysis for the PR (VdW) model for the binary system of nitrogen trifluoride (1) + perfluorohexane (2).

	$T = 283.15$ K	$T = 293.15$ K	$T = 303.15$ K
k_{12} [a]	0.013	0.022	0.022
AAD(P/MPa)	0.171	0.106	0.115
AARD(P/MPa)/%	3.93	3.06	2.82

[a] k_{12} is the binary interaction parameter for the classical mixing rule in the PR (VdW) model.

5.7.2 NF_3 + $C_{10}F_{18}$ (perfluorodecalin)

New HPVLE data were measured for the nitrogen trifluoride + perfluorodecalin binary system at three isotherms in the range of (283.15 to 303.15) K and pressures ranging from (1.9 to 9.8) MPa. The experimental data are shown in table 5-37 (SS method) and are displayed in figure 5-11. The model shows large discrepancies at the low and high-pressure range.

The solubility of NF_3 in perfluorodecalin is more than that of CF_4. The molecular structure of the perfluorodecalin consists of two attached single-bonded cycles of carbon covered with a massive electron cloud of fluorine atoms which is displayed in figure 5-10. Considering the delocalisation effect on the NF_3 molecule, the positive part of the NF_3 interacts with the perfluorodecalin molecule and improves the solubility compared to CF_4.
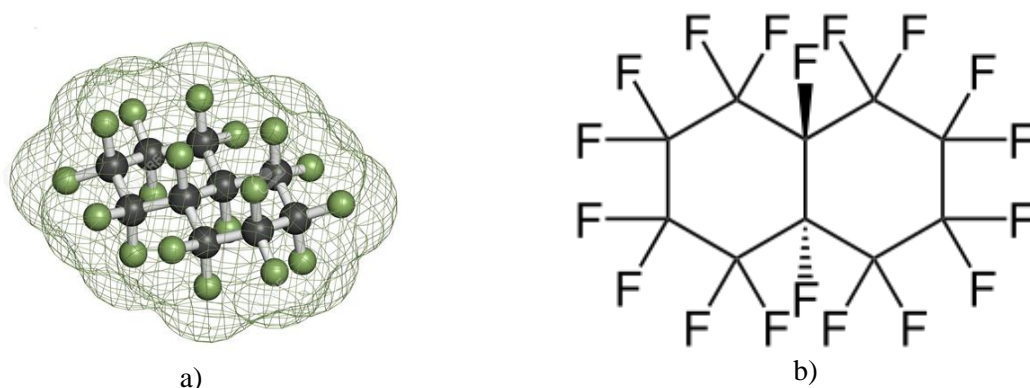
Figure 5-10. Molecular structure of perfluorodecalin a) massive electron cloud around the molecule, b) single bounded cycles of $C_{10}F_{18}$.

The greatest expanded uncertainty associated with the measured data was at the lowest composition measured with ± 0.17. A minimum volume of solvent of 3.5 ml was used to prepare the initial mixture. Due to the small volume of the gas dissolved, very small fluctuations in the mass balance causes higher uncertainties. The bubble point of this data point was measured 3 times by depressurising and pressurising the cell with the same mixture. The difference between the measured data was well within 0.01 MPa. It is clear that the uncertainty decreased as the composition increased. The minimum uncertainty of ± 0.003 was estimated at NF_3 composition of 0.697.
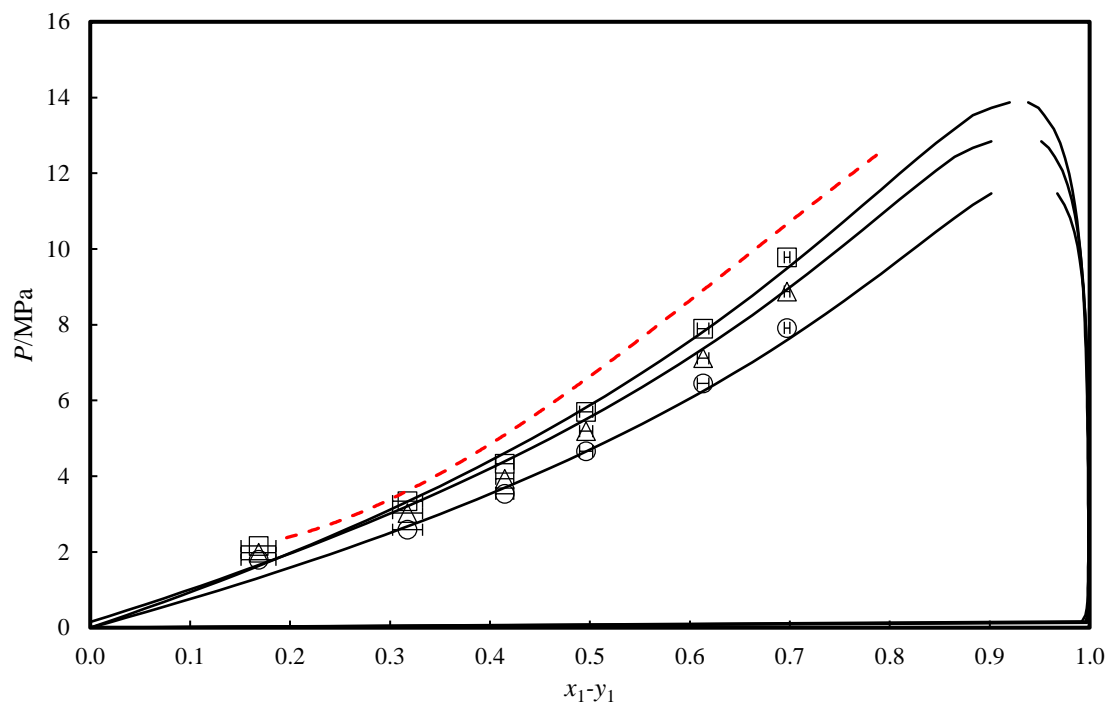
Figure 5-11. *P-x* data for the nitrogen trifluoride (1) + perfluorodecalin (2) binary system. Experimental data generated by the SS apparatus; $\bigcirc$, at 283.14 K; $\triangle$, at 293.15 K; $\square$, at 303.16 K. — PRWS (NRTL) model; --- tetrafluoromethane (1) + 1perfluorodecalin (2) at 293.15 K.

Table 5-37. Experimental *P-x* data of nitrogen trifluoride (1) + perfluorodecalin (2) binary system at temperatures between (283.15-303.15) K measured using the SS apparatus, and the expanded uncertainty[a].

T/K	*P*/MPa	x_1	$U(x_1)$
283.15	1.79	0.168	0.017
283.16	2.59	0.318	0.015
283.15	3.58	0.415	0.009
283.15	4.66	0.496	0.007
283.14	6.45	0.613	0.006
283.16	7.92	0.697	0.003
293.17	1.98	0.168	0.017
293.14	3.03	0.318	0.015
293.15	3.93	0.415	0.009
293.12	5.19	0.496	0.007
293.16	7.16	0.613	0.006
293.16	8.88	0.697	0.003
303.14	2.16	0.168	0.017
303.16	3.34	0.318	0.015
303.13	4.33	0.415	0.009
303.18	5.70	0.496	0.007
303.18	7.90	0.613	0.006
303.15	9.78	0.697	0.003

[a] $U(P) = 0.01$ MPa; $U(T) = 0.07$ K.

The regressed model parameters and results of the statistical analysis are provided in tables 5-38 (PRWS (NRTL) model) and 5-39 (PR (VdW) model). In terms of model errors, the PR (VdW) model gives a better representation of experimental data.

Table 5-38. Regressed binary interaction parameters (k_{ij} and B_{ij}) and statistical analysis for the PRWS (NRTL) model for the binary system of nitrogen trifluoride (1) + perfluorodecalin (2).

	T = 283.15 K	*T* = 293.15 K	*T* = 303.15 K
k_{12} [a]	0.763	0.770	0.776
B_{12}/ K [b]	-360	-372	-391
B_{21}/ K [b]	1282	1355	1423
AAD(*P*/MPa)	0.117	0.204	0.284
AARD(*P*/MPa)/%	5.20	5.67	5.85

[a] k_{12} is the interaction parameter of the WS mixing rule.
[b] B_{12} and B_{21} are the temperature-dependent adjustable parameters of the NRTL model, and a non-randomness factor of α_{12} set to 0.3.

Table 5-39. Regressed binary interaction parameters (k_{ij}) and statistical analysis for the PR (VdW) model for the binary system of nitrogen trifluoride (1) + perfluorodecalin (2).

	T = 283.15 K	*T* = 293.15 K	*T* = 303.15 K
k_{12} [a]	0.007	0.007	0.006
AAD(*P*/MPa)	0.188	0.175	0.166
AARD(*P*/MPa)/%	7.15	6.84	6.63

[a] k_{12} is the binary interaction parameter for the classical mixing rule in the PR (VdW) model.

5.7.3 NF₃ + C₅H₄F₈O (TFE–TFP ether)

New HPVLE data were measured for the nitrogen trifluoride + tetrafluoroethyl, tetrafluoropropyl ether binary system at three temperatures between (283.15 to 303.15) K and pressures ranging from (2.1 to 10.26) MPa. The experimental data are shown in table 5-40 (SS apparatus) and are displayed in figure 5-12.

The TFE-TFP ether is a polar asymmetric molecule. Nitrogen trifluoride is a slightly polar compound. Upon mixing of the pure components the ΔH_{mix} is positive resulting in endothermic process. Considering the nonpolar structure of tetrafluoromethane, the presence of unlike interactions decreases the solubility of CF_4.

The maximum uncertainty of the measured data is ± 0.009 for the composition of 0.130. As the composition increases, the uncertainty reduced. The minimum uncertainty is 0.004 which is estimated at the composition of 0.452. The solubility of TFE-TFP ether in nitrogen fluoride is temperature dependent with improved solubility at a lower temperature, however, its solubility changes slightly with temperature.
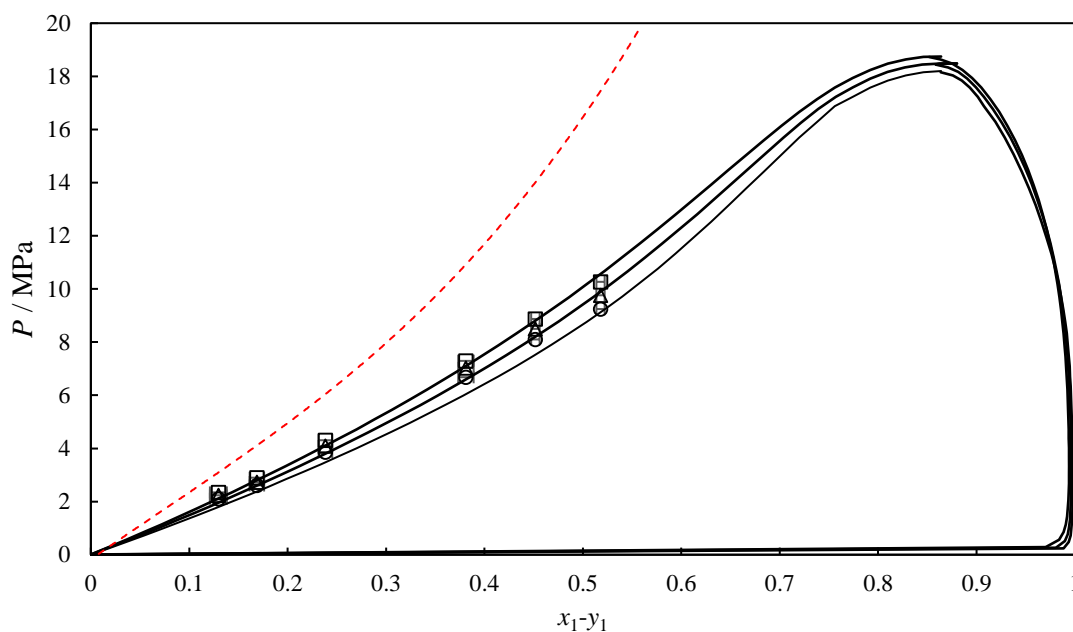
Figure 5-12. *P-x* data for the binary system of nitrogen trifluoride (1) + 1,1,2,2-tetrafluoroethyl 2,2,3,3-tetrafluoropropyl ether (2). Experimental data generated by the SS apparatus; ○, at 283.14 K; △, at 293.15 K; □, at 303.16 K. ― PRWS (NRTL) model; --- tetrafluoromethane (1) + 1,1,2,2-tetrafluoroethyl 2,2,3,3-tetrafluoropropyl ether (2) at 293.15 K.

Table 5-40. Experimental data for the nitrogen trifluoride (1) + 1,1,2,2-tetrafluoroethyl 2,2,3,3-tetrafluoropropyl ether (2) binary system using the SS apparatus listing the pressure (P), temperature (T), liquid phase composition (x_1), and the expanded uncertainty[a].

T/K	P/MPa	x_1	$U(x_1)$
283.15	1.89	0.130	0.009
283.16	2.39	0.169	0.007
283.15	3.46	0.238	0.007
283.15	6.08	0.381	0.008
283.14	7.53	0.452	0.004
283.16	8.95	0.518	0.004
293.17	2.11	0.130	0.009
293.14	2.61	0.169	0.007
293.15	3.86	0.238	0.007
293.12	6.68	0.381	0.008
293.16	8.11	0.452	0.004
293.16	9.77	0.518	0.004
303.14	2.34	0.130	0.009
303.16	2.90	0.169	0.007
303.13	4.31	0.238	0.007
303.18	7.30	0.381	0.008
303.18	8.87	0.452	0.004
303.15	10.26	0.518	0.004

[a] $U(P) = 0.01$ MPa; $U(T) = 0.07$ K.

The regressed model parameters and results of the statistical analysis are provided in table 5-41 (PRWS (NRTL) model) and (PR (VdW) model) table 5-42. Statistically, the PR (VdW) model shows a better representation of the experimental data, though the difference in errors between the two models is not significant. The magnitude of the k_{ij} from PR (VdW) model at temperatures of 283.15, 293.15, and 303.15 is 0.19, 0.15, and 0.08, respectively. This indicates the positive deviation from Raoult's law. At the higher temperature, the PR (VdW) model is better.

The AARD(P) % calculated for the PR (WS) model is 6 on average which is relatively high, while it is low for PR (VdW) model, but it is just below 4 on average. The highest AARD(P) % and AAD(P) errors were obtained at the low temperature for PR (VdW) with 4.19 % and 0.19 MPa, respectively while their PRWS (NRTL) model counterpart obtained at 303.15 K with 6.28 % and 0.16 MPa, respectively.

Table 5-41. Regressed binary interaction parameters (k_{ij} and B_{ij}) and statistical analysis for the PRWS (NRTL) model for the binary system of nitrogen trifluoride (1) + tetrafluoroethyl, tetrafluoropropyl ether (2).

	T = 283.15 K	*T* = 293.15 K	*T* = 303.15 K
k_{12} [a]	0.820	0.824	0.822
B_{12}/ K [b]	-400	-421	-428
B_{21}/ K [b]	943	1012	1021
AAD(*P*/MPa)	0.08	0.12	0.16
AARD(*P*/MPa)/%	5.74	6.07	6.28

[a] k_{12} is the interaction parameter of the WS mixing rule.
[b] B_{12} and B_{21} are the temperature-dependent adjustable parameters of the NRTL model, and a non-randomness factor of α_{12} set to 0.3.

Table 5-42. Regressed binary interaction parameters (k_{ij}) and statistical analysis for the PR (VdW) model for the binary system of nitrogen trifluoride (1) + tetrafluoroethyl, tetrafluoropropyl ether (2).

	T = 283.15 K	*T* = 293.15 K	*T* = 303.15 K
k_{12} [a]	0.080	0.082	0.087
AAD(*P*/MPa)	0.19	0.15	0.08
AARD(*P*/MPa)/%	4.19	3.54	4.07

[a] k_{12} is the binary interaction parameter for the classical mixing rule in the PR (VdW) model.

5.7.4 NF$_3$ + C$_4$H$_3$F$_7$O (heptafluoro, 1-butanol)

New HPVLE data were measured for the nitrogen trifluoride + heptafluoro, 1-butanol binary system at three temperatures between (283.15 to 303.15) K and pressures ranging from (2.5 to 8.8) MPa. The experimental data are shown in table 5-43 (SS method) and are displayed in figure 5-13. The error bars indicate the uncertainties associated with the measured experimental data. The error of the model is within the calculated uncertainty range (the maximum error is smaller than 0.008). As a polar gas, the solubility of NF$_3$ in heptafluoro, 1-butanol is higher than that of CF$_4$. It is due to the like-like interactions between NF$_3$ and perfluorinated alcohol.
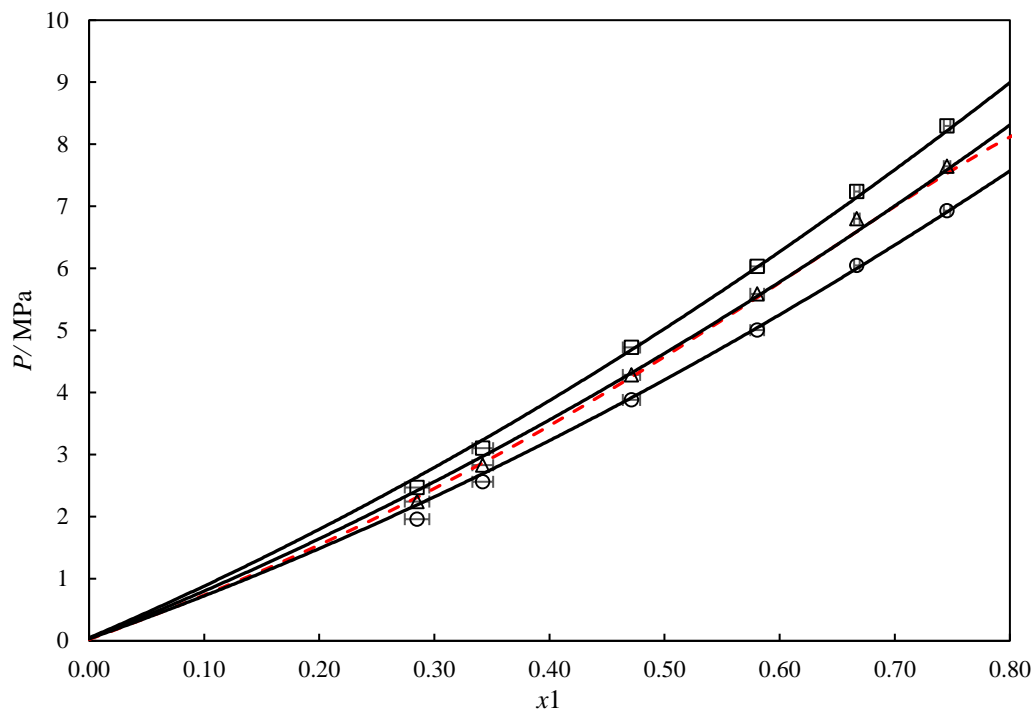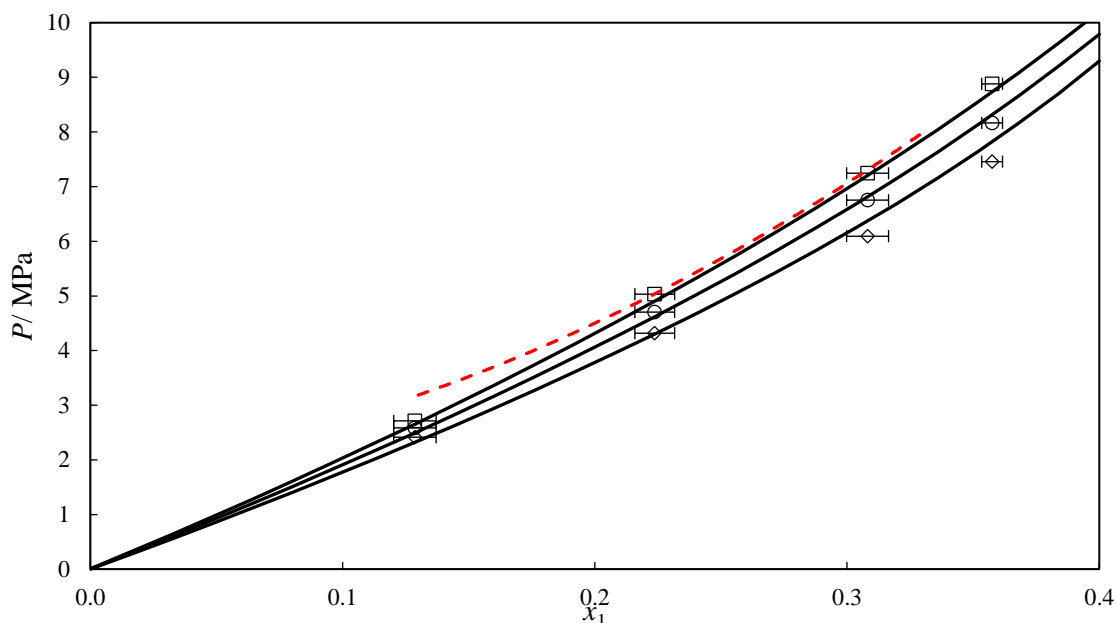
Figure 5-13. *P-x* data for the nitrogen trifluoride (1) + heptafluoro-butanol (2) binary system. Experimental data generated by the SS apparatus; ○, at 283.14 K; △, at 293.15 K; □, at 303.16 K. — Solid lines, PR (VdW) model; --- tetrafluoromethane (1) + heptafluoro butanol (2) at 293.15 K.

Table 5-43. Experimental data for the nitrogen trifluoride (1) + heptafluoro-butanol (2) binary system using the SS apparatus, including the measured pressure (P), temperature (T), liquid phase composition (x_1), and the expanded uncertainty[a].

T/K	P/MPa	x_1	$U(x_1)$
283.15	2.41	0.129	0.008
283.16	4.32	0.224	0.008
283.15	6.09	0.308	0.008
283.15	7.46	0.358	0.004
293.17	2.56	0.129	0.008
293.14	4.705	0.224	0.008
293.15	6.751	0.308	0.008
293.12	8.165	0.358	0.004
303.14	2.713	0.129	0.008
303.16	5.033	0.224	0.008
303.13	7.245	0.308	0.008
303.18	8.882	0.358	0.004

[a] $U(P) = 0.01$ MPa; $U(T) = 0.07$ K.

The regressed binary interaction parameter of the PR (VdW) model shows a positive deviation from Raoult's law. Comparison of the data fit parameters, provided in tables 5-44 (PR (VdW) model) and 5-45 (PRWS (NRTL) model), shows better AAD(P) errors associated with the data regression using the latter model as opposed to the AARD(P) errors calculated.

Table 5-44. Regressed binary interaction parameters (k_{ij} and B_{ij}) and statistical analysis for the PRWS (NRTL) model for the binary system of nitrogen trifluoride (1) + heptafluoro-butanol (2).

	T = 283.15 K	*T* = 293.15 K	*T* = 303.15 K
k_{12} [a]	0.952	0.967	0.986
B_{12}/ K [b]	-413	-445	-484
B_{21}/ K [b]	925	967	1052
AAD(*P*/MPa)	0.04	0.05	0.07
AARD(*P*/MPa)/%	3.47	3.94	3.71

[a] k_{12} is the interaction parameter of the WS mixing rule.
[b] B_{12} and B_{21} are the temperature-dependent adjustable parameters of the NRTL model, and a non-randomness factor of α_{12} set to 0.3.

Table 5-45. Regressed binary interaction parameters (k_{ij}) and statistical analysis for the PR (VdW) model for the binary system of nitrogen trifluoride (1) + heptafluoro-butanol (2).

	T = 283.15 K	*T* = 293.15 K	*T* = 303.15 K
k_{12} [a]	0.101	0.104	0.107
AAD(*P*/MPa)	0.10	0.10	0.10
AARD(*P*/MPa)/%	2.93	2.32	1.75

[a] k_{12} is the binary interaction parameter for the classical mixing rule in the PR (VdW) model.

5.8 Summary of the experimental results

The results from HPVLE data measurements showed the better selectivity of TFE-TFP ether compared to other solvents tested. The selectivity and capacity of the solvents were calculated to rank them based on their affinity to dissolve either NF_3 or CF_4. The selectivity is estimated as the ratio of the activity coefficients at infinite dilution (γ_i^∞) (Perry et al., 1997). The infinite dilution activity coefficients were correlated to the experimental bubble point data using Aspen Plus®. The solvent selectivity and capacity are then calculated as follows:

$$S = \frac{\gamma_i^\infty}{\gamma_j^\infty} \qquad 5.3$$

$$C = \frac{1}{\gamma^\infty} \qquad 5.4$$

where *i* and *j* refer to the light and heavy constituents of the gaseous mixture. The following three conditions apply to the selectivity:

- S>1: solvent has an affinity towards heavier solvent,
- S<1: solvent has an affinity towards lighter component which will reverse the relative volatility of the mixture.
- S=1: solvent has no affinity.

The solvent capacity is defined as the ratio of one to the greater infinite dilution activity coefficient and indicates the recovery of the solvent from the bottom product (Perry et al., 1997). Table 5-46 shows the selectivity of the solvents tested in this work. Figure 5-14 shows the selectivity of the solvents at the temperature of 283.15 K. While aa slight change is observed at higher temperatures, the overall proportion remains the same. It is clear that TFE-TFP ether has the greatest selectivity with an affinity upon NF_3 among others tested.
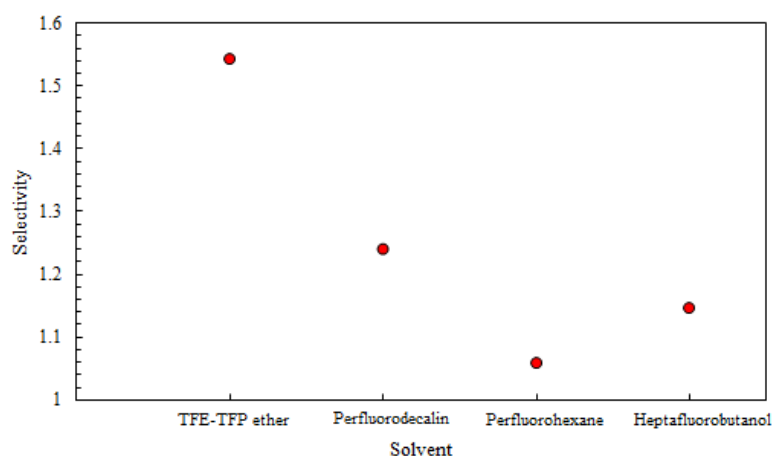
Figure 5-14. Selectivity of the solvents used in this work.

Table 5-46. Selectivity and capacity of the solvents tested in this study.

Solvent	T/ K	γ_i^∞		Selectivity	Capacity
		CF$_4$	NF$_3$		
TFE-TFP ether	283.15	3.665	2.337	1.568	0.428
	293.15	3.507	2.276	1.541	0.439
	303.15	3.347	2.209	1.515	0.453
Perfluorodecalin	283.15	1.582	1.276	1.240	0.784
	293.15	1.584	1.279	1.239	0.782
	303.15	1.578	1.275	1.237	0.784
Heptafluorobutanol	283.15	3.437	3.003	1.144	0.333
	293.15	3.315	2.888	1.148	0.346
	303.15	3.186	2.770	1.150	0.361
Perfluorohexane	283.15	1.227	1.176	1.044	0.851
	293.15	1.216	1.157	1.051	0.865
	303.15	1.197	1.131	1.058	0.884

To design a preliminary separation process using Aspen Plus®, initially physical absorption was selected to purify the NF_3 to the grades of higher than 99.999 %. Since the high-quality product was not obtained using the absorption technology, the extractive distillation was attempted to produce a high-grade product. The results from the extractive distillation obtained acceptable purities. The proposed absorption and extractive distillation processes are explained here. The purification results obtained from this work is compared to the literature data which is discussed as well.

5.9 Design of the absorption process with $C_5H_4F_8O$ using Aspen Plus®

The absorption method was selected to purify NF_3 from CF_4 impurity. The process is designed using Aspen Plus® V10. The main goal was to dissolve the maximum amount of the NF_3 in the promising solvent and to produce the high purity NF_3 using a stripping column (SC). Figure 5-15 shows the schematics of the proposed process. The feed stream of CF_4 – NF_3 enters the absorption column (AC). Another column was placed after the absorption column for stripping purposes to purify NF_3 and recover the valuable solvent. As shown in figure 5-15, the vapour product obtained from the stripping column is the NF_3 product. The solvent is mixed with a make-up flow in the mixer to compensate for the loss of solvent via the gaseous product of the absorber and stripping column. Thereafter, the solvent flow is directed to a pump and heat exchanger to regulate its pressure and temperature. A mixer is added to the process in a way that the recovered solvent from the process is used as the solvent feed to the absorption column.
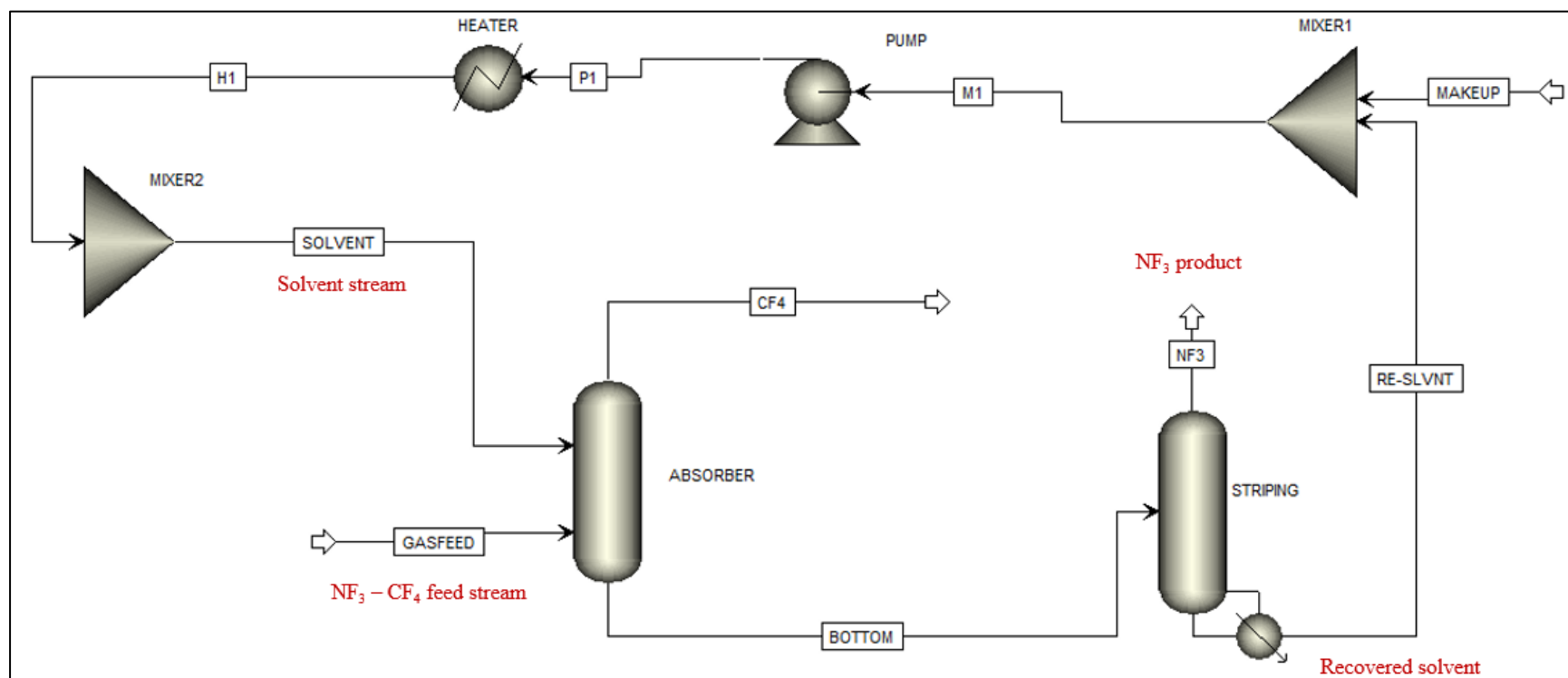
Figure 5-15. Schematic diagram of the proposed NF₃ purification process via physical absorption.

Process design

An absorption column was designed and run using a feed of NF_3 – CF_4 with the solvent of TFE-TFP ether to obtain NF_3 product with the purity of 99.999 %. The effect of several parameters was investigated on the product quality by varying operating temperature (223.15 – 323.15 K), pressure (0.20 – 2.50 MPa), theoretical stage numbers (10 – 100), solvent flow rate (1886 – 2200 $kmol.hr^{-1}$) and feed composition (50 – 90 % NF_3). From the simulation studies, a 30-stage column was obtained to be the most appropriate column which operates at 2.50 MPa and 293.15 K with the gas and solvent flow rates of 500 and 1990 $kmol.hr^{-1}$, respectively. The stream table of the highest product quality obtained from the absorption process is presented in table 5-47. It is clear that the gas feed of 50 % NF_3 is purified to 55.05 %. Several sensitivity studies were performed to obtain the highest product purity.

Table 5-48 shows the results of the absorption process for different feed composition operating in the most suitable condition. According to the results presented in the table, the final purity of the NF_3 product obtained for the feeds of 70, 80 and 90 % NF_3 are approximately 73, 78 and 86 %. This shows a decreasing percentage in the purity of NF_3 for the feed streams of 80 % and above. Looking at the stream contents, it is clear that the major part of the impurity increase is because of TFE-TFP ether which is evaporated to the NF_3 stream obtained from the stripping column. As the aim of this process design was to obtain a product with the purity of 99.999 %, the results show that the absorption column is incapable of producing a product with such grade. Therefore, extractive distillation is attempted to purify the NF_3 to the desired level.

Table 5-47. Stream table of the 30-stage absorption process for the 50 % NF_3 feed operating at 293.15 K and 2.50 MPa with gas and solvent flow rates of 500 and 1990 [a].

	Gas feed	Solvent stream	CF$_4$ (AC-top)	Bottom (AC)	RE (SC-bottom)	NF$_3$ (SC- top)	Makeup	S9 (mixer1)	S1 (pump)	S2 (heater)
T/ K	293.15	293.15	296.51	295.06	306.82	292.03	293.15	306.71	308.76	293.15
P/ MPa	2.50	2.50	2.50	2.50	0.10	0.10	2.50	0.10	2.50	2.50
					Mole flow					
Total	500	1542.5	258.4	1784.1	1530.0	254.1	12.5	1542.5	1542.5	1542.5
CF$_4$	250	2.7	147.0	105.6	2.7	103.0	0.0	2.7	2.7	2.7
NF$_3$	250	5.3	110.1	145.2	5.3	139.9	0.0	5.3	5.3	5.3
Solvent	0	1534.5	1.2	1533.3	1522.0	11.3	12.5	1534.5	1534.5	1534.5
					Mole fraction (%)					
CF$_4$	50	0.17	56.91	5.92	0.17	40.51	0.00	0.17	0.17	0.17
NF$_3$	50	0.35	42.62	8.14	0.35	55.05	0.00	0.35	0.35	0.35
Solvent	0	99.48	0.47	85.94	99.48	4.44	100.00	99.48	99.48	99.48

[a] Flow rate units are in kmol.hr^{-1}

Table 5-48. Summary of the best product streams obtained from absorption column using different feed compositions at the column pressure of 2.50 MPa, temperature of 293.15 K, absorption column theoretical stage number of 30, stripping column theoretical stage number of 2, solvent and gas feed flow rates of 1990 and 500 [a] for a 50 % NF_3 feed.

NF$_3$ % in feed	Component	Mole fraction (%)		Re-solvent (SC-bottom)	Make-up flow
		CF$_4$ (AC-top)	NF$_3$ (SC-top)		
50	CF$_4$	56.91	40.51	0.17	12.5
	NF$_3$	42.62	55.05	0.35	
	TFE-TFP ether	0.47	4.44	99.48	
70	CF$_4$	42.03	23.15	0.12	13.3
	NF$_3$	57.50	73.25	0.55	
	TFE-TFP ether	0.47	3.60	99.33	
80	CF$_4$	31.61	14.24	0.00	30.9
	NF$_3$	67.91	78.02	0.04	
	TFE-TFP ether	0.48	7.74	99.95	
90	CF$_4$	17.20	6.94	0.00	31.0
	NF$_3$	82.32	85.53	0.05	
	TFE-TFP ether	0.48	7.53	99.95	

[a] Flow rate units are in kmol.hr^{-1}

5.10 Design of the extractive distillation with $C_5H_4F_8O$ using Aspen Plus®

Due to the inability of designed absorption process to purify the NF_3 to the desired level, the two-column extractive distillation process is attempted to purify NF_3 from CF_4 impurity. The process is designed using Aspen Plus® V10. The extractive distillation uses the solvent as an entraining agent to change the relative volatility of the gaseous components through interaction with them. The presence of the entraining agent changes the fugacity of the components in the mixture, generating a repelling force. Thereby, the component possessing the stronger repulsive force moves to the vapour phase (Noll et al., 2013).

Process description

Figure 5-16 shows the schematics of the proposed process. The feed stream of CF_4 – NF_3 enters the extractive distillation column (EDC), and the simulation studies assess the separation at the different pressures and feed stream compositions with the solvent and gas feeds entering the column at the different stage numbers. A stripping column (SC) is placed after the extractive distillation column to purify NF_3 and recover the valuable solvent. Due to the price of the solvent used in this process (TFE-TFP ether) stripping is an important factor. The bottom of the stripping column is directed to a mixer. The solvent is mixed with a make-up flow in the mixer to compensate for the loss of solvent via the gaseous product of the extractive distillation and stripping columns. Thereafter, the solvent flow is directed to a pump to regulate its pressure. The solvent then enters a heat exchanger to cool down to the required temperature. A mixer is added to the process in a way that the recovered solvent from the process is used as the solvent feed to the extractive distillation column.

Design approach

The removal efficiency of the extractive distillation column depends on the properties of the material, feed and solvent flow rates, operating pressure, number of theoretical stages, feed composition and solvent/gas stage location (Fink, 2016). Usually, a range of acceptable variations is applied to find the most suitable parameters affecting the separation efficiency. Hence, several variations were tested on the removal efficiency of the column including solvent flow rate, column pressure, column temperature, the actual number of stages and feed composition to obtain the most appropriate operating condition which aims to reach the NF_3 product with a purity greater than 99.999 %.

Figure 5-16. Schematic diagram of the proposed NF$_3$ purification process using extractive distillation.

The stripping column design is affected by the several parameters including the degree of solvent and solute recovery, the operating conditions, number of theoretical stages and the heat effects. The operating conditions must be selected at the highest possible temperature and lowest possible pressure that the liquid solvent does not vaporise. The stripping column specifications targeted such that the solvent and gas recoveries are maximised. Different stage numbers between 3 to 6 were tested to find the most suitable number for the separation.

Process design

An extractive distillation column was designed and run using a feed of $NF_3 - CF_4$ with the solvent of TFE-TFP ether to obtain NF_3 product with the grade of 99.9999 %. The sensitivity of the extractive distillation tower was analysed by varying operating pressure (0.10 – 2.50 MPa), theoretical stage numbers (20 – 100), feed composition (50 – 99.2 % NF_3) and feed entrance stage number with the aim to obtain the highest purity. From the simulation studies, a 100- stage column was deemed to be the most suitable column operating at 0.10 MPa with the gas and solvent flow rates of 100 and 500 kmol.hr^{-1}, respectively. The results showed that the best entrance position for the gas and solvent feeds are at the 50th and 3rd stages, respectively with stage 1 being the top stage.

Table 5-49 shows the stream table of the proposed extractive distillation process with a 100-theoretical stage extractive distillation column and a 6-theoretical stage stripping column, operating at 0.10 MPa with the 100 kmol.hr^{-1} gas feed entering from 50th stage and 500 kmol.hr^{-1} solvent feed entering from 3rd stage. According to the table, the gaseous product of the extractive distillation column contains 99.99996 % CF_4 (0.4 ppm NF_3) obtained at 145.58 K. The bottom product of the extractive distillation column enters the 6-theoretical stage stripping column with the temperature of 165.55 K. The gaseous product of the stripping column is the NF_3 product with 99.99995 % purity (0.5 ppm CF_4). The bottom product of the stripping column is obtained at 365.27 K and purity of 99.9999996 % TFE-TFP ether and it is then combined with the makeup flow. The makeup flow is overall solvent loss through the gaseous products of the extractive distillation and stripping column which is 1.78×10^{-6} kmol.hr^{-1}, indicating a negligible amount of solvent loss. The heat exchanger then regulated the temperature of the TFE-TFP ether to the solvent feed temperature of 144.46 K.

Table 5-49. Stream table of the extractive distillation process with a 100-theoretical stage extractive distillation column and 6 theoretical stages stripping column for the 50 % NF_3 feed entering from 50th stage operating at 0.10 MPa with gas and solvent (entering from 3rd stage) flow rates of 100 and 500 kmol.hr^{-1}.

	Solvent feed (TFE-TFP ether)	Gas feed (NF_3-CF_4)	CF_4 (EDC-distillate)	Bottom (EDC)	NF_3 (SC-top)	PFE (SC-bottom)	Makeup	S1 (mixer1)	S2 (pump)	S3 (Heat exchanger)
T/ K	365.27	144.46	145.58	165.55	165.68	365.27	365.27	365.27	365.27	365.27
P/ MPa	0.100	0.100	0.100	0.101	0.100	0.100	0.100	0.100	0.100	0.100
Mole flows/ kmol.hr^{-1}										
Total	500.0000018	100	50	550	50	500	1.78E-06	500.0000018	500.0000018	500.0000018
NF_3	1.78E-06	50	2E-05	49.999978	49.999976	1.8E-06	0	1.78E-06	1.78E-06	1.78E-06
Solvent	500	0	0	500	2E-06	499.999998	1.78E-06	500	500	500
CF_4	1.30E-13	50	49.99998	2E-05	2.2E-05	0	0	1.29E-13	1.29E-13	1.29E-13
Mole fractions/ %										
NF_3	4E-07	4E-06	4E-05	9.0909051	99.99995[a]	4E-07	0	4E-07	4E-07	4E-07
Solvent	99.9999996	99.9999996	0	90.9090909	4E-06	99.9999996	100	99.9999996	99.9999996	99.9999996
CF_4	0	0	99.99996	4E-06	1E-06	0	0	0	0	0

[a] NF_3 product mole fraction (%)

A 100-theoretical stage extractive distillation column was used with a feed of 50 % NF_3 at the pressure of 0.10 MPa. Figure 5-17 shows the composition profile of the vapour and liquid phases versus the stage number. It is clear from the composition distribution of the vapour phase (figure 5-17 (a)) that the NF_3 composition decreases moving up the column; at the 72nd stage reaching the composition of 98.98. Thereafter the composition profile changes with a sharp slope until it reaches to 0.0085 in the gaseous product at 38th stage and after that, the changes can be observed only in 4th decimal places and more. It is clear from the liquid composition graph (figure 5-17 (b)) that the NF_3 composition is highest at the 100th stage and approaches zero above the 21st stage of the column. The trends show that the use of TFE-TFP ether increases the relative volatility of the CF_4, escaping to the vapour phase which is expected from the results obtained from HPVLE measurements. Table 5-50 lists the NF_3 composition at each stage.

(a)   (b)
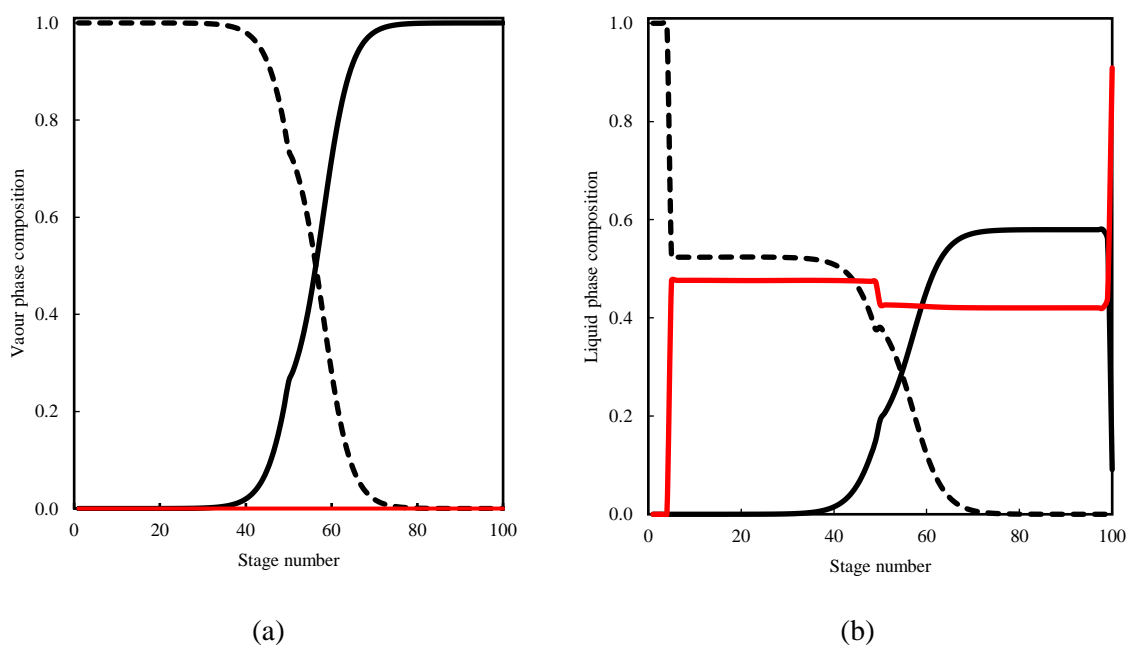
Figure 5-17. Composition profile of — NF_3, --- CF_4 and — TFE-TFP ether in a) vapour phase and b) liquid phase of the 100-stage extractive distillation columns for the 50 % NF_3 feed entering from 50th stage operating at 0.10 MPa with gas and solvent (entering stage of 3rd stage) flow rates of 100 and 500 kmol.hr^{-1}.

Table 5-50. NF_3 compositions in both liquid and vapour phases on the respective stage of the extractive distillation column operating at 0.10 MPa using a 100-theoretical stage extractive distillation column with 100 kmol.hr^{-1} gas feed of 50 % NF_3 entering from 50th stage and 500 kmol.hr^{-1} solvent entering from 3rd stage.

Stage no.	x_{NF_3}	y_{NF_3}	Stage no.	x_{NF_3}	y_{NF_3}	Stage no.	x_{NF_3}	y_{NF_3}	Stage no.	x_{NF_3}	y_{NF_3}	Stage no.	x_{NF_3}	y_{NF_3}
1	1.00E-06	1.00E-06	21	5.80E-05	7.60E-05	41	0.0199	0.0263	61	0.480	0.772	81	0.579	0.9994
2	1.00E-06	1.00E-06	22	7.80E-05	1.02E-04	42	0.0264	0.0349	62	0.502	0.818	82	0.58	0.9995
3	1.00E-06	1.00E-06	23	1.05E-04	1.37E-04	43	0.0348	0.0462	63	0.520	0.858	83	0.58	0.99967
4	0.0E+00	1.00E-06	24	1.41E-04	1.84E-04	44	0.0455	0.0608	64	0.534	0.891	84	0.58	0.99976
5	0.0E+00	1.00E-06	25	1.89E-04	2.46E-04	45	0.0591	0.0796	65	0.545	0.917	85	0.58	0.99982
6	1.00E-06	1.00E-06	26	2.53E-04	3.31E-04	46	0.0761	0.103	66	0.554	0.938	86	0.58	0.99987
7	1.00E-06	1.00E-06	27	3.40E-04	4.43E-04	47	0.0969	0.133	67	0.561	0.953	87	0.58	0.99991
8	1.00E-06	1.00E-06	28	4.56E-04	5.95E-04	48	0.122	0.169	68	0.565	0.965	88	0.58	0.99993
9	2.00E-06	2.00E-06	29	6.11E-04	7.98E-04	49	0.150	0.212	69	0.569	0.974	89	0.58	0.99995
10	2.00E-06	3.00E-06	30	8.19E-04	1.07E-03	50	0.193	0.261	70	0.572	0.981	90	0.58	0.99996
11	3.00E-06	4.00E-06	31	1.10E-03	1.43E-03	51	0.207	0.283	71	0.574	0.986	91	0.58	0.99997
12	4.00E-06	5.00E-06	32	1.47E-03	1.92E-03	52	0.224	0.309	72	0.576	0.990	92	0.58	0.99998
13	5.00E-06	7.00E-06	33	1.97E-03	2.58E-03	53	0.245	0.342	73	0.577	0.992	93	0.58	0.999986
14	7.00E-06	1.00E-05	34	2.64E-03	3.45E-03	54	0.270	0.382	74	0.577	0.995	94	0.58	0.999990
15	1.00E-05	1.30E-05	35	3.54E-03	4.63E-03	55	0.298	0.428	75	0.578	0.996	95	0.58	0.999993
16	1.30E-05	1.70E-05	36	4.74E-03	6.20E-03	56	0.329	0.481	76	0.578	0.997	96	0.58	0.999995
17	1.80E-05	2.30E-05	37	6.34E-03	8.29E-03	57	0.362	0.539	77	0.579	0.998	97	0.58	0.999996
18	2.40E-05	3.10E-05	38	8.46E-03	0.0111	58	0.394	0.599	78	0.579	0.998	98	0.58	0.999997
19	3.20E-05	4.20E-05	39	0.0113	0.0148	59	0.426	0.660	79	0.579	0.999	99	0.56	0.999998
20	4.30E-05	5.70E-05	40	0.015	0.0197	60	0.455	0.718	80	0.579	0.999	100	0.0909	0.999999

Figure 5-18 shows the pressure and temperature profile of the extractive distillation column for the above simulation. The pressure drop of 1 kPa was considered for each stage. The pressure profile indicates that the pressure changes fairly stable between (0.100 and 0.101) MPa throughout the column. The gas and solvent streams are set to enter as the liquid with zero vapour fraction, hence, the gas feed temperature at the entrance is 144 K and the temperature profile remains around that temperature over throughout the column. The solvent stream enters the column from the 3rd stage at 365.27 K which causes a slight increase in the temperature of the top 4 stages. There is a rapid temperature change near the bottom of the column which is due to the heat duty of 9.29×10^6 kJ.hr^{-1} on the re-boiler to meet the flow requirement of the extractive distillation column bottom product. This is due to the significant difference between the compositions of the last two stages.
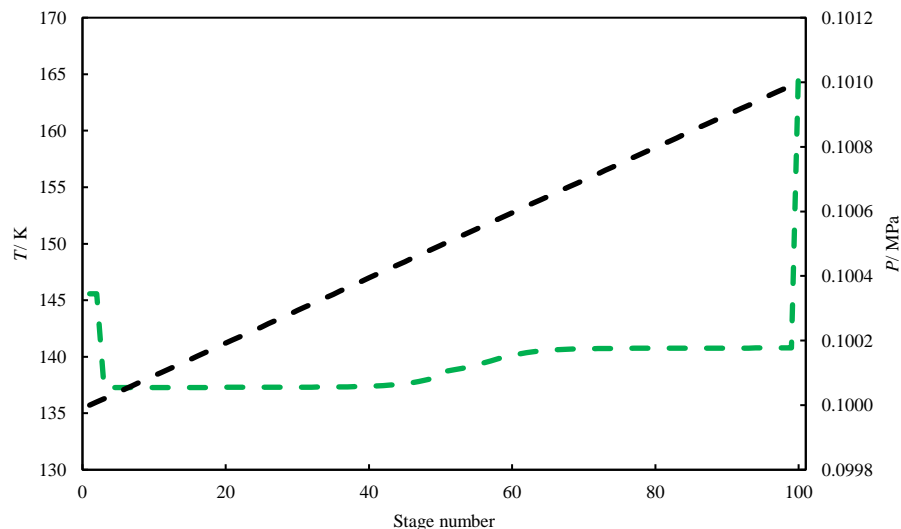
Figure 5-18. The distribution of --- temperature and --- pressure at different stages of the extractive distillation column operating at 0.10 MPa using a 100-theoretical stage extractive distillation column with 100 kmol.hr^{-1} gas feed of 50 % NF$_3$ entering from 50th stage and 500 kmol.hr^{-1} solvent entering from 3rd stage.

The 6-theoretical stage stripping column produces NF$_3$ with the purity of 99.9999 % and CF$_4$ content of below 1 ppm (0.45 ppm). Table 5-51 shows a summary of the product streams obtained from the stripping column with varying stage numbers. It is clear from the table that the best results were obtained using a stripping column with 6 theoretical stages. The number of theoretical stages affects the final CF$_4$ content in the NF$_3$ stream significantly. The minimum amount of NF$_3$ and CF$_4$ in the stripping stream is obtained using the 6-theoretical stage column with 1.78×10^{-6} and 9.33×10^{-14} kmol.hr^{-1} which consequently leads to the highest NF$_3$ grade of 99.9999 % at the gaseous stream

compared to the others. This means the reduction of CF_4 content from 5000000 to 0.45 ppm in the gaseous stream.

Looking at the make-up flow figures, while the makeup flow is not significant, the maximum flow rate (3-theoretical stage column) is approximately 1800 times more than the minimum flow rate (6-theoretical stage column) with 3.31×10^{-3} and 1.78×10^{-6} kmol.hr^{-1}, respectively. Furthermore, for the 6-theoretical stage column, NF_3 is produced at 165.68 K with just 0.13-degree temperature elevation compared to the bottom product of the extractive distillation column whereas the NF_3 obtained from 3-theoretical stage column is at 212.93 K with just below 40 degrees increase. This indicates a significant energy loss through the gaseous stream for the column with a lower theoretical stage number. The results indicate the significance of the number of theoretical stages on the solvent recovery and NF_3 grade.

Table 5-51. Summary of the product streams obtained from stripping column at the different number of theoretical stages for the extractive distillation process operating at 0.10 MPa using a 100-theoretical stage extractive distillation column with 100 kmol.hr^{-1} gas feed of 50 % NF_3 entering from 50th stage and 500 kmol.hr^{-1} solvent entering from 3rd stage [a].

stage number	T_{NF_3}/ K	Component	NF$_3$ stream (SC – top)		Recovered solvent (SC-bottom)		Make-up flow/ kmol.hr^{-1}
			Mole flow/ kmol.hr^{-1}	Mole fraction	Mole flow/ kmol.hr^{-1}	Mole fraction	
3	212.93	NF$_3$	49.997	0.99993	3.31E-03	6.61E-06	3.31E-03
		TFE-TFP ether	3.31E-03	6.61E-05	499.997	0.999993	
		CF$_4$	2.19E-05	4.38E-07	5.53E-10	1.11E-12	
4	187.06	NF$_3$	49.99989	0.999998	9.27E-05	1.85E-07	9.27E-05
		TFE-TFP ether	9.27E-05	1.85E-06	499.99991	0.9999998	
		CF$_4$	2.19E-05	4.38E-07	1.14E-11	2.27E-14	
5	168.86	NF$_3$	49.99997	0.9999995	3.44E-06	6.89E-09	3.4E-06
		TFE-TFP ether	3.44E-06	6.89E-08	499.999997	0.999999993	
		CF$_4$	2.21E-05	4.42E-07	3.00E-13	6.00E-16	
6 [b]	165.68	NF$_3$	49.99998	0.9999995	1.78E-06	3.55E-09	1.78E-6
		TFE-TFP ether	1.78E-06	3.55E-08	499.999998	0.999999996	
		CF$_4$	2.20E-05	4.40E-07	9.33E-14	1.87E-16	

[a] Temperature of the bottom product for all the cases is 365.27 K

[b] The best operating condition

5.10.1 Sensitivity analysis on the extractive distillation column pressure

The composition of 50 % NF_3 was considered as a feed stream. Results were obtained by running the simulation at the constant solvent flow rate of 500 kmol.hr^{-1} and three theoretical stage numbers of 80, 90 and 100 while varying the pressures between (0.10 – 2.50) MPa. Table 5-52 summaries the results of the pressure sensitivity analysis. Figure 5-19 shows the NF_3 mole fraction in the product stream at different pressures for the column with different stage numbers. It is clear that as the pressure increases from 0.10 MPa, the NF_3 composition in the product stream decreases at the constant stage number until it reaches the minimum composition at 2.50 MPa. The figure illustrates that as the pressure increases the further number of theoretical stages are required to reach the desired product quality.
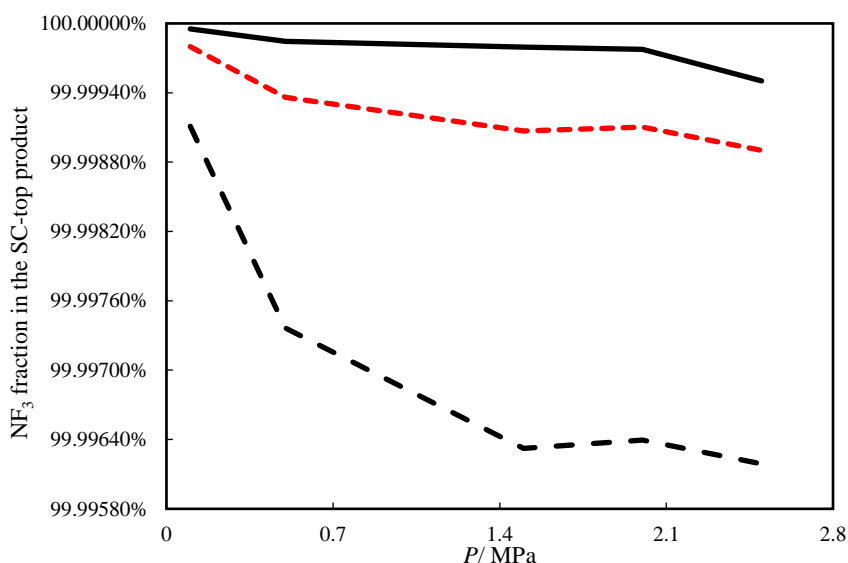
Figure 5-19. Sensitivity analysis of extractive distillation column pressure for NF_3 mole fraction obtained from columns with theoretical stage numbers of: — 100, --- 90, --- 80 with 100 kmol.hr^{-1} gas feed of 50 % NF_3 entering from the middle stage and 500 kmol.hr^{-1} solvent entering from 3rd stage.

The reflux ratio indicates the ratio of boil-off (amount returning to the column) to the take-off (amount collected as the distillate). The reflux ratio was adjusted in a way that the highest product grade is obtained. According to table 5-52, the reflux ratio figures increase as the pressure increases. This is 58 for the column with the operating pressure of 0.10 MPa which increases by three times to 190 at the pressure of 2.50 MPa. The positive outcome from the increased pressure is the improved operating temperature from 145.58 to 214.34 K for CF_4 product and from 165.55 to 220.41 K for the bottom product. However, it must be considered that the increase of the reflux ratio imposes a heavy heat duty.

Table 5-52. Summary of the pressure sensitivity analysis for three different column stages, with 100 kmol.hr^{-1} gas feed of 50 % NF_3 entering from 50th stage and 500 kmol.hr^{-1} solvent entering from 3rd stage [a].

P / MPa	T_{Bottom} / K	T_{CF_4} / K	Reflux ratio	Number of theoretical stages			Number of theoretical stages			Number of theoretical stages		
				100	90	80	100	90	80	100	90	80
				Mole fraction CF$_4$ (EDC-distillate)			Mole flow CF$_4$ (EDC-distillate)			Mole fraction of NF$_3$ (SC-top)		
0.10	165.55	145.58	58	99.99996	99.99980	99.99911	49.99998	49.99901	49.99956	99.99995[b]	99.99980	99.99911
0.50	220.41	173.21	78	99.99985	99.99936	99.99736	49.99992	49.99968	49.99868	99.99985	99.99936	99.99736
1.50	300.29	197.52	115	99.99978	99.99907	99.99632	49.99987	49.99953	49.99816	99.99980	99.99907	99.99632
2.00	367.71	207.56	140	99.99976	99.99910	99.99639	49.99988	49.99955	49.99820	99.99978	99.99910	99.99639
2.50	429.44	214.34	190	99.99936	99.99929	99.99641	49.99968	49.99964	49.99820	99.99950	99.99890	99.99619

[a] Flow rate units are in kmol.hr^{-1}

[b] The best operating condition

Figure 5-20 shows the effect of operating pressure on the temperature of the column. One of the major drawbacks of the conventional distillation methods is their operating temperature which can be down to 81.15 K imposing the high operation costs (Hart et al., 2006, Suenaga et al., 1991). It is clear that as the operating pressure increases, the column temperature is improved. As the pressure increases from 0.10 to 2.50 MPa, the temperature of the bottom product and distillate increases from 165.51 to 429.44 and from 145.58 to 214.33 K respectively. The temperature change for the bottom product is significant and fairly steep as opposed to the temperature of the distillate product.
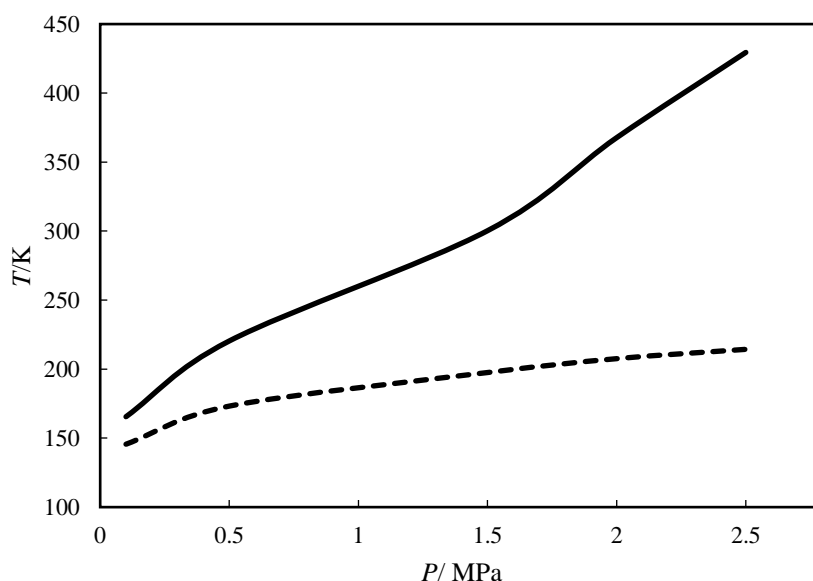
Figure 5-20. Sensitivity analysis of the pressure on the temperature of: — bottom product and --- distillate for a 100-theoretical stage extractive distillation column with 100 kmol.hr^{-1} gas feed of 50 % NF$_3$ entering from 50th stage and 500 kmol.hr^{-1} solvent entering from 3rd stage.

NF$_3$ and CF$_4$ are valuable gases that both are required in an ultra-high purity of 99.99 – 99.9999 % in the industry (Miller et al., 2002). While the aim of this study is to obtain high purity NF$_3$, it is possible to produce a high-quality CF$_4$. Figure 5-21 shows the effect of operating pressure on a) the CF$_4$ concentration and b) the CF$_4$ flow rate obtained as the gaseous product from the top of the extractive distillation column. it is clear from the figure that as the pressure increases at the constant theoretical stage numbers of 90 and 100, the impurity content of the CF$_4$ stream changes between 9 and 2 ppm which indicates a product with a significant grade. However, the use of a column with 80 theoretical stages produces CF$_4$ with the impurity content of 9 ppm at 0.10 bar which increases to almost 40 ppm at 2.50 MPa. As the product quality is high, the CF$_4$ flow rate obtained from the column of 90 and 100 theoretical stages differ only at 4th decimal place which is 3rd decimal place for that of the 80 theoretical stage column.
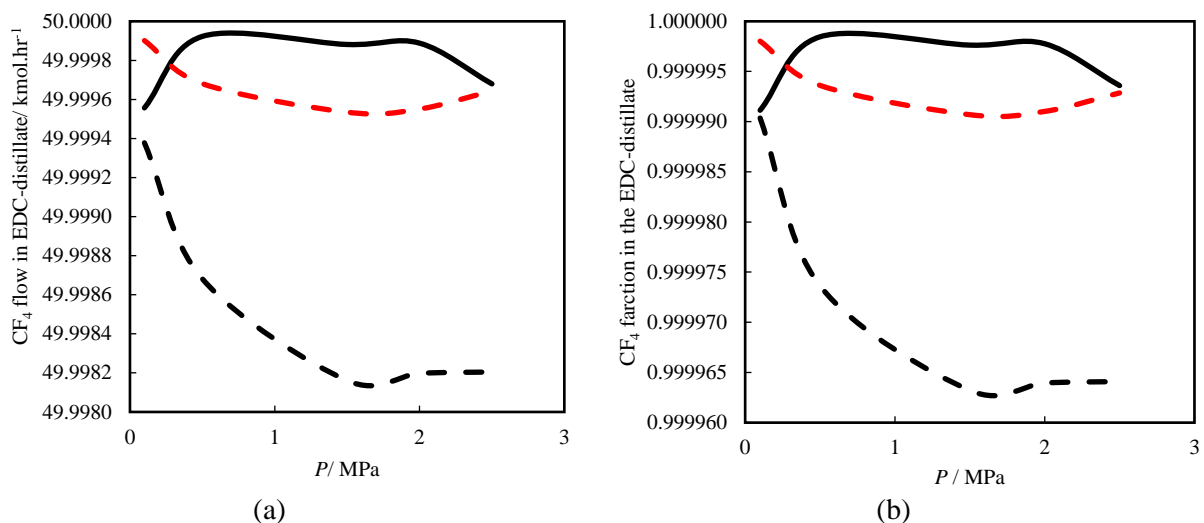
Figure 5-21. Sensitivity analysis of the pressure on a) the CF_4 fraction and b) CF_4 flow rate obtained as the gaseous product of the extractive distillation column for theoretical stage numbers of: — 100, --- 90, --- 80 with 100 kmol.hr^{-1} gas feed of 50 % NF_3 entering from the middle stage and 500 kmol.hr^{-1} solvent entering from 3rd stage.

5.10.2 Sensitivity analysis on the extractive distillation column stage number

Table 5-53 lists the summary of the results of the stage sensitivity analysis for the extractive distillation column operating at 0.10 MPa with the gas feed of 100 kmol.hr^{-1} entering from the middle stage and solvent feed of 500 kmol.hr^{-1} entering from 3rd stage. Figure 5-22 shows the effect of theoretical stage number on the a) flowrate and b) concentration of NF_3 in the product streams at the different theoretical stage numbers between 20 and 100 stages. It is clear that as the number of theoretical stages increases, the product quality increases form 94.96 % for the column with 20 theoretical stages to 99.9999 % for the column with 100 theoretical stages. According to the results listed in the table, the maximum purity for the column with 20 theoretical stages is obtained using reflux ratio of 54 which is 56 for the column of 50 theoretical stages and 58 for the rest of the columns. Overall, the makeup flow is just below 2×10^{-6} kmol.hr^{-1}, indicating a negligible solvent loss.
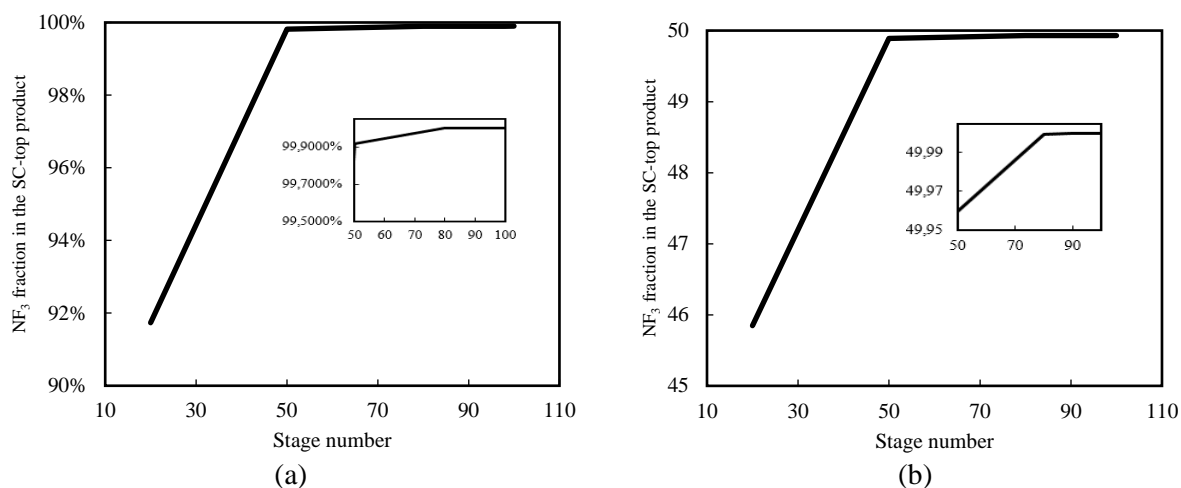
Figure 5-22. Sensitivity analysis of the theoretical stage number on the a) NF_3 fraction and b) NF_3 flow rate operating at 0.10 MPa with 100 kmol.hr^{-1} gas feed of 50 % NF_3 entering from the middle stage and 500 kmol.hr^{-1} solvent entering from 3rd stage.

Table 5-53. Summary of the theoretical stage number sensitivity analysis for the extractive distillation column operating at 0.10 MPa with the 50 % NF_3 gas feed of 100 kmol.hr^{-1} entering from the middle stage and solvent flow rate of 500 kmol.hr^{-1} entering from 3rd stage [a].

No. of stages	Reflux ratio	NF_3 mole fraction % (SC-top)	Mole flow NF_3 (SC-top)	CF_4 mole fraction % (EDC-distillate)	Mole flow CF_4 (EDC-distillate)	Makeup flow
20	54	94.96983	47.48491	94.96983	47.484915	1.55E-06
50	56	99.94732	49,97366	99.94732	49.973662	1.77E-06
80	58	99.99911	49.99955	99.99911	49.999557	1.78E-06
90	58	99.99980	49.99989	99.99980	49.999901	1.78E-06
98	58	99.99994	49,99997	99.99994	49.999973	1.78E-06
100 [b]	58	99.99995	49.99998	99.99996	49.999978	1.78E-06

[a] Flow rate unit is in kmol.hr^{-1}

[b] The best operating condition

Figure 5-23 shows the results of the theoretical stage number sensitivity analysis on the CF_4 a) mole fraction and b) flow rate obtained from extractive distillation column as the distillate. Comparing the results illustrated in figures 5-23 and 5-23 shows that the same trend is observed for both NF_3 in the bottom product and CF_4 in the distillate. The minimum product quality of just below 92 % is obtained using 20 theoretical stage column whereas the CF_4 with the impurities less than 1 ppm is obtained using the column with 100 theoretical stages. It is clear that the extra number of theoretical stages operate as the further mass transfer units which enhance the separation due to the improved mass transfer surface.

(a)   (b)
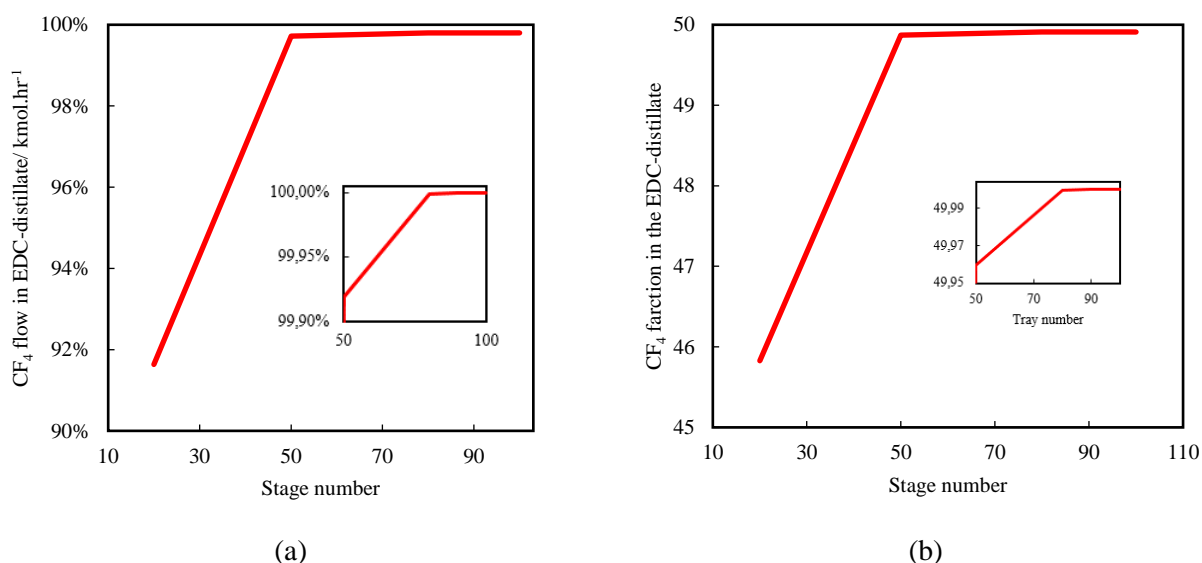
Figure 5-23. Sensitivity analysis of the theoretical stage number on the a) CF_4 fraction and b) CF_4 flow rate for the extractive distillation column operating at 0.10 MPa with the 50 % NF_3 gas feed of 100 kmol.hr^{-1} entering from the middle stage and solvent flow rate of 500 kmol.hr^{-1} entering from 3rd stage.

5.10.3 Sensitivity analysis on the solvent stage location

Table 5-54 summaries the results of varying solvent stage location with different theoretical stage numbers. The NF_3 and CF_4 fractions reported in the table are obtained from the stripping and extractive distillation columns, respectively. The simulation was run at the pressure of 0.10 MPa and solvent flow rate of 500 kmol.hr^{-1} varying the theoretical stages between (20 and 100) stages. Overall, the solvent stage number of 3 obtained the best results among others. The makeup flow is almost the same and only differs in 7th decimal place and more which the average figures are reported. According to the table, the minimum product concentration is obtained using the second stage as the solvent stage location. As the NF_3 fraction obtained from the stripping column increases, the CF_4 concentration in the product increases and the makeup flow remains the same. This indicates that the

solvent simply acts as a powerful entraining agent with low volatility which poses major alteration on the fugacity of the CF_4 to escape the liquid phase which could be separated via extractive distillation.

Table 5-54. Summary of the solvent stage location sensitivity analysis for the columns with different theoretical stage numbers at 0.10 MPa, 100 kmol.hr^{-1} feed composition of 50 % NF_3 entering from the middle stage and solvent flow rate of 500 [a] (NF_3 and CF_4 fractions are obtained from top of the stripping and extractive distillation columns, respectively).

No. of stages	Variable	Stage no. of solvent				Makeup flow
		2	3 [b]	4	5	
20	NF_3 fraction %	94.54	94.97	93.62	91.84	1.55E-06
	NF_3 flow	47.27	47.48	46.81	45.92	
	CF_4 fraction %	94.62	94.97	93.62	91.84	
	CF_4 flow	47.31	47.48	46.81	45.92	
50	NF_3 fraction %	99.94	99.95	99.93	99.92	
	NF_3 flow	49.970	49.974	49.965	49.960	1.67E-06
	CF_4 fraction %	99.94	99.95	99.93	99.92	
	CF_4 flow	49.970	49.974	49.965	49.960	
80	NF_3 fraction %	99.9986	99.9991	99.9988	99.9984	1.78E-06
	NF_3 flow	49.9993	49.9996	49.9994	49.9992	
	CF_4 fraction %	99.9984	99.9991	99.9988	99.9984	
	CF_4 flow	49.9993	49.9996	49.9994	49.9992	
90	NF_3 fraction %	99.9997	99.9998	99.9997	99.9996	1.78E-06
	NF_3 flow	49.9998	49.9999	49.9998	49.9998	
	CF_4 fraction %	99.9997	99.9998	99.9997	99.9996	
	CF_4 flow	49.9998	49.9999	49.9998	49.9998	
100	NF_3 fraction %	99.99991	99.99995	99.99994	99.99992	1.78E-06
	NF_3 flow	49.99996	49.99998	49.99997	49.99996	
	CF_4 fraction %	99.99992	99.99996	99.99994	99.99992	
	CF_4 flow	49.99996	49.99998	49.99997	49.99996	

[a] Flow rate unit is in kmol.hr^{-1}
[b] The best operating condition

5.10.4 Sensitivity analysis on the gas feed stage location

Table 5-55 summaries the results of varying gas feed stage location with different stage numbers. The NF_3 and CF_4 fractions are obtained from stripping and extractive distillation columns, respectively. The simulation was run at the pressure of 0.10 MPa and solvent flow rate of 500 kmol.hr^{-1} varying the theoretical stages between (20 and 100) stages. According to the table, the gas feed stage location is more efficient when it is just in the middle of the tower, obtaining the best product purity. The makeup flow is almost the same for the different gas feed stage location and only differs in 7th decimal place and more. The trends show a lower solvent loss at lees number of stages which is due to the less efficient separation of CF_4 – NF_3 mixture and it is not attributed to the number of stages. Here, only the average figures are reported. According to the table, moving up the tower for the gas feed stage location has a more negative effect as compared to the case that the gas feed stage is placed

below the middle of the column. This is due to the less number of mass transfer stages for the case with a gas stage located above the middle. Therefore, the lower CF_4 concentration is collected as a distillate.

Table 5-55. Summary of the gas feed location sensitivity analysis for the columns with different theoretical stage numbers at 0.10 MPa, 100 kmol.hr^{-1} gas feed composition of 50 % NF_3 and solvent flow rate of 500 [a] entering from 3rd stage.

No. of stage	Gas feed stage	SC – top		EDC – distillate		Makeup
		NF_3 mole fraction %	NF_3 mole flow	CF_4 mole fraction %	CF_4 mole flow	
20	7	92.52	46.26	92.52	46.26	1.55E-06
	10 [b]	94.97	47.48	94.97	47.48	
	14	94.78	47.39	94.78	47.39	
50	15	99.44	49.72	99.44	49.72	1.77E-06
	25 [b]	99.94	49.97	99.95	49.97	
	35	99.82	49.91	99.83	49.91	
80	30	99.992	49.9960	99.992	49.9960	1.77E-06
	40 [b]	99.999	49.9996	99.999	49.9996	
	50	99.998	49.9991	99.998	49.9992	
90	43	99.9997	49.99987	99.9997	49.99987	1.77E-06
	45 [b]	99.9998	49.99989	99.9998	49.99990	
	55	99.9996	49.99983	99.9996	49.99983	
100	49	99.99994	49.999974	99.99995	49.999975	1.77E-06
	50 [b]	99.99995	49.999976	99.99996	49.999978	
	56	99.99989	49.999947	99.99990	49.999949	

[a] Flow rate unit is in kmol.hr^{-1}
[b] The best operating condition

5.10.5 Sensitivity analysis on the feed composition

Table 5-56 lists the summary of the sensitivity analysis on the feed composition for an extractive distillation column with 100 theoretical stages operating at the pressure of 0.10 MPa and solvent flow rate of 500 kmol.hr^{-1}. Figure 5-24 shows the sensitivity analysis results on the temperature and makeup flow. It is clear that as the NF_3 content of the feed increases the bottom product temperature decreases from 165.68 to 154.57 K which is not a significant change. A similar trend is observed for the makeup flow which decreases by approximately ten times form 1.78×10^{-6} to 2.67×10^{-7} kmol.hr^{-1}, however, the values are insignificant.

Table 5-56. Summary of the feed composition sensitivity analysis for a 100-theoretical stage extractive distillation column operating at 0.10 MPa with the gas feed of 100 kmol.hr^{-1} entering from the 50th stage and solvent flow rate of 500 kmol.hr^{-1} entering from 3rd stage (flow rate unit is in kmol.hr^{-1}).

Feed (NF$_3$ %)	SC – top			EDC – distillate		Makeup
	T_{NF_3}/ K	NF$_3$ mole fraction %	NF$_3$ mole flow	CF$_4$ mole fraction %	CF$_4$ mole flow	
50	165.68	99.999953	49.999976	99.999956	49.99998	1.78E-06
60	162.21	99.999955	59.999992	99.999958	39.99999	9.98E-07
70	159.58	99.999957	69.999957	99.999960	29.99996	6.38E-07
80	157.51	99.999960	79.999965	99.999963	19.99997	4.46E-07
90	155.83	99.999971	89.999974	99.999975	9.999998	3.33E-07
99	154.57	99.9999999	99	99.9999999	1	2.67E-07
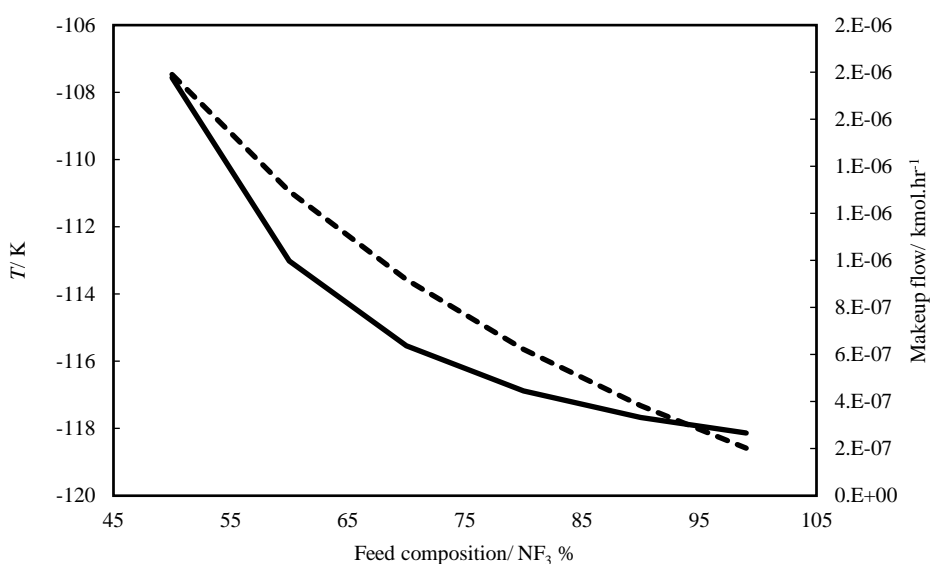
Figure 5-24. Sensitivity analysis of the gas feed composition on the temperature and makeup flow for a 100-theoretical stage extractive distillation column operating at 0.10 MPa with the gas feed of 100 kmol.hr^{-1} entering from the 50th stage and solvent flow rate of 500 kmol.hr^{-1} entering from 3rd stage.

Figure 5-25 shows the feed composition sensitivity analysis for the NF$_3$ and CF$_4$ composition obtained from the stripping column and distillate, respectively. It is clear that as the feed composition increases at the constant pressure and stage number, the product quality increases from 99.99995 at 50 % NF$_3$ feed to 99.99999 at 99 % NF$_3$ feed. The trends from both of the gases prove the fact that there is a negligible amount of solvent present in the product streams. This indicates that the TFE-TFP ether is a good separator agent with a low solvent capacity which can be recovered with a trivial loss.

(a)   (b)
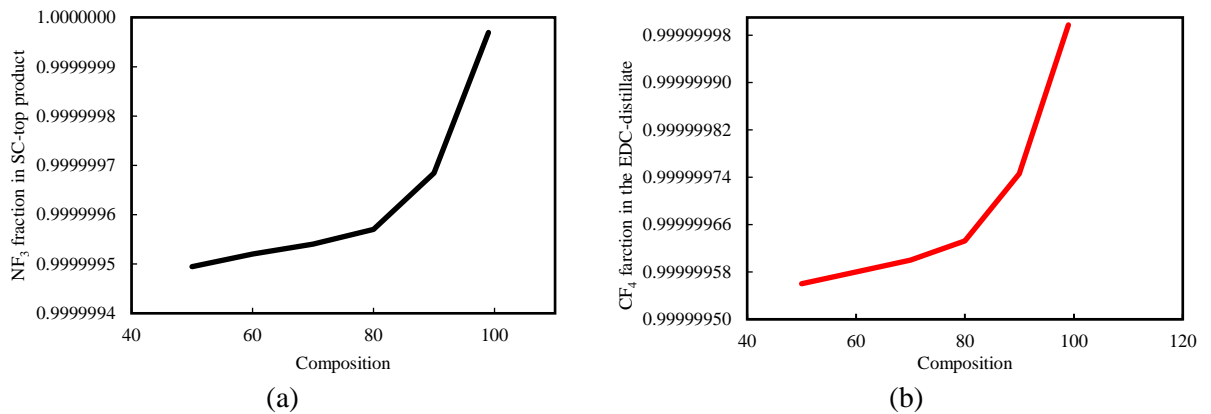
Figure 5-25. Sensitivity analysis of the gas feed composition on the a) NF_3 b) CF_4 fraction in the product for a 100-theoretical stage extractive distillation column operating at 0.10 MPa with the gas feed of 100 kmol.hr^{-1} entering from the 50th stage and solvent flow rate of 500 kmol.hr^{-1} entering from 3rd stage.

5.10.6 Sensitivity analysis on the reflux ratio

Table 5-57 shows the summary of the reflux ratio sensitivity analysis for the extractive distillation column with 100 theoretical stages, 100 kmol.hr^{-1} the gas feed composition of 50 % NF_3 entering from 50th stage, the solvent flow rate of 500 kmol.hr^{-1} entering from 3rd stage and pressure of 0.10 MPa. Figure 5-26 shows the reflux ratio sensitivity analysis results for the makeup flow. It is clear that as the reflux ratio increases from 58 to 100 the makeup flow decreases from 1.78×10^{-6} to 1.50×10^{-6} kmol.hr^{-1}. While it shows that as the reflux ratio increases the solvent loss through distillate decreases, the high reflux ratio requires more energy for boiling off.

Table 5-57. Reflux ratio sensitivity analysis for the extractive distillation column with 100 theoretical stages, 100 kmol.hr^{-1} the gas feed of 50 % NF_3 entering from 50th stage, the solvent flow rate of 500 ^{a} entering from 3rd stage and pressure of 0.10 MPa.

Reflux ratio	SC – top		EDC – distillate		Makeup
	NF$_3$ content %	NF$_3$ mole flow	CF$_4$ content %	CF$_4$ mole flow	
58	99.99995	49.99998	99.99996	49.99998	1.78E-06
60	99.99987	49.99994	99.99988	49.99994	1.78E-06
65	99.9985	49.9993	99.9986	49.9993	1.78E-06
70	99.989	49.994	99.989	49.995	1.77E-06
75	99.947	49.97	99.94	49.97	1.77E-06
80	99.8	49.9	99.8	49.90	1.77E-06
85	99.4	49.7	99.4	49.7	1.74E-06
90	98.6	49.3	98.6	49.3	1.70E-06
95	97.1	48.6	97.1	48.6	1.62E-06
100	94.8	47.4	94.8	47.4	1.50E-06

^{a} Flow rate unit is in kmol.hr^{-1}
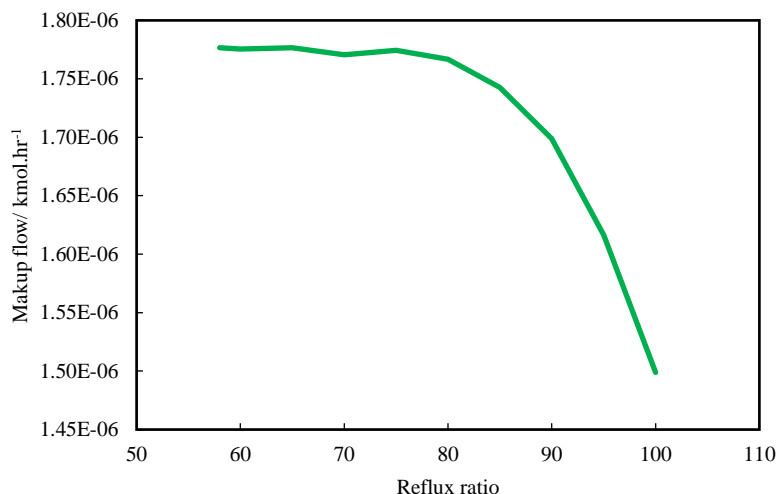
Figure 5-26. Sensitivity analysis of the reflux ratio on the makeup flow for the extractive distillation column with 100 theoretical stages, 100 kmol.hr^{-1} the gas feed composition of 50 % NF$_3$ entering from 50th stage, the solvent flow rate of 500 kmol.hr^{-1} entering from 3rd stage and pressure of 0.10 MPa.

Figure 5-27 shows the sensitivity analysis of the reflux ratio on the CF$_4$ and NF$_3$ mole fractions in the product streams obtained from the extractive distillation and stripping column, respectively. It is clear that as the reflux ratio increases from 58 to 100 the NF$_3$ fraction decreases from 99.9999 to 94.83, respectively which is a similar trend obtained for CF$_4$. Given the makeup flow reduction versus the increase of the reflux ratio and looking at the impurity content in the product streams, it can be concluded that the decrease in product quality is only attributed to the smaller alteration of the relative volatility of the gaseous mixture at higher reflux ratios than the best value. It must be born in mind that the best operating value is obtained considering only the final NF$_3$ purity.

(a)　　　　　　　　　　　　　　　　　　　(b)
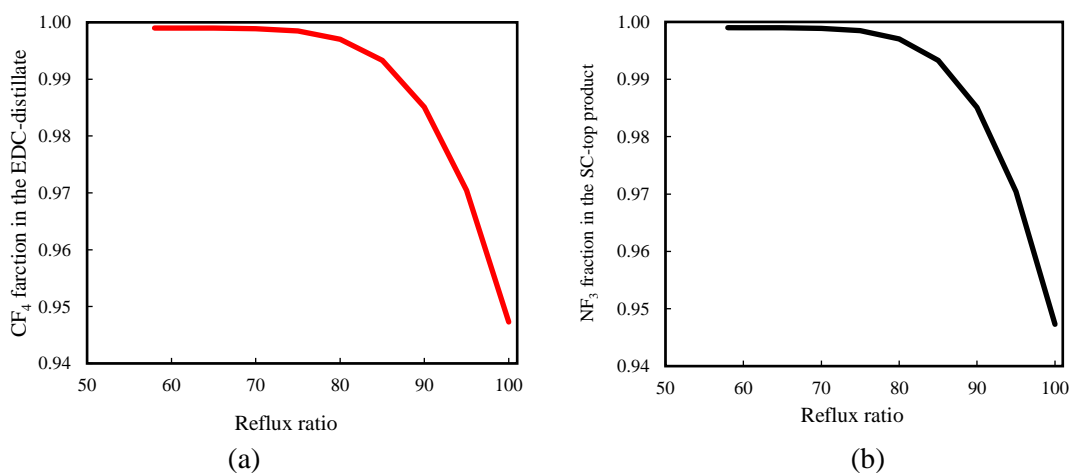
Figure 5-27. Sensitivity analysis of the reflux ratio on the a) NF$_3$ b) CF$_4$ fraction in the product streams for the extractive distillation column with 100 theoretical stages, 100 kmol.hr^{-1} the gas feed composition of 50 % NF$_3$ entering from 50th stage, the solvent flow rate of 500 kmol.hr^{-1} entering from 3rd stage and pressure of 0.10 MPa.

5.11 O'Connell's overall efficiency

The number of stages that have been used so far are the theoretical number of stages. The efficiency of a specific section of the extractive distillation column is used to translate the number of theoretical stages to the actual number of trays. The efficiency is calculated as follows (Duss and Tylor, 2018):

$$\eta_{section} = \frac{n_{theoretical}}{n_{actual\,trays}} \qquad 5.5$$

The empirical correlation proposed by O'Connell to calculate the section efficiencies of bubble cap trays for the hydrocarbons (O'Connell, 1964). Among the other efforts to develop the theoretical based rigorous models, the O'Connell's efficiency is still in use, however, it lacks a theoretical explanation (Duss and Tylor, 2018). The correlation is as follows (O'Connell, 1964):

$$\eta_{section} = 0.503 \times \left(\mu_l \times \alpha\right)^{-0.226} \qquad 5.6$$

where μ and α denote the liquid viscosity in mPa-s and relative volatility, respectively. The viscosity of the TFE-TFP ether was measured to be 1.27 mPa-s at 298.15 K. Due to the limitations in the experimental apparatus (Anton Paar; DMA 5000; expanded uncertainty of 0.001 g/ml) it is not possible to measure the viscosity at 140 K and it is assumed constant with no temperature dependence. The O'Connell's correlation is proposed for hydrocarbons and it is assumed that it can be used for TFE-TFP ether, reducing its reliability. The below section presents the comparisons between the results of the literature and these simulations. The stages are presented in actual tray numbers considering the efficiency of each process for the comparison purposes.

5.12 Evaluation of the proposed process compared to literature

Due to the industrial importance of the high-grade NF_3, there have been several attempts to produce NF_3 with 6-nine grades which were mentioned in chapter 2.2. The use of extractive distillation has been reported by the use of 16 different ionic liquids (Shiflett and Yokozeki, 2014) as well as a long list of entraining agents such as HCl and several refrigerates (Miller et al., 2002). While the use of ionic liquids has shown the potential to produce NF_3 with impurity content of just above 200 ppm at best, the use of HCl obtains an excellent product with below 10 ppm impurity.

The infinite dilution activity coefficient is a crucial factor in the design of the extractive distillation column which indicates the solvent selectivity and affinity upon the selection of the gases and

consequently the solvent capacity for its recovery. The work done by (Shiflett and Yokozeki, 2014) focuses on reporting a long list of the ionic liquids based on their infinite dilution correlated from the experimental phase equilibrium data. The actual phase equilibria are only reported for the [bmim][PF_6] binary data with either CF_4 or NF_3 along with the infinite dilution activity coefficients at the 5 different temperatures. The maximum selectivity is obtained at 283.15 K with 5.53 which is significantly high whereas the best selectivity obtained from current work is approximately 1.57 for TFE-TFP ether at 283.15 K. While there is a remarkable difference between the selectivities obtained, it is clear that due to the electrolyte nature of the ionic liquids there is an improved interaction force between [bmim][PF_6] and the target gaseous mixture. Due to the oxidising property of nitrogen trifluoride and the probable interaction with ionic liquids (depending on the thermo-physical condition), there is a chance of initiation of explosion regimes. Besides, the ionic liquids listed are not produced on an industrial scale within a feasible price range. Due to the specifications of the ionic liquids, it has been noted in the patent manuscript that the best quality product obtained from this mixture is a NF_3 stream with an impurity of just above 200 ppm (Shiflett and Yokozeki, 2014).

The use of strong acids is controversial in the disposal point of view, environmental issues and their corrosive properties. It is worth to mention that except for one case, the product grades reported in (Miller et al., 2002) exclude the solvent traces available in the product. While it has not been mentioned in the patent manuscript, according to the experimental phase data presented, HCl forms an azeotrope with both gases which turns the proposed process into an azeotropic distillation rather than an extractive distillation process. The extractive distillation is advantageous over the azeotropic distillation due to its considerably improved mass transfer (Noll et al., 2013).

Here the feed stream composition and operation condition of the abovementioned systems are considered for the simulation studies with the aim to gauge the proposed process. The first two cases refer to the use of HCl as the separator agent for the separation of 60 % NF_3 feed in the extractive distillation column with two different tray numbers of 122 (gas feed tray of 61) and 244 trays (gas feed tray of 122). Table 5-58 lists the summary of the results for the two cases and the results obtained from this work. According to the table for the case of 122 tray column, the reflux ratio of 70 and operating pressure of 1.50 MPa, the product purity of 58.3084 is obtained which is reported excluding the solvent traces. The increase of reflux ratio and tray number to 700 and 244, respectively led to the lower product quality of 57.4897. The results from simulations performed in the current work showed that it is possible to obtain NF_3 with an impurity traces of 0.4 ppm which includes both CF_4 and solvent traces. This was achieved using a 100-theoretical stage column with 50th and 3rd stages as the

solvent and gas feed stage locations, respectively as well as the reflux ratio of 110. The O'Connell efficiency of the column is 43.5 % obtaining 230 trays numbers. The results showed that there is a temperature enhancement of approximately 116 and 6 degrees for the bottom product and distillate, respectively obtained from this work.

Table 5-58. Summary of simulation comparison for purification of 60 % NF_3 gas feed at 1.50 MPa.

No. of trays	Gas feed stage	Solvent feed stage	Reflux ratio	Product purity	$T_{distillate}/$ K	$T_{bottom}/$ K	Source
122	61	-NA	70	58.3084	193.15	193.15	(Miller et al.,
244	122	-NA	700	57.4897	193.15	193.15	2002)
230	50	3	110	99.99996	199.11	309.97	This work

In addition to HCl, (Miller et al., 2002) reported using 15 other solvents which include some PFCs, HFCs, CFCs, refrigerants and hydrocarbons. Table 5-59 shows the summary of the results for purification of 99 % NF_3 feed in a 120-tray extractive distillation column (gas and solvent tray locations of 20 and 10, respectively) with a reflux ratio of 2000, operating pressure of 1.20 MPa and a product temperature of 193.15 K (bottom and distillate). According to the table, the use of C_3F_8 and C_2F_6 is inefficient as the product quality remains almost similar to the feed composition. The impurity level of 1.3 and 0.3 ppm was obtained using CH_2FCF_3 and CHF_3 as the entraining agent. Very good product grade of 0.1 ppm was achieved using N_2O, C_2H_6, CH_3F, HCl, CH_3Cl, $CHClF_2$, CH_2F_2 and C_2H_5F. It is necessary to note that the impurity results were reported without considering the solvent traces which would have compromised the product quality due to the high L/V ratios of the extractive distillation column. Most of the separating agents reported in this work (HFCs and CFCs) are banned by the Kyoto and Montreal protocols and are to be phased out.

Simulation studies related to this part were performed at the pressure of 1.20 MPa and the feed composition of 99 % NF_3 to compare the results between the two processes. In the first case scenario, given the O'Connell efficiency of 44 %, 52 theoretical stage column was attempted with gas feed stage of 26 and solvent feed stage of 3 to test the use of 120 trays. The results showed that with the reflux ratio of 95 the product with 4.251 ppm impurity is obtained. While the reflux ratio of (Miller et al., 2002) is significantly high, better product quality of 0.1 ppm impurity is obtained for some of the proposed solvents. In the second case, it was aimed to obtain a product with an impurity of below 1 ppm. The results showed that a column of only 68 theoretical stages (gas feed stage of 34 and solvent stage of 3) and reflux ratio of 100 is required to obtain an ultra-pure product with impurity content of 0.199 ppm. The O'Connell efficiency is 43.95 % obtaining 155 actual tray numbers. The third simulation results showed that a column with only 96 theoretical stages (gas feed stage of 48

and solvent stage of 3) is required to obtain an extremely pure product with 0.012 ppm (12 ppb) impurity. The O'Connell efficiency is 44.48 % obtaining 216 actual tray numbers. In addition to the improved NF_3 product quality counting the solvent traces, an extremely pure CF_4 can also be produced. The temperature of the bottom product is approximately 90 degrees warmer than that of miller's work in a lower number of stages.

Table 5-59. Comparison of the simulation results for the feed of 99 % NF_3 at the column pressure of 1.20 MPa.

Solvent	No. of trays	Gas stage	Solvent stage	Reflux ratio	Impurity /ppm	$T_{distillate}$/ K	T_{bottom}/ K	Source
C_3F_8	120	20	10	2000	9110			
C_2F_6	120	20	10	2000	10100			
$CClF_3$	120	20	10	2000	1820			
C_2ClF_5	120	20	10	2000	1650			
C_2HF_5	120	20	10	2000	1150			
CO_2	120	70	10	2000	50.7			
CH_2FCF_3	120	20	10	2000	1.3			
CHF_3	120	20	10	2000	0.3	193.15	193.15	(Miller et al., 2002)
N_2O	120	20	10	2000	0.1			
C_2H_6	120	20	10	2000	0.1			
CH_3F	120	20	10	2000	0.1			
HCl	120	20	10	2000	0.1			
CH_3Cl	120	60	10	2000	0.1			
$CHClF_2$	120	20	10	2000	0.1			
CH_2F_2	120	20	10	2000	0.1			
C_2H_5F	120	20	10	2000	0.1			
TFE-TFP	119	26	3	95	4.251	192.36	282.10	This
ether	155	38	3	100	0.199	192.36	282.10	work
	216	44	3	110	0.012	192.36	282.10	

The last case is the purification of 99.1946 % NF$_3$ using a 200-stage column with the reflux ratio of 5000 and operating pressure of 1.50 MPa. Table 5-60 shows a summary of the results obtained for this case. According to the table, HCl is capable of decreasing the impurity from 8054 to 170 ppm (excluding solvent traces) using 200 stages and the reflux ratio of 5000. The results from simulations showed that the NF$_3$ with an impurity of 0.05 ppm (52 ppb) is achieved in an extractive distillation column with only 72 theoretical stages and a reflux ratio of 110. Considering the O'Connell's efficiency of 43.83 %, 164 actual trays obtained for this case. In addition, it is possible to obtain an extremely pure product with an impurity of 0.013 ppm (13 ppb) in a column with 87 theoretical stages and a reflux ratio of 110. The O'Connell's efficiency for this case is 43.82 %, obtaining 199 actual trays. Furthermore, the bottom product temperature is improved by approximately 111 degrees.

Table 5-60. Comparison of the simulation results for the feed of 99.1946 % NF$_3$ at the column pressure of 1.50 MPa.

No. of trays	Gas feed stage	Solvent feed stage	Reflux ratio	Impurity/ ppm	$T_{distillate}$/ K	T_{bottom}/ K	Source
200	100	-NA	5000	170	198.15	198.15	(Miller et al., 2002)
164	34	3	110	0.05	198.44	309.97	This work
199	44	3	110	0.01	198.44	309.97	This work

In summary, the experimental phase equilibrium data for the binary mixtures of several solvents with the two gases of NF$_3$ and CF$_4$ were presented in this chapter. The solvents were characterised prior to measurements via density, refractive index and GC peak area. The experimental data were fitted to PR (VdW) and PRWS (NRTL) models. The PR (VdW) model was used to design the absorption and extractive distillation processes. Ternary measurements of NF$_3$ + CF$_4$ + solvents were not possible due to the lack of analytical devices to analyse the samples in the SA apparatus. It is one of the future tasks that is recommended. Moreover, it was not possible to generate binary data for NF$_3$ – CF$_4$ mixture and due to the lack of this type of data in the literature, for the sake of process design, it was assumed that the NF$_3$ – CF$_4$ mixture does not form an azeotrope.

The extractive distillation process proposed in this study operates at a more desirable temperature (144 – 440 K) than current industrial-scale operations. This includes the cryogenic distillation process proposed by (Fidkowski, et al., 2001) operating at 81.5 K and 0.30 MPa and the process proposed by (Nagamura et al., 1994) operating at 107.15 K and 0.9 MPa with the final product of 10 ppm for both processes. However the process proposed by (Hyakutake et al., 1990) operates almost at the same temperature and pressure of 144.15 K and 0.10 MPa, respectively compared to the current work, it

obtains product purity of 100 ppm. Due to the change in relative volatility, the number of stages in the extractive distillation is reduced compared to cryogenic, whereas the wider column diameter is required in the extractive distillation demanding more material.

Membrane and adsorption separations are reported to operate at operating temperatures in the ranges of $323.15 < T < 433.15$ K and $77.15 < T < 873.15$ K, respectively (Branken et al., 2014, Hart et al., 2006, Igumnov and Kharitonov, 2006, Singh et al., 2008, Jin and Fisher, 1996, Fisher and Jin, 1997, Fisher, 1998, Nagamura and Yamamoto, 1994). The results from simulations showed that it is possible to the recovery of up to 100 % of the NF_3 from the feed of 100 kmol.hr^{-1} flow rate with the product purity of greater than 99.9999 % (CF_4 content of 0.002 ppb). Membrane and adsorption technologies are unable to handle this scale of production which is added to the other disadvantages of maintenance and cleaning costs associated with adsorbents and membranes.

Additional to their high prices, the GWP of CF_4 and NF_3 are 6500 (Hurley et al., 2005) and 17200 (Forster et al., 2007) compared to that of CO_2 which is 1, making it necessary to recover the maximum possible amount of those gases. Results from this process show almost the total recovery of both gases with high purity from the mixture which has not been reported in any of the available technologies in the literature. The L/V ratio in extractive distillation is regularly high and between 5-8 which is 5 for this study indicating another advantage to the proposed extractive distillation process using TFE-TFP ether.

Results obtained from absorption column simulations runs showed that it was not possible to achieve the product purity of 99.999 %. While the results obtained from extractive distillation runs showed that it is possible to achieve extremely high purity NF_3 with 0.002 ppm (2 ppb), the cost analysis and optimisation has not been performed and more efforts need to be done in that regard. Over the duration of the study, the price of the solvent has increased dramatically also weakening the feasibility of the proposed process, however, the solvent loss is very negligible and the major cost is attributed to the initial solvent charge to the process. Perfluorodecalin is the second best solvents after TFE-TFP ether with lower selectivity towards NF_3 which do not exhibit the ability to purify NF_3.

Chapter 6: Conclusions

From a thorough literature review and solvent screening procedure, physical separation technology was selected for the separation of CF_4 and NF_3 because of the advantages over other techniques such as cryogenic, adsorption and membrane separation.

From solvent screening, 6 suitable solvents were selected for further investigations.

The thermodynamic HPVLE data were generated for the binary system of: CF_4 + (perfluorohexane, perfluoroheptane, perfluorooctane, perfluorodecalin, heptafluoro butanol, tetrafluoroethyl-tetrafluoropropyl ether) and NF_3 + (perfluorohexane, heptafluoro butanol, perfluorodecalin and tetrafluoroethyl-tetrafluoropropyl ether).

The optimal solvent (tetrafluoroethyl-tetrafluoropropyl ether) based on the pre-screening process was determined based on the pricing. The cost of this solvent was R15/ml in 2016 however the recent price for this solvent is R400/ml as of April 2019.

Successful HPVLE experiments were performed for the NF_3 system generating the first HPVLE data. While the solvents were screened on the basis of absorbing CF_4, experimental results showed the affinity of the solvents to dissolve NF_3.

Based on the results obtained, tetrafluoroethyl-tetrafluoropropyl ether was the best performing chemical among the selected solvents, followed by perfluorodecalin and heptafluoro butanol.

Preliminary absorption process simulation studies were performed using Aspen Plus® V10 using a column temperature in the range of (233.15 – 333.15) K, a pressure range of (0.20 – 2.50) MPa, solvent flow rate range of (1880 – 2200) $kmol.hr^{-1}$, a feed composition range of (50 – 90) % of NF_3 and theoretical stage number of (10 – 100) stages.

The absorption process designed is not capable of purifying NF_3 up to 99.99 mole % in several case scenarios of pressure, temperature, solvent flow rate, theoretical stage numbers and feed composition, hence, the extractive distillation was attempted.

The extractive distillation simulation runs using Aspen Plus® V10 showed the ability of the proposed process in producing ultra-high purity CF_4 and NF_3 streams with impurity contents of below 1 ppm.

The most appropriate conditions to obtain high purity NF_3 are the pressure of 0.10 MPa, column number of theoretical stages of 100, gas stage location of 50, solvent stage location of 3, stripping column with 6 theoretical stages and reflux ratio of 58. The average O'Connell's efficiency of 44 % was obtained for different case scenarios.

A comparison between the results obtained from this study and the literature data showed an improved product quality in a higher temperature range and significantly lower reflux ratio.

The benefit of this process is the high solvent, CF_4 and NF_3 recovery which is considered important due to their price as well as high GWP of the gases.

While the price of the solvent increased dramatically over the duration of the study, weakening the feasibility of the process, the solvent loss through the gaseous products of the proposed process is negligible and only the initial solvent charge is required.

The main conclusions obtained from this work are as follows:

•   Absorption is not a feasible method to purify NF_3

•   The results from the theoretical simulation design showed that purification of the feed mixture to an NF_3 product quality of 6-nine grades and impurity below 1 ppm CF_4 is theoretically possible via extractive distillation.

Chapter 7: Recommendations

In terms of the detailed simulation point of view, binary data may not be sufficient. The ternary phase equilibrium data combination between major and minor constituents (NF_3 + CF_4) + solvent systems is required, in order to develop a more detailed design to achieve the proposed separation.

For the purpose of validating the design and getting information on the operation of an extractive distillation column, pilot plant trials for this separation should be conducted. A prototype of an extractive distillation column will provide the opportunity to study the effect of pressure, temperature, liquid flow rate as well as the time required to attain equilibrium and separation.

It is recommended to investigate the possibility of using a cheaper solvent and performing an intensive energy analysis which could help to develop a process overcoming the current industrial issues.

To complement the experimental work, it is necessary to establish a functional group for the UNIFAC group contribution method specific for NF_3. Due to the toxic nature of the fluorinated chemicals, measurements are dangerous, hence the development of a predictive tool is essential.

References

ABBOTT, M. M. 1979. Cubic Equations of State: An Interpretive Review. *Equations of State in Engineering and Research.* American Chemical Society.

ABRAMS, D. S. & PRAUSNITZ, J. M. 1975. Statistical thermodynamics of liquid mixtures: a new expression for the excess Gibbs energy of partly or completely miscible systems. *AIChE Journal,* 21**,** 116-128.

AHMAD, M., HASHIM, H., YUNUS, N., LIM, J., HO, W. & HO, C. 2017. A physical absorption assessment of a new alternative solvent for carbon capture. *Chemical Engineering Transactions,* 56**,** 625-630.

ALCÁNTARA-AVILA, J. R., GÓMEZ-CASTRO, F. I., GABRIEL SEGOVIA-HERNÁNDEZ, J., SOTOWA, K.-I. & HORIKAWA, T. 2014. Energy Minimization in Cryogenic Distillation Columns Through Intermediate Side Heat Exchangers. *In:* KLEMEŠ, J. J., VARBANOV, P. S. & LIEW, P. Y. (eds.) *Computer Aided Chemical Engineering.* Elsevier.

AMEEL, B., T'JOEN, C., DE KERPEL, K., DE JAEGER, P., HUISSEUNE, H., VAN BELLEGHEM, M. & DE PAEPE, M. 2013. Thermodynamic analysis of energy storage with a liquid air Rankine cycle. *Applied Thermal Engineering,* 52**,** 130-140.

ARAMAKI, M., KOBAYASHI, Y., NAKAMURA, T., NAKANO, H. & SUENAGA, T. 1985. *Process of preparing nitrogen trifluoride by gas-solid reaction.*

ARTIOLI, Y. 2008. Adsorption. *In:* JØRGENSEN, S. E. & FATH, B. D. (eds.) *Encyclopedia of Ecology.* Oxford: Academic Press.

BAVETTA, L. A. & DEUEL JR, H. J. 1942. The effect of adrenalectomy on the absorption of hydrogenated cottonseed oil, corn oil, tributyrin and sodium butyrate. *American Journal of Physiology-Legacy Content,* 136**,** 712-715.

BEN-MANSOUR, R., HABIB, M., BAMIDELE, O., BASHA, M., QASEM, N., PEEDIKAKKAL, A., LAOUI, T. & ALI, M. 2016. Carbon capture by physical adsorption: materials, experimental investigations and numerical modeling and simulations–a review. *Applied Energy,* 161**,** 225-255.

BLINOV, I., MUKHORTOV, D., PASHKEVICH, D., PETROV, V., ALEKSEEV, U., KAMBUR, M. & KURAPOVA, E. 2011. Absorption technology of fine cleaning of nitrogen trifluoride from tetrafluoromethane. *Russian Journal of Applied Chemistry,* 84**,** 2159-2163.

BORGHI, D., ABREU, C. & GUIRARDELLO, R. 2015. Use of COSMO-SAC to Determine the Activity Coefficient and Predict Phase Equilibrium of Binary Systems Involving Methanol, Glycerol and Water. *Chemical Engineering Transactions,* 43**,** 1879-1884.

BRANKEN, D., KRIEG, H., LE ROUX, J. & LACHMANN, G. 2014. Separation of NF_3 and CF_4 using amorphous glassy perfluoropolymer Teflon AF and Hyflon AD60 membranes. *Journal of Membrane Science,* 462**,** 75-87.

BRANKEN, D. J., LE ROUX, J. P., KRIEG, H. M. & LACHMANN, G. 2013. A dual-channel gas chromatography method for the quantitation of low and high concentrations of NF3 and CF4 to study membrane separation of the two compounds. *Journal of Chromatography A,* 1307**,** 180-190.

BRASLAVSKY, S. E. 2007. Glossary of terms used in photochemistry, (IUPAC Recommendations 2006). *Pure and Applied Chemistry,* 79**,** 293-465.

BRITT, H. I. & LUECKE, R. H. 1973. The estimation of parameters in nonlinear, implicit models. *Technometrics,* 15**,** 233-247.

BRONKALA, W. J. 2000. Magnetic separation. *Ullmann's Encyclopedia of Industrial Chemistry.*

BRUICE, P. Y. 2003. *Organic Chemistry 4th Edition*, Pearson.

BYRNE, J. E., BATTINO, R. & WILHELM, E. 1975. The solubility of gases in liquids 8. Solubility of He, Ne, Ar, Kr, CO2, CH4, CF4, and SF6 in o-, m-, and p-xylene at 283 to 313 K. *The Journal of Chemical Thermodynamics,* 7**,** 515-522.

CEROFOLINI, G. F., MEDA, L. & BANDOSZ, T. J. 1999. Adsorption with soft adsorbents or adsorbates. Theory and practice. *In:* DĄBROWSKI, A. (ed.) *Studies in Surface Science and Catalysis.* Elsevier.

CHAKMA, A. 1995. An energy efficient mixed solvent for the separation of CO_2. *Energy Conversion and Management,* 36**,** 427-430.

CHEN, D. & CHEN, W. 1992. Phase equilibria of n-hexane and n-octane in critical carbon dioxide. *Huaxue Gongcheng,* 20**,** 66-69.

CHENG, J.-H., BARTOS, S. C., LEE, W. M. & LI, S.-N. 2013. SF6 usage and emission trends in the TFT-LCD industry. *International Journal of Greenhouse Gas Control,* 17**,** 106-110.

CHRISTOV, M. & DOHRN, R. 2002. High-pressure fluid phase equilibria: Experimental methods and systems investigated (1994–1999). *Fluid Phase Equilibria,* 202**,** 153-218.

CORMOS, C.-C. 2015. Assessment of chemical absorption/adsorption for post-combustion CO_2 capture from Natural Gas Combined Cycle (NGCC) power plants. *Applied Thermal Engineering,* 82**,** 120-128.

COSGROVE, B. A. & WALKLEY, J. 1981. Solubilities of gases in H_2O and ^2H_2O. *Journal of Chromatography A,* 216**,** 161-167.

COSTELLO, M. G., FLYNN, R. M. & OWENS, J. G. 2000. *Fluoroethers and fluoroamines*.

CROLL, I. M. & SCOTT, R. L. 1964. Fluorocarbon solutions at low temperatures. IV. The liquid mixtures CH_4 + $CClF_3$, CH_2F_2 + $CClF_3$, CHF_3 + $CClF_3$, CF_4 + $CClF_3$, C_2H_6 + $CClF_3$, C_2H_6 + CF_4, and CHF_3 + CF_4. *The Journal of Physical Chemistry,* 68**,** 3853-3860.

DE LOOS, T. W., POOT, W. & ARONS, J. D. S. 1989. Fluid-phase equilibria and critical phenomena in (tetrafluoromethane+ n-butane). *The Journal of Chemical Thermodynamics,* 21**,** 113-124.

DOHRN, R. & BRUNNER, G. 1995. High-pressure fluid-phase equilibria: Experimental methods and systems investigated (1988–1993). *Fluid Phase Equilibria,* 106**,** 213-282.

DOHRN, R., FONSECA, J. M. S. & PEPER, S. 2012. Experimental Methods for Phase Equilibria at High Pressures. *Annual Review of Chemical and Biomolecular Engineering,* 3**,** 343-367.

DOHRN, R., PEPER, S. & FONSECA, J. M. 2010. High-pressure fluid-phase equilibria: experimental methods and systems investigated (2000–2004). *Fluid Phase Equilibria,* 288**,** 1-54.

DURAN-VALENCIA, C., VALTZ, A., GALICIA-LUNA, L. A. & RICHON, D. 2001. Isothermal vapor−liquid equilibria of the carbon dioxide (CO_2)−n,n-dimethylformamide (DMF) system at temperatures from 293.95 K to 338.05 K and pressures up to 12 MPa. *Journal of Chemical & Engineering Data,* 46**,** 1589-1592.

EBERLY JR, P., KIMBERLIN JR, C., MILLER, W. & DRUSHEL, H. 1966. Coke formation on silica-alumina cracking catalysts. *Industrial & Engineering Chemistry Process Design and Development,* 5**,** 193-198.

EDENHOFER, O. 2015. *Climate change 2014: mitigation of climate change*, Cambridge University Press.

EVANS, F. D. & BATTINO, R. 1971. The solubility of gases in liquids 3. The solubilities of gases in hexafluorobenzene and in benzene. *The Journal of Chemical Thermodynamics,* 3**,** 753-760.

FIDKOWSKI, Z. T., CIRUCCI, J. F., AGRAWAL, R., SUCHDEO, S. R. & AUVIL, S. R. 2001. *Purification of nitrogen trifluoride by continuous cryogenic distillation*.

FIELD, L. R., WILHELM, E. & BATTINO, R. 1974. The solubility of gases in liquids 6. Solubility of N_2, O_2, CO, CO_2, CH_4, and CF_4 in methylcyclohexane and toluene at 283 to 313 K. *The Journal of Chemical Thermodynamics,* 6**,** 237-243.

FINK, J. K. 2016. *Guide to the Practical Use of Chemicals in Refineries and Pipelines*, Gulf Professional Publishing.

FISHER, T. F. 1998. *Cryogenic rectification system for recovery of fluorine compounds*. US-5771713-A.

FISHER, T. F. & JIN, Y. 1997. *Cryogenic rectification system for fluorine compound recovery using additive liquid.* US-5626023-A.

FLAMM, D. L. 1993. Feed gas purity and environmental concerns in plasma etching. *Solid state technology,* 36**,** 43-48.

FLAMM, D. L., DONNELLY, V. M. & IBBOTSON, D. E. 1983. Basic chemistry and mechanisms of plasma etching. *Journal of Vacuum Science & Technology B: Microelectronics Processing and Phenomena,* 1**,** 23-30.

FONSECA, J. M. S., DOHRN, R. & PEPER, S. 2011. High-pressure fluid-phase equilibria: Experimental methods and systems investigated (2005–2008). *Fluid Phase Equilibria,* 300**,** 1-69.

FORNARI, R. E., ALESSI, P. & KIKIC, I. 1990. High pressure fluid phase equilibria: experimental methods and systems investigated (1978–1987). *Fluid Phase Equilibria,* 57**,** 1-33.

FORSTER, P., RAMASWAMY, V., ARTAXO, P., BERNTSEN, T., BETTS, R., FAHEY, D. W., HAYWOOD, J., LEAN, J., LOWE, D. C. & MYHRE, G. 2007. Changes in atmospheric constituents and in radiative forcing. Chapter 2. *Climate Change 2007. The Physical Science Basis.*

FOURNIER, J. A., PHAN, C. L. & BOHN, R. K. 2011. Microwave spectroscopy and characterization of the helical conformer of perfluorohexane. *ARKIVOC,* 5.

FREDENSLUND, A., JONES, R. L. & PRAUSNITZ, J. M. 1975. Group-contribution estimation of activity coefficients in nonideal liquid mixtures. *AIChE Journal,* 21**,** 1086-1099.

FRENCH, R. H., WHELAND, R. C., QIU, W., LEMON, M., ZHANG, E., GORDON, J., PETROV, V. A., CHERSTKOV, V. F. & DELAYGINA, N. I. 2003. Novel hydrofluorocarbon polymers for use as pellicles in 157 nm semiconductor photolithography: fundamentals of transparency. *Journal of Fluorine Chemistry,* 122**,** 63-80.

FRENKEL, M., CHIRICO, R., DIKY, V., YAN, X., DONG, Q. & MUZNY, C. 2005. NIST ThermoData Engine 6.0. National Institute of Standards and Technology. Thermodynamics Research Center (TRC). NIST Applied Chemicals and Materials Division: USA.

GALLARDO, M. A., MELENDO, J. M., URIETA, J. S. & LOSA, C. G. 1987. Solubility of non-polar gases in cyclohexanone between 273.15 and 303.15 K at 101.32 kPa partial pressure of gas. *Canadian Journal of Chemistry,* 65**,** 2198-2202.

GIBANEL, F., LÓPEZ, M., GALLARDO, M., URIETA, J. & LOSA, C. G. 1988. Solubility of nonpolar gases in hexamethylenoxide. *Fluid Phase Equilibria,* 42**,** 261-268.

GONG, Y., GRANT, D. J. & BRITTAIN, H. G. 2007. Principles of solubility. *Solvent systems and their selection in pharmaceutics and biopharmaceutics.* Springer.

GONZÁLEZ, B., GONZÁLEZ, E. J., DOMÍNGUEZ, I. & DOMÍNGUEZ, A. 2010. Excess properties of binary mixtures hexane, heptane, octane and nonane with benzene, toluene and ethylbenzene at T = 283.15 and 298.15 K. *Physics and Chemistry of Liquids,* 48**,** 514-533.

GRAHAM, T. 1866. The solution-diffusion model. *London Edinburgh Dublin Phil. Mag. Sci. Serie,* 32**,** 401-425.

GREENWOOD, N. N. & EARNSHAW, A. 2012. *Chemistry of the Elements*, Elsevier.

HARADA, I., HOKONOHARA, H. & YAMAGUCHI, T. 1990. *Process for purifying nitrogen trifluoride gas*. US-4948571-A.

HARADA, I., HOKONOHARA, H. & YAMAGUCHI, T. 1993. *Method for purifying nitrogen trifluoride gas.* US-5183647-A.

HART, J. J., HENDERSON, P. B., WITHERS JR, H. P., RAO, M. B. & SUBAWALLA, H. 2006. *Process for the purification of NF_3.*

HENDERSON, P. B. & UNDERWOOD, R. P. 2016. *Purification of nitrogen trifluoride by pressure swing absorption.*

HERNÁNDEZ-GARDUZA, O., GARCíA-SÁNCHEZ, F. & NEAU, E. 2001. Generalization of composition-dependent mixing rules for multicomponent systems: prediction of vapor–liquid and liquid–liquid equilibria. *Chemical Engineering Journal,* 84**,** 283-294.

HESSE, P. J., BATTINO, R., SCHARLIN, P. & WILHELM, E. 1996. Solubility of gases in liquids. 20. Solubility of He, Ne, Ar, Kr, N_2, O_2, CH_4, CF_4, and SF_6 in n-Alkanes n-$C_l H_{2l+2}$ ($6 \leq l \leq 16$) at 298.15 K. *Journal of Chemical & Engineering Data,* 41**,** 195-201.

HO, Y.-S. 1995. *Absorption of heavy metals from waste streams by peat.* University of Birmingham, Birmingham, United Kingdom.

HOLLERAN, E. M. & GERARDI, G. J. 1969. Corresponding states of methane, tetrafluoromethane, and their mixtures. *The Journal of Physical Chemistry,* 73**,** 528-533.

HORSTMANN, S., JABŁONIEC, A., KRAFCZYK, J., FISCHER, K. & GMEHLING, J. 2005. PSRK group contribution equation of state: comprehensive revision and extension IV, including critical constants and α-function parameters for 1000 components. *Fluid Phase Equilibria,* 227**,** 157-164.

HOWE-GRANT, M. 1993. Kirk-Othmer Encyclopedia of Chemical Technology, 4th edn, vol. 6. Wiley, New York.

HURLEY, M., WALLINGTON, T., BUCHANAN, G., GOHAR, L., MARSTON, G. & SHINE, K. 2005. IR spectrum and radiative forcing of CF4 revisited. *Journal of Geophysical Research: Atmospheres,* 110.

HYAKUTAKE, H., HARADA, I., IWANAGA, N. & NISHITSUJI, T. 1990. *Method of liquefying and condensing nitrogen trifluoride and a method of purifying nitrogen trifluoride.* US-4975259-A.

IANNUCCI, E. 2009. Necsa launches fluorochemical expansion initiative. *engineering news.*

IGUMNOV, S. M. & KHARITONOV, V. P. 2006. *Method of purifying gaseous nitrogen trifluoride.*

ISLAM, M. R. & CHEN, C.-C. 2015. COSMO-SAC sigma profile generation with conceptual segment concept. *Industrial & Engineering Chemistry Research,* 54**,** 4441-4454.

JESCHKE, P. & SCHNEIDER, G. M. 1982. Phase equilibria in binary mixtures containing fluorocarbons at high pressures and low temperatures V. Liquid-liquid and gas-gas equilibria for tetrafluoromethane+ propane and+ butane up to 200 MPa. *The Journal of Chemical Thermodynamics,* 14**,** 547-554.

JIN, Y. & FISHER, T. F. 1996. *Cryogenic rectification system for fluorine compound recovery*. US-5502969-A.

KEESOM, W. 1915. The second viral coefficient for rigid spherical molecules, whose mutual attraction is equivalent to that of a quadruplet placed at their centre. *Proc. R. Acad. Sci,* 18**,** 636-646.

KISTER, H. Z., HAAS, J. R., HART, D. R. & GILL, D. R. 1992. *Distillation design*, McGraw-Hill New York.

KNAPP, H., DÖRING, R., OELLRICH, L., PLÖCKER, U. & PRAUSNITZ, J. 1981. Vapor–Liquid Equilibria for Mixtures of Low-Boiling Substances, DECHEMA Chem. *Data Series VI, Dechema, Frankfurt.*

KRAFFT, M. P. & RIESS, J. G. 2007. Perfluorocarbons: Life sciences and biomedical uses Dedicated to the memory of Professor Guy Ourisson, a true RENAISSANCE man. *Journal of Polymer Science Part A: Polymer Chemistry,* 45**,** 1185-1198.

KUBIC JR, W. L. & STEIN, F. P. 1981. An experimental and correlative study of the vapor-liquid equilibria of the tetrafluoromethane-chlorotrifluoromethane system. *Fluid Phase Equilibria,* 5**,** 289-304.

LANGE, H. B. & STEIN, F. P. 1970. Volumetric behavior of a polar-nonpolar gas mixture: trifluoromethane-tetrafluoromethane system. *Journal of Chemical & Engineering Data,* 15**,** 56-61.

LAWSON, K. W. & LLOYD, D. R. 1997. Membrane distillation. *Journal of membrane Science,* 124**,** 1-25.

LI, Y.-H., DILLARD, K. H. & ROBINSON JR, R. L. 1981. Vapor-liquid phase equilibrium for carbon dioxide-n-hexane at 40, 80, and 120. degree. C. *Journal of Chemical and Engineering Data,* 26**,** 53-55.

LIDE, D. R. 2005. Physical constants of organic compounds. *CRC handbook of chemistry and physics,* 89**,** 3-1.

LIU, Y., GUO, K. & LU, L. 2012. Vapor–liquid equilibrium measurements for a tetrafluoromethane+ propane system over a temperature range from (142.96 to 293.23) K. *Journal of Chemical & Engineering Data,* 57**,** 3611-3616.

LOBO, L., STAVELEY, L., VENKATASUBRAMANIAN, V., CLANCY, P., GUBBINS, K., GRAY, C. & JOSLIN, C. 1985. Thermodynamic properties of liquid mixtures of hydrogen chloride and tetrafluoromethane. *Fluid Phase Equilibria,* 22**,** 89-105.

LOEB, S. & SOURIRAJAN, S. Advances in Chem. Ser, 1963. 117.

LOWE, K. 1987. Perfluorocarbons as oxygen-transport fluids. *Comparative Biochemistry and Physiology Part A: Physiology,* 87**,** 825-838.

MAINAR, A. M., PARDO, J., ROYO, F. M., LÓPEZ, M. C. & URIETA, J. S. 1996. Solubility of nonpolar gases in 2, 2, 2-trifluoroethanol at 25 C and 101.33 kPa partial pressure of gas. *Journal of Solution Chemistry,* 25**,** 589-595.

MARINA, J. M. & TASSIOS, D. P. 1973. Effective local compositions in phase equilibrium correlations. *Industrial & Engineering Chemistry Process Design and Development,* 12**,** 67-71.

MARTIN, J. J. 1979. Cubic equations of state-which? *Industrial & Engineering Chemistry Fundamentals,* 18**,** 81-97.

MARTIN, J. J. & HOU, Y. C. 1955. Development of an equation of state for gases. *AIChE Journal,* 1**,** 142-151.

MCCABE, W. L., SMITH, J. C. & HARRIOTT, P. 1993. *Unit operations of chemical engineering*, McGraw-hill New York.

MEHRA, Y. R. 1996. *Absorption process for recovering ethylene and hydrogen from refinery and petrochemical plant off-gases*.

MESHRI, D. T. 2000. Chapter 20 - Industrial Applications of Inorganic Fluorides. *In:* NAKAJIMA, T., ŽEMVA, B. & TRESSAUD, A. (eds.) *Advanced Inorganic Fluorides.* Switzerland: Elsevier.

MILLER, R. N., KAO, C.-P. C. & MAHLER, B. A. 2002. *Process for purifying perfluorinated products*.

MILLER, W. T. 1966. *Process for preparing fluorocarbon polyethers*.

MOFARAHI, M., KHOJASTEH, Y., KHALEDI, H. & FARAHNAK, A. 2008. Design of CO_2 absorption plant for recovery of CO_2 from flue gases of gas turbine. *Energy,* 33**,** 1311-1319.

MOLEKUUL.BE. 2010. *Tetrafluoromethane (carbon tetrafluoride, CF4) greenhouse gas molecule. 3D rendering.* [Online]. Available: https://stock.adobe.com/images/tetrafluoromethane-carbon-tetrafluoride-cf4-greenhouse-gas-molecule-3d-rendering/112262760 [Accessed 2010].

MÜHLBAUER, A. 1997. *Phase Equilibria: Measurement & Computation*, CRC press.

MÜHLBAUER, A. L. & RAAL, J. D. 1995. Computation and thermodynamic interpretation of high-pressure vapour—liquid equilibrium—a review. *The Chemical Engineering Journal and the Biochemical Engineering Journal,* 60**,** 1-29.

MUKHORTOV, D., BLINOV, I., KURAPOVA, E. & KAMBUR, P. 2010. Solubility of nitrogen trifluoride and tetrafluoromethane in perfluorinated and highly halogenated fluids. *Russian Journal of Applied Chemistry,* 83**,** 31-35.

MULLINS, E., OLDLAND, R., LIU, Y., WANG, S., SANDLER, S. I., CHEN, C.-C., ZWOLAK, M. & SEAVEY, K. C. 2006. Sigma-profile database for using COSMO-based thermodynamic methods. *Industrial & Engineering Chemistry Research,* 45**,** 4389-4415.

NAGAMURA, T. & YAMAMOTO, T. 1994. *Method and apparatus for the production of ultra-high purity nitrogen*.

NAKAJIMA, T., ŽEMVA, B. & TRESSAUD, A. 2000. *Advanced inorganic fluorides: synthesis, characterization and applications*, Elsevier.

NARASIGADU, C. 2011. *Design of a static micro-cell for phase equilibrium measurements: measurements and modelling.* École Nationale Supérieure des Mines de Paris; University of KwaZulu-Natal

NARASIGADU, C., NAIDOO, P., COQUELET, C., RICHON, D. & RAMJUGERNATH, D. 2013. A novel static analytical apparatus for phase equilibrium measurements. *Fluid Phase Equilibria,* 338**,** 188-196.

NECSA. 2012. *Necsa Integrated Annual Report* [Online]. Available: http://www.necsa.co.za/wp-content/uploads/2018/10/b3.pdf [Accessed].

NECSA. 2018. *Necsa Integrate Annual Report* [Online]. Available: http://www.necsa.co.za/wp-content/uploads/2019/02/Necsa-Annual-Report-2018.pdf [Accessed].

NELSON, W. 2012. *The Separation of Trichlorosilane: Measurement, Modeling and Simulation.* Ph. D. Thesis (Eng.), University of KwaZulu-Natal, Durban, South Africa.

NELSON, W. M., HASSANALIZADEH, R. & RAMJUGERNATH, D. 2017. Phase equilibrium and critical point data for ethylene and chlorodifluoromethane binary mixtures using a new "static-analytic" apparatus. *Fluid Phase Equilibria,* 451**,** 106-113.

NELSON, W. M. & RAMJUGERNATH, D. 2017. Experimental solubility data for binary mixtures of ethane and 2,2,4-trimethylpentane at pressures up to 6 MPa using a new variable-volume sapphire cell. *Journal of Chemical & Engineering Data,* 62**,** 3915-3920.

NOLL, O., GEHRKE, H., LUEBBECKE, C. & KOLBE, B. 2013. *Recovery of benzene and benzene derivatives from gasoline fractions and refinery streams*.

O'HAGAN, D. 2008. Understanding organofluorine chemistry. An introduction to the C–F bond. *Chemical Society Reviews,* 37**,** 308-319.

ORBEY, H., SANDLER, S. I. & WONG, D. S. H. 1993. Accurate equation of state predictions at high temperatures and pressures using the existing UNIFAC model. *Fluid Phase Equilibria,* 85**,** 41-54.

PANDEY, P. & CHAUHAN, R. S. 2001. Membranes for gas separation. *Progress in Polymer Science,* 26**,** 853-893.

PANKRATOV, A. 1973. *Chemistry of Nitrogen Fluorides*, Khimiya, Moscow, Russia.

PARK, S., KANG, W. R., KWON, H. T., KIM, S., SEO, M., BANG, J., HYUP LEE, S., JEONG, H. K. & LEE, J. S. 2015. The polymeric upper bound for N_2/NF_3 separation and beyond; ZIF-8 containing mixed matrix membranes. *Journal of Membrane Science,* 486**,** 29-39.

PENG, D.-Y. & ROBINSON, D. B. 1976. A new two-constant equation of state. *Industrial & Engineering Chemistry Fundamentals,* 15**,** 59-64.

PEPER, S., FONSECA, J. M. S. & DOHRN, R. 2019. High-pressure fluid-phase equilibria: Trends, recent developments, and systems investigated (2009–2012). *Fluid Phase Equilibria,* 484**,** 126-224.

PERRY, R. H., GREEN, D. W. & MALONEY, J. O. 1997. *Perry's Chemical Engineers' Handbook*, McGraw-Hill.

POHANISH, R. P. 2017. *Sittig's handbook of toxic and hazardous chemicals and carcinogens*, William Andrew.

POWELL, R. J. 1972. Solubility of 16 gases in heptacosafluorotributylamine and carbon disulfide. *Journal of Chemical and Engineering Data,* 17**,** 302-304.

PRAUSNITZ, J. M. 1980. *Computer calculations for multicomponent vapor-liquid and liquid-liquid equilibria*, Prentice Hall.

PUMMER, W. J. & WALL, L. A. 1958. Reactions of hexafluorobenzene. *Science,* 127**,** 643-644.

RAAL, J. & MÜHLBAUER, A. 1998. *Phase equilibria: measurement and computation*, Washington, D.C: Taylor and Francious.

RAMJUGERNATH, D., VALTZ, A., RICHON, D., WILLIAMS-WYNN, M. D. & COQUELET, C. 2018. Isothermal vapor–liquid equilibrium data for binary mixtures of hexafluoroethane (R116) + n-pentane or n-hexane at two temperatures, 288 and 296 K. *Journal of Chemical & Engineering Data,* 63**,** 1228-1233.

REDLICH, O. & KWONG, J. N. 1949. On the thermodynamics of solutions. V. An equation of state. Fugacities of gaseous solutions. *Chemical Reviews,* 44**,** 233-244.

REIJERKERK, S. R., KNOEF, M. H., NIJMEIJER, K. & WESSLING, M. 2010. Poly (ethylene glycol) and poly (dimethyl siloxane): Combining their advantages into efficient CO_2 gas separation membranes. *Journal of Membrane Science,* 352**,** 126-135.

REISIG, H., WISOTZKI, K.-D. & SCHNEIDER, G. 1989. Phase equilibria of the binary systems CF_4+ methylpropane and CF_4+ dimethylpropane measured in a new low-temperature high-pressure apparatus. *Fluid Phase Equilibria,* 51**,** 269-283.

REISS, H., FRISCH, H. & LEBOWITZ, J. 1959. Statistical mechanics of rigid spheres. *The Journal of Chemical Physics,* 31**,** 369-380.

RENON, H. & PRAUSNITZ, J. M. 1968. Local compositions in thermodynamic excess functions for liquid mixtures. *AIChE journal,* 14**,** 135-144.

RIESS, J. G. & LE BLANC, M. 1982. Solubility and transport phenomena in perfluorochemicals relevant to blood substitution and other biomedical applications. *Pure and Applied Chemistry,* 54**,** 2383-2406.

ROBBINS, L. 1980. Liquid-liquid- extraction- a pretreatment process for waste- water. *Chemical Engineering Progress,* 76**,** 58-61.

RUBIO, R. G., CALADO, J. C. G., CLANCY, P. & STREETT, W. B. 1985. A theoretical and experimental study of the equation of state of tetrafluoromethane. *The Journal of Physical Chemistry,* 89**,** 4637-4646.

RUTHVEN, D. M. 1984. *Principles of adsorption and adsorption processes*, John Wiley & Sons.

SCOTT, R. L. 1956. Corresponding states treatment of nonelectrolyte solutions. *The Journal of Chemical Physics,* 25**,** 193-205.

SHIFLETT, M. B. & YOKOZEKI, A. 2014. *Process for purifying perfluorinated products*.

SIGMAALDRICH. 2019. Available: https://www.sigmaaldrich.com/ [Accessed].

SINGH, R. R., PAONESSA, M. R., LULY, M. H. & ORLOWSKI, D. F. 2008. *Purification of nitrogen trifluoride*.

SMITH, A. R. & KLOSEK, J. 2001. A review of air separation technologies and their integration with energy conversion processes. *Fuel Processing Technology,* 70**,** 115-134.

SMITH, J., VAN NESS, H. & ABBOTT, M. 2005. *Vapor/liquid equilibrium: introduction. introduction to chemical engineering thermodynamics*, Singapore: McGraw Hill. p.

SMITS, P., SMITS, R., PETERS, C. & DE SWAAN ARONS, J. 1997. High pressure phase behaviour of $\{xCF_4+ (1- x) H_2O\}$. *The Journal of Chemical Thermodynamics,* 29**,** 23-30.

SOAVE, G. 1972. Equilibrium constants from a modified Redlich-Kwong equation of state. *Chemical Engineering Science,* 27**,** 1197-1203.

SOLOMONS, S.-L. 2018. *Emerging South African fluorspar producer pursues aggressive strategy* [Online]. Available: https://www.miningreview.com/top-stories/emerging-south-african-fluorspar-producer-pursues-aggressive-strategy/ [Accessed].

SOO, C.-B., THÉVENEAU, P., COQUELET, C., RAMJUGERNATH, D. & RICHON, D. 2010. Determination of critical properties of pure and multi-component mixtures using a "dynamic–synthetic" apparatus. *The Journal of Supercritical Fluids,* 55**,** 545-553.

SOUSA, J. M. & FONSECA, I. M. 2014. Solubility of hydrofluorocarbons in halobenzene solvents. *Journal of Chemical & Engineering Data,* 59**,** 3605-3609.

SOUSA, J. M. M. V., FERREIRA, A. G. M., FACHADA, H. C. & FONSECA, I. M. A. 2010. Solubility of CF_4 in lower alcohols. *Fluid Phase Equilibria,* 296**,** 95-98.

SPEXCERTIPREP. 2017. United States of America. Available: https://www.spexcertiprep.com/MSDS/140-2003-D.pdf [Accessed 25.07.2017 2017].

STROBRIDGE, T. R. 1962. *The Thermodynamic Properties of Nitrogen from 64 to 300 K between 0.1 and 200 Atmospheres*, US Department of Commerce, National Bureau of Standards.

SUENAGA, T., FUJII, T. & KOBAYASHI, Y. 1991. *Method of refining nitrogen trifluoride gas*.

TASAKA, A. 2007. Electrochemical synthesis and application of NF3. *Journal of Fluorine Chemistry,* 128**,** 296-310.

TRO, N. J., FRIDGEN, T. & SHAW, L. 2011. *Chemistry: A Molecular Approach, 2e*.

TSAI, W.-T. 2008. Environmental and health risk analysis of nitrogen trifluoride (NF_3), a toxic and potent greenhouse gas. *Journal of Hazardous Materials,* 159**,** 257-263.

TSAI, W.-T., CHEN, H.-P. & HSIEN, W.-Y. 2002. A review of uses, environmental hazards and recovery/recycle technologies of perfluorocarbons (PFCs) emissions from the semiconductor manufacturing processes. *Journal of Loss Prevention in the Process Industries,* 15**,** 65-75.

TUINIER, M. J., HAMERS, H. P. & VAN SINT ANNALAND, M. 2011. Techno-economic evaluation of cryogenic CO_2 capture—A comparison with absorption and membrane technology. *International Journal of Greenhouse Gas Control,* 5**,** 1559-1565.

TWU, C. H., BLUCK, D., CUNNINGHAM, J. R. & COON, J. E. 1991. A cubic equation of state with a new alpha function and a new mixing rule. *Fluid Phase Equilibria,* 69**,** 33-50.

UUSI-KYYNY, P., IONITA, S., QURESHI, M. S., ALOPAEUS, V. & RICHON, D. 2016. Design of equilibrium cells for phase equilibria and PVT measurements in large ranges of temperatures and pressures. I. vapor–liquid–liquid equilibria. *Journal of Chemical & Engineering Data,* 61**,** 2700-2711.

VALTZ, A., COQUELET, C. & RICHON, D. 2004. Vapor–Liquid Equilibrium Data for the Sulfur Dioxide (SO_2) + Difluoromethane (R32) System at Temperatures from 288.07 to 403.16 K and at Pressures up to 7.31 MPa. *International Journal of Thermophysics,* 25**,** 1695-1711.

VAN DER WAALS, J. D. 1873. *On the continuity of the gas and liquid state* Doctoral dissertation, Ph. D. thesis, University of Leiden, Leiden, The Netherlands.

WAGNER, Z. & WICHTERLE, I. 1987. High-pressure vapour—liquid equilibrium in systems containing carbon dioxide, 1-hexene, and n-hexane. *Fluid Phase Equilibria,* 33**,** 109-123.

WALAS, S. M. 2013. *Phase equilibria in chemical engineering*, Butterworth-Heinemann.

WANG, S., LIN, S.-T., WATANASIRI, S. & CHEN, C.-C. 2009. Use of GAMESS/COSMO program in support of COSMO-SAC model applications in phase equilibrium prediction calculations. *Fluid Phase Equilibria,* 276**,** 37-45.

WIJMANS, J., HE, Z., SU, T., BAKER, R. & PINNAU, I. 2004. Recovery of perfluoroethane from chemical vapor deposition operations in the semiconductor industry. *Separation and Purification Technology,* 35**,** 203-213.

WILCOCK, R. J., BATTINO, R. & WILHELM, E. 1977. The solubility of gases in liquids 10. The solubility of He, Ne, Ar, Kr, N_2, O_2, CO, CO_2, CH_4, CF_4, and SF_6 in cyclooctane at 289 to 313 K. *The Journal of Chemical Thermodynamics,* 9**,** 111-115.

WILCOCK, R. J., MCHALE, J. L., BATTINO, R. & WILHELM, E. 1978. Solubility of gases in liquids. 12 Solubility of He, Ne, Ar, Kr, N_2, O_2, CO, CO_2, CH_4, CF_4, and SF_6 in octamethylcyclotetrasiloxane at 292 to 313 K. *Fluid Phase Equilibria,* 2**,** 225-230.

WILLIAMS-WYNN, M. D. 2018. *Discovering New Solvents For Supercritical Extraction Processes* [Online]. Sciencetrends. Available: https://sciencetrends.com/discovering-new-solvents-for-supercritical-extraction-processes/ [Accessed].

WILLIAMSON, T. H. 2013. *Vitreoretinal surgery*, Springer Science & Business Media.

WILSON, G. M. 1964. Vapor-liquid equilibrium. XI. A new expression for the excess free energy of mixing. *Journal of the American Chemical Society,* 86**,** 127-130.

WIRTHS, M. & SCHNEIDER, G. M. 1985. High-pressure phase studies on fluid binary mixtures of hydrocarbons with tetrafluoromethane and trifluoromethane between 273 and 630 K and up to 250 MPa. *Fluid Phase Equilibria,* 21**,** 257-278.

WONG, D. S. H. & SANDLER, S. I. 1992. A theoretically correct mixing rule for cubic equations of state. *AIChE Journal,* 38**,** 671-680.

WOYTEK, A. J. & LILECK, J. T. 1978. *Preparation of nitrogen trifluoride*.

ZAKHAROV, N., MATYASH, Y. I., DEMENKOV, A. & DOMNINA, E. 1977. Phase equilibria in the nitrogen-freon-13 and freon-14-freon-13 systems at high pressures. *Russian Journal of Physical Chemistry A,* 51**,** 1640-1642.

ZARZYCKI, R. & CHACUK, A. 2013. *Absorption: fundamentals & applications*, Elsevier.

ZHU, H., GONG, M., ZHANG, Y. & WU, J. 2006. Isothermal vapor−liquid equilibrium data for tetrafluoromethane + ethane over a temperature range from (179.68 to 210.03) K. *Journal of Chemical & Engineering Data,* 51**,** 1201-1204.

ZIONMARKETRESEARCH 2018. Fluorochemicals market by product (fluoropolymers, specialty, fluorocarbons, and inorganics) and by end-user (aluminum production, home & industrial appliances, refrigeration, pharmaceuticals, electrical & electronics and other end users) - global industry perspective, comprehensive analysis and forecast, 2017 – 2024. *zionmarketresearch.*

Appendices

Appendix A: A review of the literature data

As a part of the solvent selection process, it is essential to consider the thermodynamic data presented in the literature. In the following appendix, more than 117 systems presented in the literature and their results were studied and classified into three groups of *T-x*, *P-x-y*, and *P-x* data sets.

A.1 Temperature – composition data

In the literature, a wide range of *T-x* data is presented at 0.1 MPa for the systems, including tetrafluoromethane and various solvents. The published data are generally (except for a few sets) in the range of 273.15 to 313.15 K. Tetrafluoromethane exhibited the highest solubility in two solvents, namely hexaflurobenzene (C_6F_6) and perfluorotributalamine ($C_{12}F_{27}N$). Given that the data were measured at 0.1 MPa, it will certainly show significant growth in the case of increased pressure. The comparative *T-x* diagram of the CF_4 solubility is shown in figure A-1.
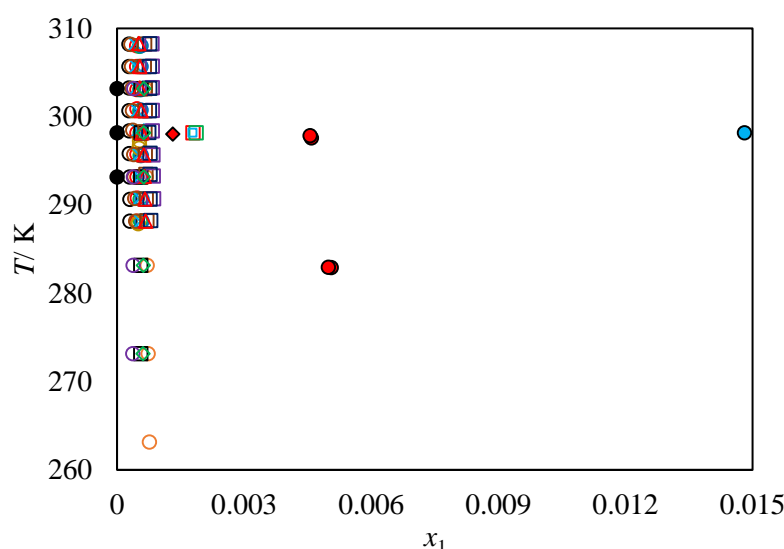

Figure A-1. The comparative *T-x* diagram for some of the published data of CF_4 + solvents. The solvents include; ○ methanol (Borghi et al., 2015), ○ ethanol (Sousa et al., 2010), ○ propanol (Sousa et al., 2010), ○ butanol (Sousa et al., 2010), ○ benzene (Evans and Battino, 1971), × toluene (Field et al., 1974), □ m-xylene (Byrne et al., 1975), □ mesitylene (Byrne et al., 1975), ○ 2-butanol (Borghi et al., 2015), ○ bromobenzene (Sousa and Fonseca, 2014), □ 2-methylcyclohexane (Field et al., 1974), □ dodecane (Wilcock et al., 1977), □ decane (Hesse et al., 1996), □ tetradecane (Wilcock et al., 1977), ● water (Cosgrove and Walkley, 1981), ○ cyclohexanone (Gallardo et al., 1987), ● hexafluorobenzane (Evans and Battino, 1971), ● perfluorotributalamine (Powell, 1972), ◆ 2,2,2-trifluoroethanol (Mainar et al., 1996), ◇ hexamethylenoxide (Gibanel et al., 1988).

A.2 Pressure-composition data

The number of P-x-y data sets in the literature for the CF_4 systems is limited, which were in most of the cases published for the vapour phase. The P-x-y data published in the literature did not introduce a solvent with a significant ability to absorb CF_4. The P-x-y plot is shown in figure A-2.
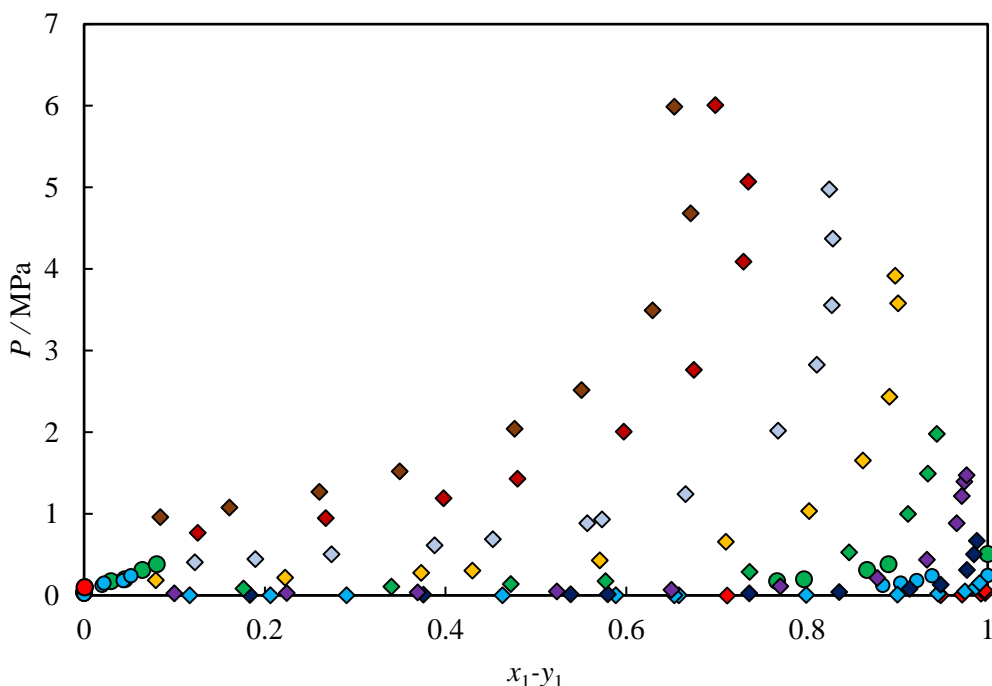

Figure A-2. The comparative P-x-y diagram for some of the published data of CF_4 + solvents. The solvents include HCl (● 173.1 and ● 159 K) (Lobo et al., 1985), propane (◆ 142.96, ◇ 163.07, ◆ 183.1, ◆ 203.16, ◆ 223.17, ◆ 243.12, ◇ 263.15, ◆ 283.01 and ◆ 293.23 K) (Liu et al., 2012) and ● cyclooctane (Wilcock et al., 1977).

A.3 Bubble point data

There are some bubble point data published for the CF_4 systems using the static-synthetic apparatus. The higher absorption capacity was observed at remarkably elevated pressures, however, the above-mentioned solvents were among the systems measured and published. There is not a distinguished solvent among the systems published. The liquid-liquid equilibrium results are presented in figure A-3.
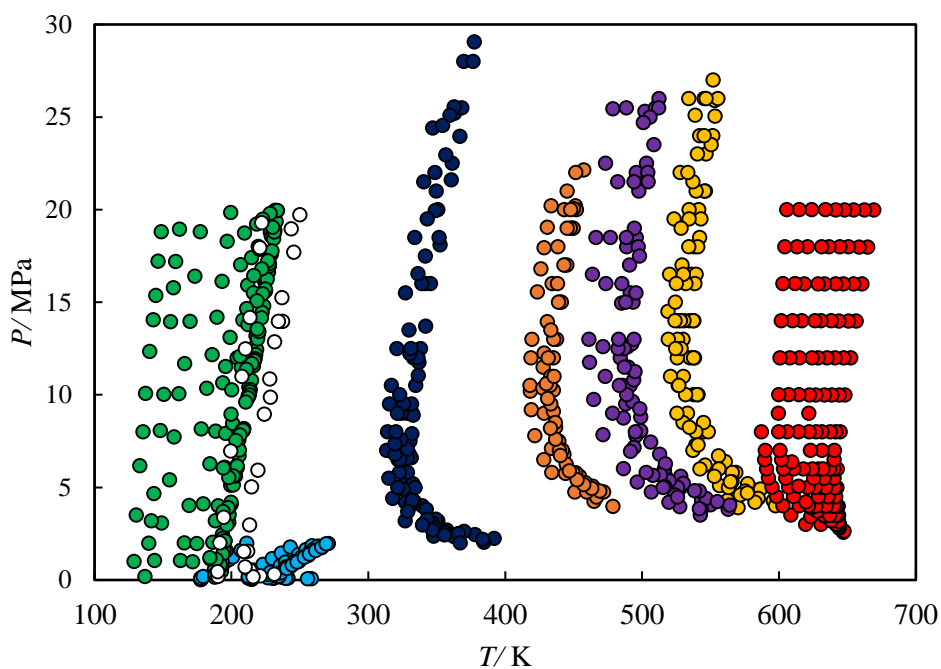
Figure A-3. The comparative *P-T* diagram for some of the published LLE data of CF$_4$ + solvents. The solvents include ● butane (De Loos et al., 1989), ● dodecane (Hesse et al., 1996), ● heptane (Wirths and Schneider, 1985), ● tetralin (Wirths and Schneider, 1985), ● water (Smits et al., 1997), ● propane (Jeschke and Schneider, 1982), ● cis-decalin (Wirths and Schneider, 1985), and ○ methylpropane (Reisig et al., 1989).

In summary, the overall review of the data presented in the literature showed that the chemicals from perfluorinated families exhibited improved solubility for CF$_4$. The perfluorotributylamine (CAS no. 311-89-7) and hexafluorobenzene (CAS no. 392-56-3) are the solvents which CF$_4$ showed the highest solubility.

Appendix B: Chemical compatibility table

The chemical compatibility of the material used in this work with the O-rings is presented in table B-1.

Table B-1. Chemical compatibility of the gas and liquids used in this work.

Chemical	Teflon	PTFE	Viton	Polyurethane
Carbon dioxide	1	1	2	1
Tetrafluoromethane	1	1	1	1
Nitrogen trifluoride	1	1	1	1
Hexane	1	1	1	1
Perfluorohexane	1	1	3	1
Perfluoroheptane	1	1	3	1
Perfluorooctane	1	1	3	1
Perfluorodecalin	1	1	3	1
Perfluoroalcohol	3	1	3	1
Perfluoroether	3	1	3	1

[1] Compatible

[2] Compatible in low pressures

[3] Non-compatible
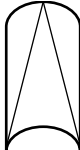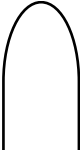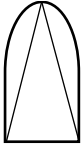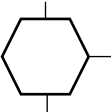
Appendix C: Fault tree analysis

The fault tree analysis (FTA) was based on the potential hazards for the phase equilibrium measurements of the nitrogen trifluoride systems. At first, potential risks were identified, and the degree of importance and hazard degree was indicated. After assigning the hazard code, an FTA was drawn up, and the gates for each hazard were linked in place to the previous source. Table C-1 lists each of the gate icons.

C.1 Gate symbols

For each gate symbol, a specific definition states the relation of each input and output based on their degree of influence on each other.

- OR gate - the output occurs if any input occurs.
- AND gate - the output occurs only if all inputs occur (inputs are independent).
- Exclusive OR gate - the output occurs if exactly one input occurs.
- Priority AND gate - the output occurs if the inputs occur in a specific sequence specified by a conditioning event.
- Inhibit gate - the output occurs if the input occurs under an enabling condition specified by a conditioning event.

Table C-1. Gate symbols and their meanings

| OR gate | And gate | Exclusive OR gate | Priority AND gate | Inhibit gate |

The Hazards are classified into three groups of:

- The gas release under the fume hood
- The potential release of gas by dropping the cell outside the fume hood

C.2 The gas release under the fume hood

The chance of occurrence of this set of gas release is due to human mistakes including negligence, fatigue, or lack of attention to possible gas leakage signs. The human errors may include a fault in the fitting connected to the apparatus, filling the cell up to a pressure higher than the permissible pressure leakage of the NF_3 cylinder or leakage during the process of filling the vapour-liquid mixture.

In the event that the equilibrium cell exceeds the pressure limit (10.00 MPa for the transducer and 17.50 MPa for the Swagelok valve), there is a likelihood of failure in the respective compartment, which will lead to gas leakage. All of the above release gas to the environment only if there is a problem in the fume hood suction, with the most important factor being the failure of the power supply. According to the calculations performed for the concentration of gas in the fume hood, in the event of a power failure and simultaneously releasing the total gas from the equilibrium cell (a completely unlikely event), the impurity concentration does not exceed IDLH. Due to the use of special masks and cartridges, the gas concentration is below the PEL (100 ppm) that does not threaten the user's risk.

In the event of such an accident, the laboratory area should be evacuated immediately so that other laboratory members are not exposed to the gas leaked. The fault tree analysis of the gas leakage is shown in figure C-1.

Given that the molecular mass of nitrous trifluoride (71 g/mole) is higher than air (29 g/mole), if there is a major leakage, it will direct to the floor and until the full evacuation of the laboratory area, there is the low possibility of a large inhalation of this gas. It should be noted that the lab should be evacuated immediately after the electricity tripping.
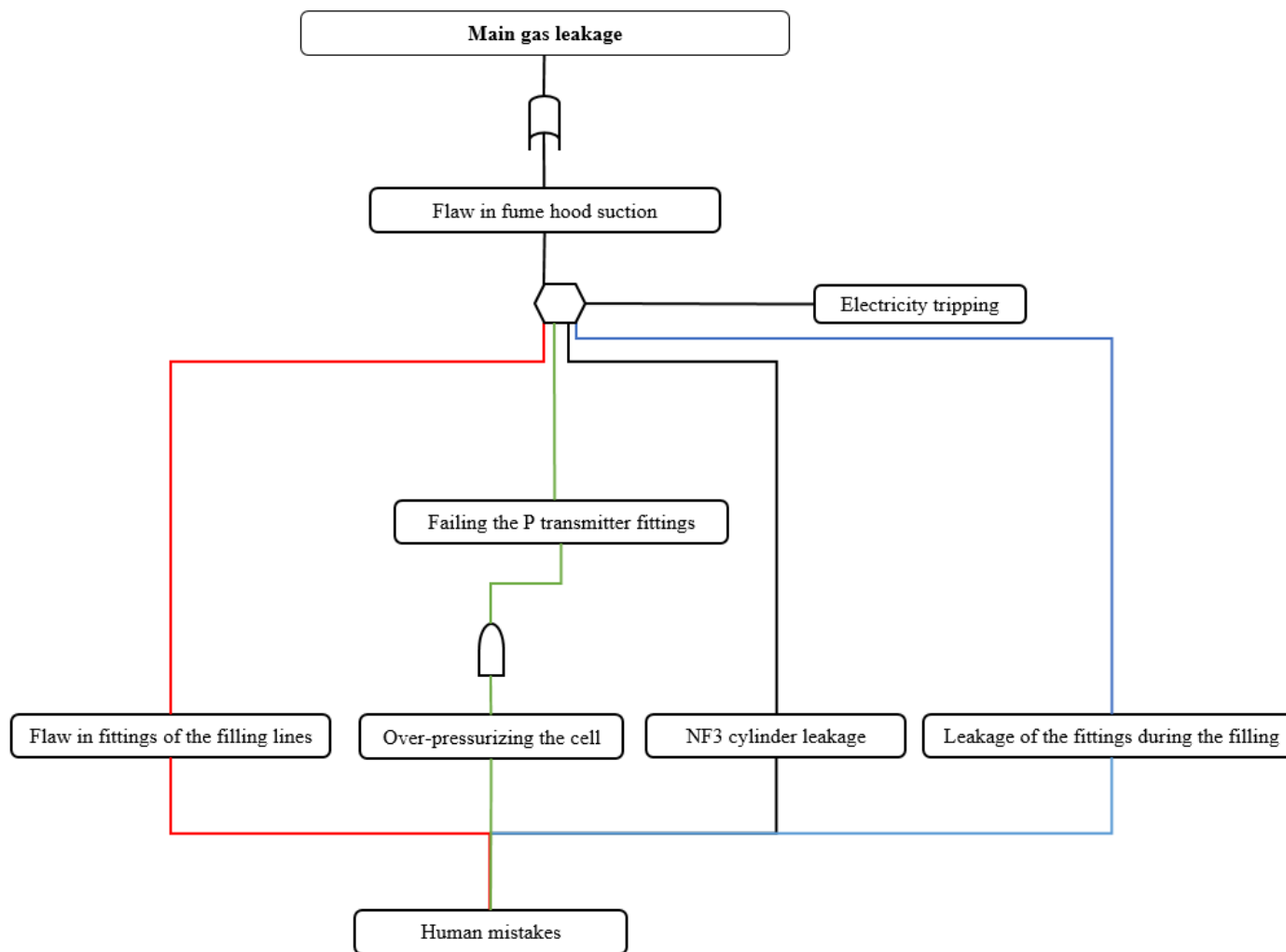
Figure C-1. Fault tree analysis for the *P-x* measurements of NF$_3$ + identified solvents (gas leakage).

C.3 Release of gas outside the fume hood

The cell weighing is required to prepare the vapour-liquid mixture. The corresponding balance is located outside the fume hood, and the cell is weighed three times while carrying the gas (four times in total). The weighing requires manual handover of the cell. There must be sufficient precaution during the cell transfer to prevent it from dropping. Due to the fact that the Sapphire tube is protected by two flanges made of SSL 316, there is a low possibility of sapphire tube breakage as it is enclosed by two thick flanges from top and bottom, respectively. In the event of cell breakage or fracturing, the concentration of gas in the laboratory environment reaches less than 10 ppm. In any case, the lab environment should be evacuated quickly to prevent any risk. The FTA for this case of leakage is shown in figure C-2.
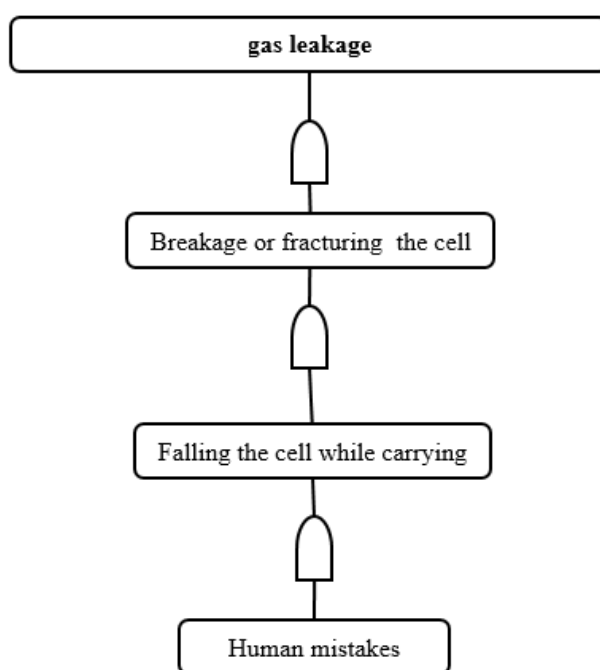
Figure C-2. Fault tree analysis for the case of weighing the cell out of the fume hood.

C.4 Exposure limits

The maximum allowed limit for working with nitrogen trifluoride has been presented in various work environments by different organisations. In different exposure limits including threshold limit value (TLV) by the ACGIH 2001, permissible exposure limit (PEL) by the OSHA 2003, recommended exposure limit (REL) by the NIOSH 2004, and permissible concentration standard by the COLA 2003 the limits are set to be 10 ppm for 8 hrs of working per 5 days of week. Immediately dangerous to life or health (IDLH) limit is set to be 1000 ppm, which can severely affect vital organs such as blood system, liver, and kidneys. With the use of a 3 M, 6500 masks with a fluorinated gas specified cartridge and filter; the IDLH limit is multiplied by 10, reaching 10000 ppm (OSHA). The affected organs and exposure routes of the NF_3 are listed in table C-2.

Table C-2. NF_3 target organs and limits.

Material	Exposure route	Critical effect
Nitrogen trifluoride	Inhalation, blood	Blood, liver and kidneys

C.4.1 NF₃ Decomposition and reactivity

The NF_3 decomposes at temperatures higher than 100 °C as well as the presence of sparks, even if they are not visible. Rogers (1961) investigated the reactivity of NF_3 with water at 373 K for seven days, resulting in HF formation:

$$NF_3 + 2H_2O \rightarrow 3HF + HNO_2$$ C.1

Klapotke (2006) ignited the gaseous mixture containing NF_3 and water vapour by sparking and then reacted according to the following equation:

$$2NF_3 + 3H_2O \rightarrow 6HF + NO + NO_2$$ C.2

Sinke (1965), studied the reaction of hydrogen and NF_3:

$$2NF_3 + 3H_2 \rightarrow N_2 + 6HF$$ C.3

The NF_3 decomposition and reactions lead to the production of different material including NF_3O, F_2, HF, NO_2, NO, N_2O, HNO_2, and HNO_3. The health issues (NIOSH 2004 and ACGIH 2012) and toxicity information of the decomposed material are listed in the tables C-3 and C-4.

Table C-3. Hazards and decomposition products of NF_3 to health.

Material	Exposure routes	Target organs	TLV basis-critical effect
Fluorides	Inhalation	Blood, liver, kidneys	Anoxia, Irritation, bone; fluorosis
Fluorine (F_2)	Inhalation, skin and eye contact	Eyes, skin, respiratory system, liver, kidneys	Irritation
Nitric acid (HNO_3)	Inhalation, ingestion, skin and eye contact	Eyes, skin, respiratory system, central nervous system	Irritation; corrosion; pulmonary oedema
Nitric oxide (NO)	Inhalation	Blood, liver, kidneys	Anoxia; irritation; cyanosis
Nitrogen dioxide (NO_2)	Inhalation, skin and eye contact	Eyes, respiratory system, central nervous system	Irritation; pulmonary oedema
Nitrous oxide (N_2O)	Inhalation, skin and eye contact	Eyes, skin, respiratory system	Reproduction; blood; CNS
Hydrogen fluoride (HF)	Inhalation, skin absorption (liquid), ingestion (solution), skin and/or eye contact	Eyes, skin, respiratory system, bones	Irritation; bone; teeth; fluorosis

Table C-4. Occupational exposure limits/levels of NF_3 and its probable decomposition products based on the time-weighted average (TWA) concentration for 8-h (or up to a 10-h) workday and a 40-h workweek.

MATERIAL	TLV	PEL	REL	OEL	MAC	PCS	IDLH
Fluorine (F2)	1 ppm	0.1 ppm	——	——	0.1 ppm	1 ppm	25 ppm
Nitric acid (HNO3)	2 ppm	2 ppm	2 ppm	2 ppm	2 ppm	2 ppm	25 ppm
Nitric oxide (NO)	25 ppm	25 ppm	——	——	25 ppm	25 ppm	100 ppm
Nitrogen dioxide (NO2)	3 ppm	1 ppm	1 ppm	——	5 ppm	5 ppm	1000 ppm
Nitrous oxide (N2O)	50 ppm	——	25 ppm	——	100 ppm	——	——
Hydrogen fluoride (HF)	3 ppm	3 ppm	3 ppm	——	——	——	40 ppm

TLV: Threshold limit value, American Conference of Governmental Industrial Hygienists (ACGIH 2002).
PEL: Permissible Exposure Limit, Occupational Safety and Health Administration (OSHA 2003).
REL: Recommended Exposure Limit, National Institute for Occupational Safety and Health (NIOSH 2004).
OEL: Occupational Exposure Limit, Japan Society for Occupational Health (JSOH 2006).
MAC: Maximum Allowable Concentration, Deutsche Forschungsgemeinschaft (DFG 2002).
PCS: Permissible Concentration Standard, Council of Labor Affairs (COLA 2003).
IDLH: Immediately Dangerous to Life or Health (NIOSH 2004).

The hydrogen fluoride and nitric acid among the decomposed material are highly soluble in water. The fluorine forms HF in water. The nitrous oxide and nitric oxide are slightly soluble and nitrogen dioxide react with water (Dean, 1999 and Lewis 2004). Considering the systems measured and the molecular structure of nitrogen fluoride, and taking into account the structural characteristics of the considered solvents, the probability of solubility of this gas in the perfluorohexane substance is anticipated to be larger than the rest of the solvents. Therefore, the system is modelled with by Peng Robinson equation of state and $k_{ij} = 0$. Using the static-synthetic apparatus, the composition of various percentages was calculated. Figure C-3 shows the phase equilibrium prediction of the $NF_3 + C_6F_{14}$ system at 283.15 K.

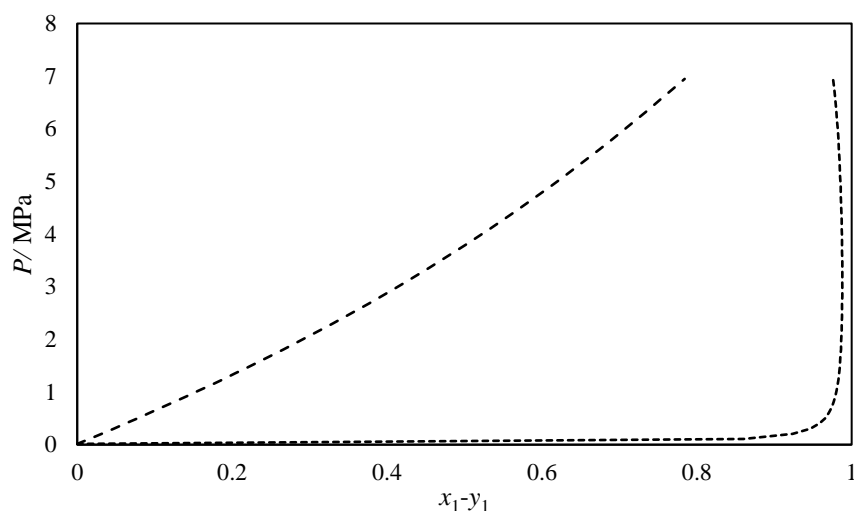**Figure C-3.** Modelling results for the $NF_3 + C_6F_{14}$ system using Peng Robinson EoS at 283.15 K with $k_{ij}=0$.

At least 3 ml of the solution is required to start the experiment via a static synthetic apparatus. With this in mind and the densities of the solvent and gas, the compositions were calculated to provide the minimum and maximum amount of materials needed for each data point.

The fume hood volume is calculated to be 2 m^3 (2×10^6 ml). The worst-case for the measurement is the situation in which there is an electricity trip together with the total release of the gas from the equilibrium cell. The concentration of the NF_3 inside the fume is presented in table C-5 for the worst possible case.

Table C-5. Maximum possible leakage of the NF_3 from the equilibrium cell.

Z	P (MPa)	NF_3 volume (ml)	NF_3 concentration (ppm)
0.229	1.5	333	167
0.405	2.9	333	167
0.576	4.5	667	334
0.671	5.6	1000	500
0.731	6.4	1333	667
0.773	6.9	1667	834

Figure C-4 shows the IDLH and the maximum possible gas leakage from the equilibrium cell. The red arrow is the exposure limit.
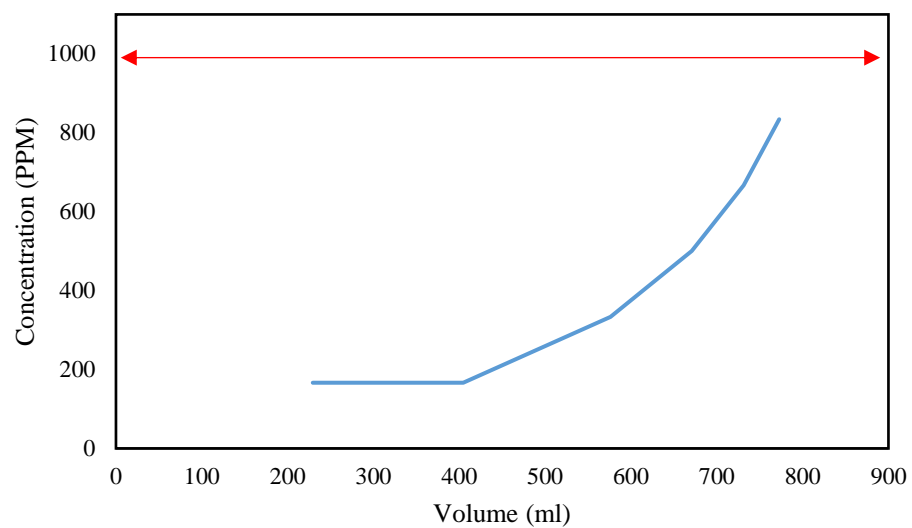
Figure C-4. The maximum possible release of NF_3 for each point. The red arrow shows the IDLH limit.

Appendix D: Uncertainty Estimation

It is very important to report all possible sources of uncertainty while providing the main measurement data. When there is more than one source of uncertainty, overall uncertainty is combined as standard uncertainty. The reader is referred to the works of (Soo et al., 2010) and (Nelson, 2012) for a detailed discussion of the procedures used in computing compositional uncertainty. In this report, the uncertainty was evaluated per the NIST guidelines for uncertainty reporting. The basic equation used for the uncertainty evaluation is as follows:

$$u_c^2(y) = \sum_{i=1}^{N} \left(\frac{\partial f}{\partial x_i}\right)^2 u^2(x_i) + 2 \sum_{i=1}^{N-1} \sum_{j=i+1}^{N} \frac{\partial f}{\partial x_i} \frac{\partial f}{\partial x_j} u(x_i, x_j) \qquad \text{D.1}$$

Where $u_c(\theta)$ is defined as the standard uncertainty of (θ). The uncertainty components of the equation (D.1) can be carried out using types A and B:

$$\text{Type A} \qquad u_i(\theta) = \frac{\sigma}{\sqrt{N_{rp}}} \qquad \text{D.2}$$

$$\text{Type B} \qquad u_i(\theta) = \frac{b}{\sqrt{3}} \qquad \text{D.3}$$

Where N_{rp}, σ and b are the number of data points repeated, standard deviation and the maximum error of the calibration polynomial. The combined expanded standard uncertainty is calculated with the coverage factor (K) of 2, giving a confidence level of 95 %.

$$U(\theta) = K u_c(\theta) \qquad \text{D.4}$$

D.1 Temperature and pressure

The combined standard uncertainty in temperature is calculated as follows:

$$u_c(T) = \pm\sqrt{u_{calibration}(x)^2 + u_{repeatability}(x)^2} \qquad \text{D.5}$$

The repeatability component is calculated through equation D.2. However, the calibration component is classified as Type B and is evaluated as follows:

$$u_{calibration}(T) = \pm\sqrt{u_{correlation}(T)^2 + u_{standard}(T)^2} \qquad \text{D.6}$$

Where the correlation component is obtained from calibration polynomial and standard component is the manufacturer uncertainty of the temperature sensor.

The pressure standard uncertainty is calculated following the same concept which is as follows:

$$u_{calibration}(P) \qquad \text{D.7}$$
$$= \pm\sqrt{u_{correlation}(P)^2 + u_{standard}(P)^2 + u_{atmosphere}(P)^2 + u_{repeatability}(P)^2}$$

Where correlation, standard, atmosphere and repeatability components denote the uncertainties of calibration polynomial, pressure transmitted manufacturer, barometer and repeatability. The repeatability standard uncertainty is evaluated as type A and the other three components estimated using type B equation.

D.2 Uncertainty in composition

The experimental measurements of this work were done using two different high-pressure apparatuses following the SA and SS methods to fast track the measurements and validate the measured data. The compositional uncertainties are estimated differently for each method.

D.2.1. SA apparatus

The composition uncertainty of this apparatus is attributed to the measurements repeatability and the GC detector calibration.

$$u_c(x_i) = \pm\sqrt{u_{correlation}(x_i)^2 + u_{calibration}(x_i)^2 + u_{repeatability}(x_i)^2} \qquad \text{D.8}$$

As the calibration is performed via direct injection of the chemical, the standard calibration uncertainty is obtained from the standard uncertainty in the number of moles of both components in the mixture and its mole fraction:

$$u_{calibration}(x_i) = \sqrt{\left(\frac{n_j}{n_i + n_j}u(n_i)\right)^2 + \left(\frac{n_i}{n_i + n_j}u(n_j)\right)^2} \qquad \text{D.9}$$

Where the standard uncertainty in the number of moles of the gas and liquid components injected to the GC are calculated as follows:

$$\text{Gas} \qquad u(n_i) = \sqrt{u_{correlation}(n_i)^2 + u_{ideal\,gas}(n_i)^2} \qquad \text{D.10}$$

$$\text{Liquid} \qquad u(n_i) = \sqrt{u_{correlation}(n_i)^2 + u_{ideal\,density}(n_i)^2} \qquad \text{D.11}$$

Where $u_{ideal\,gas}$ and $u_{ideal\,density}$ denote the standard uncertainty in the number of moles of injected gas and liquid, respectively. These can be evaluated using the law of propagation of the errors which are as follows:

$$u_{ideal\,gas}(x_i) = \sqrt{\frac{u(P)^2}{P} + \frac{u(V_g)^2}{V} + \frac{u(T)^2}{T}}$$

D.12

$$u_{ideal\,density}(x_i) = \sqrt{\frac{u(P)^2}{P} + \frac{u(V_l)^2}{V}}$$

D.13

Where the components required for evaluation of the standard uncertainties are presented in table C-1. Another component for the evaluation of standard uncertainty in the number of moles is polynomial of the calibration which is calculated as follows:

$$u_{correlation}(n_i) = n_i \frac{\left(\left| \frac{n_{i,true} - ni_{i,calculated}}{n_{i,true}} \right| \right)}{\sqrt{3}}$$

D.14

D.2.1. SS apparatus

The standard uncertainty of composition measured using this type of experimental equipment is dependent on the standard uncertainties of the mass balance, masses of the components loaded to the cell as well as their mole fraction. This is calculated as follows:

$$u(x_i) = x_i x_j \sqrt{\frac{u(m_1)^2}{m_i} + \frac{u(m_1)^2}{m_j}}$$

D.15

Where $u(m_1)$ is the standard uncertainty of the mass balance.

Table D-1. Standard uncertainty influences and estimates for the variables reported in this study.

Source of uncertainty	Estimate	Distribution
Pressure (P)		
P reference/MPa: Mensor CPC 8000 (25 MPag)	0.01%	normal
P reference/MPa: Mensor CPC 6000 (300 kPa)	0.01%	normal
Correlation for P/MPa (25 MPag)	0.002	rectangular
Correlation for P/MPa (12 MPag)	0.001	rectangular
Correlation for P/kPa (500 kPa)	0.1	rectangular
Repeatability (average) of bubble-point P/MPa	0.01	rectangular
Temperature (T)		
T reference /K: CTH 6500	0.03	rectangular
Correlation for T/K	0.05	rectangular
Composition SA apparatus (x_i, y_i)		
Correlation for n_i of CF_4	2.5%	rectangular
Correlation for n_i of CF_4 (dilute mixtures)	4.0%	rectangular
Correlation for n_i of C_6F_{14}, C_7F_{16}, $C_5H_4F_8O$	2.0%	rectangular
Correlation for n_i of CO_2	1.5%	rectangular
Correlation for n_i of C_6H_{14}	3.0%	rectangular
V of injected gas/liquid from syringe[a]	2.0%	rectangular
T of injected gas from syringe/K[a]	2	rectangular
P of injected gas from syringe/kPa[a]	1	rectangular
Liquid density of the solvents used for TCD calibration	1.5%	rectangular
Repeatability (average of *max-min*) of x_i C_6H_{14} + CO_2	0.001	rectangular
Repeatability (average of *max-min*) of x_i C_6F_{14} + CF_4	0.001	rectangular
Repeatability (average of *max-min*) of x_i C_7F_{16} + CF_4	0.003	rectangular
Repeatability (average of *max-min*) of x_i C_8F_{18} + CF_4	0.001	rectangular
Repeatability (average of *max-min*) of x_i $C_5H_4F_8O$ + CF_4	0.005	rectangular
Repeatability (average of *max-min*) of y_i C_6H_{14} + CO_2	0.0001	rectangular
Repeatability (average of *max-min*) of y_i C_6F_{14} + CF_4	0.0001	rectangular
Repeatability (average of *max-min*) of y_i C_7F_{16} + CF_4	0.0004	rectangular
Repeatability (average of *max-min*) of y_i C_8H_{18} + CF_4	0.0001	rectangular
Repeatability (average of *max-min*) of y_i $C_5H_4F_8O$ + CF_4	0.0009	rectangular
Composition SS apparatus (x_i)		
Mass balance uncertainty/g	0.03	rectangular

[a] Uncertainties inherent to the direct injection method